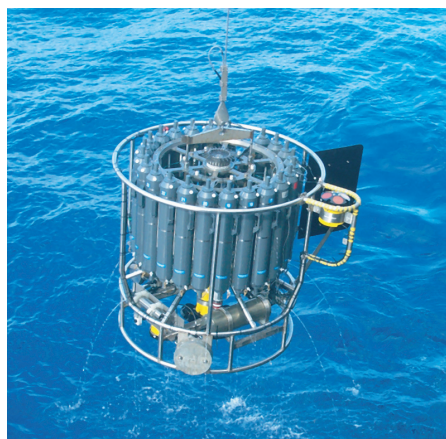




Climate Change Impacts on
Flood Related Hydrological Processes:
Further Development and Application
of a Global Scale Hydrological Model

Kerstin Verzano



Hinweis

Die Berichte zur Erdsystemforschung werden vom Max-Planck-Institut für Meteorologie in Hamburg in unregelmäßiger Abfolge herausgegeben.

Sie enthalten wissenschaftliche und technische Beiträge, inklusive Dissertationen.

Die Beiträge geben nicht notwendigerweise die Auffassung des Instituts wieder.

Die "Berichte zur Erdsystemforschung" führen die vorherigen Reihen "Reports" und "Examensarbeiten" weiter.



Notice

The Reports on Earth System Science are published by the Max Planck Institute for Meteorology in Hamburg. They appear in irregular intervals.

They contain scientific and technical contributions, including Ph. D. theses.

The Reports do not necessarily reflect the opinion of the Institute.

The "Reports on Earth System Science" continue the former "Reports" and "Examensarbeiten" of the Max Planck Institute.

Anschrift / Address

Max-Planck-Institut für Meteorologie
Bundesstrasse 53
20146 Hamburg
Deutschland

Tel.: +49-(0)40-4 11 73-0
Fax: +49-(0)40-4 11 73-298
Web: www.mpimet.mpg.de

Layout:

Bettina Diallo, PR & Grafik

Titelfotos:

vorne:

Christian Klepp - Jochem Marotzke - Christian Klepp

hinten:

Clotilde Dubois - Christian Klepp - Katsumasa Tanaka

Climate Change Impacts on Flood Related Hydrological Processes: Further Development and Application of a Global Scale Hydrological Model

Dissertation zur Erlangung des Doktorgrades der Naturwissenschaften (Dr. rer. nat)
im Fachbereich Elektrotechnik/Informatik der Universität Kassel
vorgelegt von

Kerstin Verzano

aus Kassel

Hamburg 2009

Kerstin Verzano
International Max Planck Research School
on Earth System Modelling
Bundesstrasse 53
20146 Hamburg
Germany

Als Dissertation angenommen
vom Fachbereich Elektrotechnik/Informatik der Universität Kassel

auf Grund der Gutachten von
Prof. Dr. Joseph Alcamo
und
Prof. Dr. Petra Döll

Die Disputation fand am 10. Juli 2009 statt.

Climate Change Impacts on
Flood Related Hydrological Processes:
Further Development and Application of a
Global Scale Hydrological Model



Kerstin Verzano

Kassel 2009

Cover picture sources

MODIS Snow Cover over Europe during the winter of 2001-02

<http://svs.gsfc.nasa.gov/vis/a000000/a002400/a002486/SnowEurope1.tif>

NASA/Goddard Space Flight Center

Scientific Visualization Studio. Snow Data Preparation was done by The MODIS Snow & Ice Team, Janet Y. L. Chien. Blue Marble data courtesy of Reto Stockli.

Contents

Zusammenfassung	1
Motivation	1
Hintergrund und Rahmen der Dissertation	1
Zusammenfassung der wesentlichen Resultate	2
Schlussbemerkungen und Ausblick	6
Abstract	9
1 Introduction	11
1.1 Motivation	11
1.2 Background	12
1.3 Scope of the thesis	14
1.4 Thesis outline	14
2 WaterGAP	17
2.1 Overview	17
2.2 Development of WaterGAP3	18
2.2.1 Background	18
2.2.2 Technical Realization of WaterGAP3	19
2.3 Model versions applied in this thesis	22
2.4 Simulation of Hydrological Processes within WaterGAP	22
2.4.1 Vertical Hydrological Processes	23
2.4.2 Lateral Hydrological Processes	24
2.4.3 Recent Developments	24
2.5 Model Input and Driving Forces	26
2.5.1 Static Input Maps	26
2.5.2 Climate Time Series - Historic Simulations	26
2.5.3 Climate Time Series - Future Projections	26
2.6 Water Use	28
3 A New Approach to Simulate Snow Accumulation and Melt	31
3.1 Introduction	31
3.2 Methodology	32
3.2.1 Snow Modelling Within the WaterGAP Model	32
3.2.2 Investigated River Basins	33
3.3 Results	36
3.3.1 Simulation of discharge hydrographs	36

3.3.2	Northern Hemisphere Snow Cover	37
3.4	Discussion	39
4	Snow Hydrological Conditions in Mountains and Cold Regions	43
4.1	Introduction	43
4.2	Material and methods	44
4.2.1	Definition of mountains	44
4.2.2	Definition of arctic regions	46
4.2.3	Forcing data	46
4.3	Results current situation	47
4.3.1	Results for Mountain Regions	47
4.3.2	Northern Hemisphere	52
4.4	Scenarios based on GCM output	54
4.4.1	Climate change impacts on mountain snow cover	55
4.4.2	Climate change impacts on Northern Hemisphere Snow Cover	57
4.4.3	Climate Change impact on Arctic River discharge	58
4.5	Summary and Conclusions	59
5	Simulating River Flow Velocity on Global Scale: a Pre-Study	63
5.1	Introduction	63
5.2	Methodology	64
5.3	Results	65
5.3.1	Testing the Approach	65
5.3.2	Integrating the algorithm into a global hydrology model	68
5.4	Conclusions	68
6	Modeling Variable River Flow Velocity on Continental Scale	71
6.1	Introduction	71
6.2	Methodology	72
6.2.1	River Bed Slope	72
6.2.2	Hydraulic Radius	73
6.2.3	River roughness (Manning's n)	75
6.2.4	Lateral Routing	77
6.3	Results for the Current Situation	79
6.3.1	River flow velocity in Europe	79
6.3.2	Validation of river flow velocities	79
6.3.3	Effect of the dynamic flow velocity on river discharge	81
6.3.4	Effect of the dynamic flow velocity on floods	82
6.3.5	Residence time in rivers	84
6.4	Climate change impacts on flow velocities and residence time	86
6.5	Discussion and Conclusion	89
7	Future Flood Risks in Europe	93
7.1	Introduction	93
7.2	Methodology	95
7.2.1	Forcing data	95
7.2.2	Flood Indicators	97

7.2.3	Validation of WaterGAP for Flood Calculations	99
7.3	Results	103
7.3.1	Changes in future precipitation	103
7.3.2	Changes in future flood magnitudes	105
7.3.3	Future changes in 100-year flood discharge	105
7.3.4	Comparison between scenario methods (delta change vs. future time series)	111
7.4	Discussion	115
7.5	Summary and Conclusions	119
8	Summary and Outlook	121
8.1	General Summary	121
8.2	Concluding Remarks and Outlook	125
	Appendixes	126
A	Appendix to Chapter 4	127
B	Appendix to Chapter 7	131
	Bibliography	135
	Danksagung	147

List of Figures

2.1	Soft-linking between the three global scale water models that are developed at CESR	19
2.2	Wetland distribution in South America and the river networks for WaterGAP2 and WaterGAP3	20
2.3	Comparison of WaterGAP2 and WaterGAP3 model output: Snow Water Equivalent and Water Availability	21
2.4	Division of continents within WaterGAP3 and the location of calibration stations (state January 2009).	22
2.5	Schematic representation of the vertical and lateral water balance considered in WaterGAP, including human water use.	23
3.1	Example for the altitude dependent, subscale distribution of temperature T and SWE within one 0.5° grid cell.	33
3.2	Long term average monthly discharge of the Aare at Untersiggenthal (1961-1990) and the Rhone at Chancy (1961-1978).	36
3.3	MME of 50 river basins before (grey) and after (black) implementation of sub grids into the snow routine.	37
3.4	Snow dominated river basins chosen for testing the subscale approach.	38
3.5	Global snow cover in January 1990 by WaterGAP and ISLSCP satellite data.	39
3.6	Figure of Merit in Space of the snow covered areas of the Northern Hemisphere in 1990 based on WaterGAP calculations and the ISLSCP data set. Further the modeled and satellite derived snow covered area is shown.	40
4.1	Global map of mountains and high plateaus, classified according to the definition developed within this study.	46
4.2	Typical discharge regimes (mean monthly discharges) of mountains. The examples come from seven different mountain ranges which have been selected for a detailed analysis in this paper.	48
4.3	Average January or April temperature and SWE 1961-1990 and annual number of snow days over the altitude of seven selected mountain ranges.	49
4.4	Intercomparison of average temperature, SWE and snow days per year for 1961-1990 between the different mountains.	51
4.5	Simulated and measured average monthly discharge of the Mackenzie River at Arctic Red River (Canada) showing the typical winter discharge underestimation of WaterGAP results.	55
4.6	Climate change impacts on temperature and snow characteristics for different mountain regions for the reference period 1961-1990 and for the 2080s.	56

4.7	Snow dominated area of the reference period and the A1b scenario for the 2080s as calculated by WaterGAP based on Echem climate.	58
5.1	Modeled values of river velocity compared to measured values for three selected stations	67
6.1	Approximated river bed slopes in Europe [m/m]	74
6.2	Histograms of river roughness in entire Europe and European mountains . .	77
6.3	Approximated roughness values for Europe.	78
6.4	Routing scheme of WaterGAP	79
6.5	Average annual river flow velocities for 1971-2000 in Europe (WaterGAP results)	80
6.6	Comparison of average simulated and measured river flow velocity at 22 US gauges.	82
6.7	Effect of the variable flow velocity on average long term monthly discharges.	83
6.8	Effect of the variable flow velocity on 100-year-flood discharges	84
6.9	Number of days that the water needs on average to reach the river mouth (residence time)	85
6.10	Climate change effects on average annual river flow velocity between reference period (1971-2000) and the three scenarios	89
6.11	Climate change effects on residence time in rivers between reference period and the tree scenarios	90
7.1	Daily discharge at the Weser River in Hann. Münden (Germany). The dashed line indicates the Q1 discharge level.	98
7.2	Comparison of 100-year flood discharge at 119 Europe an gauging stations derived from measured and simulated time series.	101
7.3	AMS of two gauging stations showing examples of average over- and under-estimation of annual maximum daily flood peaks.	102
7.4	Characteristical relationship between a change in flood intensity and the corresponding change in the flood return period.	103
7.5	Discharge that is exceeded statistically in 1 of 100 days. Comparison between measured and WaterGAP3 modeled data for the period 1971-2000. .	104
7.6	Changes in average annual precipitation between the baseline (1961-1990) and corresponding scenario period (2050s) derived from time series of the three GCMs.	106
7.7	Seasonal changes in precipitation of IPCM-A2 (2050s) compared to the corresponding control run (1961-1990).	107
7.8	Change in 100-year flood discharge magnitude between the 2050s and the baseline (1961-1990) of the corresponding GCM.	108
7.9	Future return periods of floods with the intensity of a 100-year flood of the control period (1961-1990).	109
7.10	Projected changes in the discharge level that is exceeded by 1% of all discharges (daily Q1)	110
7.11	Absolute change in days over bankfull flow between reference period and scenario.	111

7.12	Comparison between the flood indicators calculated from MPEH5 climate (DC and TS).	112
7.13	Changes in Annual Maximum Discharge (AMS) and the corresponding flood frequency distribution for rivers showing opposed results in change in 100-year flood discharge for the DC and TS methods.	115
7.14	Hydrographs of the same stations as in Figure 7.13 but for 1981-1990 only .	116
8.1	Validation of 100-year flood discharge modeled by two WaterGAP versions: before and after implementing the improvements performed within the scope of this dissertation.	125
A.1	Average January or April temperature and SWE and annual number of snow days over the altitude of seven selected mountain ranges during the reference period and four scenarios of the 2080s.	128
A.2	Snow dominated area of the reference period and four scenarios of the 2080s	129
B.1	Seasonal changes in precipitation of the MIMR scenario compared to the corresponding control run	131
B.2	Seasonal changes in precipitation of the MPEH scenario (2050s) compared to the corresponding control run	132
B.3	Month with maximum discharge for reference period (CRU-climate), control period (GCM) and the scenarios derived by DC and TS, respectively	133

List of Tables

2.1	Differences between WaterGAP 2.1f and WaterGAP 3.1 features	24
2.2	Data sources for static input maps used in WaterGAP 2.1f and WaterGAP 3	27
3.1	Characteristics and MMEs of the 50 watersheds that were selected for this study	34
4.1	Characteristics and quality criteria of catchments located in the selected mountains.	53
4.2	Characteristics of major rivers draining into the Arctic Ocean	54
4.3	Change in annual river discharge (Q_{annual}) of the nine largest Arctic Rivers until the 2080s compared to 1961-1990.	60
5.1	Gauging stations used for model testing with optimized roughness and modeling efficiency (NSC)	66
6.1	River lengths [km] of exemplary rivers with and without considering the individual meandering ratio (MR).	73
6.2	Values used to estimate the river roughness for the application in WaterGAP. After Cowan (1956), modified:	76
6.3	Gauging Stations with flow velocity data	81
6.4	Mean residence time in selected European rivers during the reference period and projected future changes due to climate change impacts.	87
7.1	Pros and Cons of the flood indicators as calculated by WaterGAP3	105
7.2	Gauging stations selected for further investigations with changes in 100-year flood discharge for DC and TS.	114

Zusammenfassung

Motivation

Hochwasser gehören zu den häufigsten Naturkatastrophen und verursachen oft immense wirtschaftliche Schäden. So wurden in den 1990er Jahren Kosten von über 200 Milliarden US\$ durch Hochwasser verursacht und alleine das Hochwasser in Europa im August 2002 hat zu einem wirtschaftlichen Schaden von über 20 Milliarden Euro geführt (MunichRe). Aus diesem Grund ist das Interesse von Wissenschaftlern, Politikern aber auch der Bevölkerung an Erkenntnissen über zukünftige Hochwasserrisiken groß.

Der Klimawandel führt zu einer erhöhten Klimavariabilität (e.g. IPCC, 2007a; Beniston et al., 2007) und aktuelle Forschungsergebnisse zeigen, dass die Zunahme von extremem Niederschlag zu einer erhöhten Hochwassergefährdung in vielen Regionen der Welt führt (Kundzewicz et al., 2007). Jedoch kann eine Zu- oder Abnahme der Hochwassergefährdung nicht alleine an die Entwicklung von extremen Niederschlägen gekoppelt werden, denn Hochwasser werden in schneedominierten Regionen regelmäßig durch Schneeschmelze verursacht. Wie groß der Einfluss des Klimawandels auf den Durchfluss in Flüssen ist, hängt von einer Reihe gebietspezifischer Eigenschaften ab. Um die komplexen hydrologischen Prozesse in Flusseinzugsgebieten zu untersuchen, werden hydrologische Modelle eingesetzt. Die meisten hydrologischen Studien, die sich mit dem Einfluss des Klimawandels auf Hochwassergefährdungen befasst haben, wurden auf Flusseinzugsgebietsskala durchgeführt (e.g. Graham et al., 2007; Menzel et al., 2006; Pinter et al., 2006; Booi, 2005; Dale, 2005; Menzel and Burger, 2002b) oder haben einzelne große Einzugsgebiete der Erde miteinander verglichen (Kleinen and Petschel-Held, 2007; Milly et al., 20002). Die unterschiedlichen Untersuchungsgebiete, Szenarien und Auswertungen dieser Studien lassen jedoch keine konsistenten Aussagen auf kontinentaler oder gar globaler Skala zu. Bisher wurden nur zwei Studien veröffentlicht, die die zukünftige Hochwassergefährdung in ganz Europa untersucht haben (Dankers and Feyen, 2008; Lehner et al., 2006) und es fehlt an Modellen, die in der Lage sind Hochwasserstudien auf globaler Skala durchzuführen. Diese Lücke soll im Rahmen der vorliegenden Dissertation geschlossen werden. Das Ziel dieser Arbeit ist die (Weiter-)Entwicklung eines globalen hydrologischen Modells, um damit den Einfluss des Klimawandels auf zukünftige Hochwassergefährdung weltweit beurteilen zu können.

Hintergrund und Rahmen der Dissertation

Lehner et al. (2006) haben mit Hilfe des globalen hydrologischen Modells WaterGAP (Alcamo et al., 2003a; Döll et al., 2003) erste Hochwasserberechnungen für Europa durchgeführt. Die Autoren weisen jedoch darauf hin, dass ihre Studie erste und vorläufige Ergebnisse präsentiert, die durch weitere Studien untermauert werden sollten. Die Berechnungen und Auswertungen für die Lehner-Studie wurden am Center for Environmental Systems Research (CESR) der Universität Kassel durchgeführt. Am CESR wird das hydrologische Modell WaterGAP seit den frühen 1990er Jahren entwickelt. Auf Grundlage der Erfahrungen, die die Forscher am CESR durch erste Hochwasseranalysen mit WaterGAP gewonnen haben, wurden vier hochwasserrelevante Einflussgrößen definiert,

die im Rahmen dieser Dissertation näher untersucht und verbessert werden:

- Die räumliche Auflösung von WaterGAP,
- die Simulation von Schneeakkumulation und -schmelze,
- der laterale Wassertransport durch das Flussnetz, und
- das Klima der Gegenwart und Zukunft, insbesondere Niederschlag und Temperatur.

Dadurch soll eine verbesserte WaterGAP Version entstehen, mit der auf Grundlage unterschiedlicher Szenarien Regionen definiert werden können, in denen sich die Hochwassergefahr zukünftig ändern könnte. Es ist jedoch wichtig, auch die modellinternen Prozesse näher zu untersuchen, um herauszufinden, ob die hochwasserrelevanten hydrologischen Prozesse korrekt wiedergegeben werden. Aus diesem Grund wurde die Dynamik der Schneedecke und der laterale Wassertransport bzw. die Fließgeschwindigkeit des Wassers in den Flüssen, näher untersucht. Das beinhaltet sowohl die Validierung der WaterGAP Berechnungen als auch die Untersuchung des Einflusses des Klimawandels auf diese Prozesse.

Auf Grundlage der oben beschriebenen hochwasserrelevante Einflussgrößen wurden verschiedene Forschungsfragen definiert, die innerhalb der einzelnen Kapitel dieser Dissertation bearbeitet und beantwortet werden:

- Wie kann die Simulation der Schneedynamik so verbessert werden, dass die Abflussganglinien und Hochwasserspitzen schneedominierter Einzugsgebiete verbessert dargestellt werden? Welchen Einfluss hat der Klimawandel auf die Schneebedeckung verschiedener schneedominierter Regionen der Welt?
- Wie kann der laterale Wassertransport durch das Flussnetz verbessert werden? Beeinflusst der Klimawandel die Fließgeschwindigkeit in europäischen Flüssen?
- Wie können Hochwasser auf globaler Skala modelliert werden und wie beeinflusst der Klimawandel die Hochwassergefährdung für Europa? Welchen Einfluss hat die Methode, mit der Klimazeitreihen für verschiedene Szenarien abgeleitet werden, auf die Berechnung von Hochwasserindikatoren?

Zusammenfassung der wesentlichen Resultate

Um eine optimale räumliche Auflösung für die Untersuchung von Hochwassern auf kontinentaler Skala zu erlangen, wurde die Auflösung von 0.5° der ursprünglichen Modellversion WaterGAP2 auf 5 Bogenminuten erhöht (WaterGAP3). Dies wurde dadurch ermöglicht, dass die meisten Eingangskarten, die WaterGAP verwendet inzwischen global hoch aufgelöst vorliegen. Das gilt sowohl für statische Karten als auch für Klima auf (sub-)kontinentaler Skala. Das erhöht die Informationsdichte der Eingangsgrößen des Modells und auch das Flussnetz wird realistischer dargestellt. Die oben definierten schneebezogenen Forschungsfragen wurden mit WaterGAP2 bearbeitet, die anderen Forschungsfragen im Wesentlichen mit WaterGAP3. Im folgenden wird die Beantwortung der Forschungsfragen zusammengefasst, die sich an den einzelnen Kapiteln orientieren.

Wie kann die Simulation der Schneedynamik so verbessert werden, dass die Abflussganglinien und Hochwasserspitzen schneedominierter Einzugsgebiete verbessert dargestellt werden?

Bevor der Schneealgorithmus von WaterGAP überarbeitet wurde, sind die Abflussspitzen in schneebeeinflussten Einzugsgebieten, die durch Schneeschmelze entstanden sind, oftmals überschätzt worden. Das lag daran, dass die Schneedecke in den 0.5° Rasterzellen von WaterGAP2 einheitlich simuliert wurde. Sobald die Temperatur über 0°C stieg, schmolz der Schnee in der gesamten Rasterzelle und verursachte vor allem in gebirgigen Regionen die erwähnte Überschätzung der Hochwasserpeaks. Dieser Effekt wurde durch subskalige Simulation von Schneeakkumulation und -schmelze in den einzelnen Rasterzellen verbessert. Auf Grundlage einer hoch aufgelösten Höhenkarte wurden jeweils 100 Teilzellen jeder 0.5° Rasterzelle eine individuelle Höhe über N.N. sowie eine individuelle Temperatur zugewiesen. Dadurch schmilzt der Schnee im Frühjahr in niedrig gelegenen Teilzellen zuerst und der Abflusspeak wird in vielen Einzugsgebieten realistischer dargestellt (Kapitel 3).

Die Validierung der Schneedecke der nördlichen Hemisphäre mit Hilfe von Satellitendaten hat gezeigt, dass WaterGAP die Ausdehnung der Schneebedeckung zufriedenstellend wiedergibt, insbesondere in Nordamerika, Teilen Europas und in großräumig ebenen Regionen wie Nordrussland. Die größten Unterschiede zwischen der modellierten und beobachteten Schneedecke treten in orographisch heterogenen Gegenden wie z.B. Mitteleuropa auf, aber auch in Regionen, in denen die Qualität der Klimadaten, mit denen WaterGAP angetrieben wird, verhältnismäßig ungenau ist. Das trifft zum Beispiel auf die Hindukush-Himalaya Region oder Ostasien zu.

Welchen Einfluss hat der Klimawandel auf die Schneebedeckung verschiedener schneedominierter Regionen der Erde?

Die globale Erwärmung hat bereits während der letzten Jahre einen Rückgang der globalen Schneebedeckung verursacht, der sich sehr wahrscheinlich im Laufe dieses Jahrhunderts fortsetzen wird (IPCC, 2007a). Mithilfe von WaterGAP2 wurde der Einfluss des Klimawandels auf sieben große Gebirgsregionen sowie die großräumige Schneebedeckung der gesamten nördlichen Hemisphäre untersucht (Kapitel 4). Dazu wurde das Klima zweier Szenarien für die 2080er Jahre verwendet, die jeweils von zwei unterschiedlichen Globalen Klimamodellen (GCMs) berechnet wurden. Wie zu erwarten war, werden alle untersuchten Gebirge massiv vom Klimawandel beeinflusst. Die Schneedecke wird in den meisten der untersuchten Gebirgsregionen dünner und die Schneegrenze wird steigen. Südlich gelegene Gebirge sind vom Klimawandel stärker betroffen als Gebirge in den hohen nördlichen Lagen. Die am meisten betroffenen untersuchten Gebirge sind die Alpen, das südliche Hindukusch-Himalaya und die Anden. Im Gegensatz zu den anderen Gebirgen der Studie, projizieren alle Szenarien und GCMs eine Erhöhung der Schneedecke im zentralasiatischen Altai. Dies wird durch einen massiven Anstieg des Winterniederschlags verursacht, da die Wintertemperatur trotz Klimaerwärmung noch weit unter dem Gefrierpunkt liegen wird.

Wie kann der laterale Wassertransport durch das Flussnetz verbessert werden?

In der ursprünglichen WaterGAP Version wurde der Abfluss mit einer konstanten Fließgeschwindigkeit von 1 m/s durch das virtuelle Flussnetz des Modells transportiert. Dadurch wurde die räumliche und zeitliche Variabilität der Fließgeschwindigkeit nicht berücksichtigt, die im Wesentlichen vom aktuellen Durchfluss, dem Flussgefälle und der Rauigkeit des Flussbetts abhängt. Die Abbildung der Fließgeschwindigkeit im Modell wurde im Rahmen dieser Dissertation durch die folgenden Maßnahmen verbessert: (i) die Erhöhung der räumlichen Auflösung von WaterGAP und die dadurch realistischere Abbildung der Fließlänge (Kapitel 2) und (ii) die Implementierung eines Algorithmus zur variablen Simulation der Fließgeschwindigkeit (Kapitel 5 und 6). Die Erhöhung der räumlichen Auflösung an sich führt schon zu einer realistischeren Darstellung des schematischen Flussnetzes, die durch die Berücksichtigung eines individuellen Mäandrierungsfaktors für jede Rasterzelle zusätzlich verbessert wurde. Für die Implementierung der variablen Fließgeschwindigkeit musste ein Ansatz entwickelt werden, der es ermöglicht, Faktoren zu verwenden, die global für jede 5 Bogenminuten Rasterzelle abgeleitet werden können aber dennoch die charakteristischen räumlichen Eigenschaften verschiedener Regionen wiedergeben soll. Die in WaterGAP3 implementierte variable Fließgeschwindigkeit wird nach der Manning-Strickler-Formel berechnet. Die Formel besteht aus drei Faktoren, die folgendermaßen abgeleitet werden: Die Rauigkeit des Flussbetts wird basierend auf der Topographie, der Verteilung von Stadt- und Landbevölkerung und der Flussmäandrierung abgeleitet. Der Hydraulische Radius wird in Abhängigkeit vom aktuellen Durchfluss jedes Zeitschritts berechnet und das Gefälle des Flussbetts wird auf Grundlage der Topographie und eines Mäandrierungsfaktors bestimmt. Die Validierung der berechneten Fließgeschwindigkeit an entsprechenden Messungen an 22 Flüssen in den USA hat gezeigt, dass WaterGAP die Größenordnung der Fließgeschwindigkeit gut wiedergibt. Jedoch wird sie in den meisten der untersuchten Flüsse im Mittel überschätzt. Trotz dieser Ungenauigkeit wurde der hydrologische Prozess des lateralen Transports im Vergleich zu der konstanten Fließgeschwindigkeit wesentlich verbessert, da vor allem die langsamen Fließgeschwindigkeiten in den zahlreichen Nebenflüssen, die deutlich unter 1 m/s liegen besser dargestellt werden und der Anstieg der Fließgeschwindigkeiten bei Hochwassern gut wiedergegeben werden kann. Der Einfluss der variablen Fließgeschwindigkeit auf den Durchfluss zeigt sich am deutlichsten bei Abflussspitzen, die in der Regel erhöht werden. Dadurch verbessert sich die Wiedergabe von Abflussspitzen, die zuvor unterschätzt wurden und umgekehrt. Der mittlere Durchfluss wird durch die Fließgeschwindigkeit kaum beeinflusst.

Beeinflusst der Klimawandel die Fließgeschwindigkeit in europäischen Flüssen?

Auf Grundlage von drei Klimaprojektionen für die 2050er Jahre (Ergebnisse von drei Klimamodellen für zwei Szenarien (A2 und B1)) wurden die Veränderungen der mittleren Fließgeschwindigkeit und der Verweilzeit des Wassers in europäischen Flüssen untersucht (Kapitel 6). Die drei Projektionen zeigen unterschiedliche Ergebnisse in Zentral- und Osteuropa. Sie stimmen allerdings darin überein, dass die Fließgeschwindigkeit in Nordeuropa zunimmt und in Teilen des Mittelmeerraumes abnimmt, was auf die Abnahme des mittleren Durchflusses in dieser Region zurückzuführen ist. Als Fazit kann

gezogen werden, dass der Klimawandel die mittlere Fließgeschwindigkeit beeinflusst, die mit der Entwicklung des mittleren Abflusses zusammenhängt. Die Veränderungen sind jedoch relativ gering. Ein größerer Einfluss auf den mittleren Abfluss und somit auch auf die mittlere Fließgeschwindigkeit als durch den Klimawandel wird durch Änderungen der anthropogenen Wasserentnahme erwartet.

Wie können Hochwasser auf globaler Skala modelliert werden und wie beeinflusst der Klimawandel die Hochwassergefährdung für Europa?

Mit WaterGAP3 wurde die Abflussmenge 100-jährlicher Hochwasser sowie der Q1, definiert als Abfluss, der statistisch an einem von 100 Tagen überschritten wird, für jede Rasterzelle in Europa berechnet. 100-jährliche Hochwasser sind, wie der Name schon sagt, extreme Hochwasserereignisse und der Q1 deckt regelmäßige Hochwasser ab. Die modellierten Hochwasserabflüsse wurden mit den zugehörigen aus gemessenen Abfluss berechneten Hochwasserabflüssen verglichen (Kapitel 7). Es hat sich gezeigt, dass WaterGAP3 die Abflussspitzen zufriedenstellend wiedergibt, wobei die modellierten Q1-Ergebnisse näher am gemessenen Q1 sind als die entsprechenden 100-jährlichen Hochwasserabflüsse. Daraus kann gefolgert werden, dass der Q1 robuster gegenüber fehlerhaft berechneten Abflussspitzen ist, da mit WaterGAP3 derzeit die Abflussspitzen oftmals nicht exakt wieder gegeben werden können. Aus diesem Grund werden bei den Untersuchungen des Klimawandels auf Hochwasser die Veränderung (und nicht die absoluten Werte) der Hochwasserabflüsse im Szenariozeitraum im Vergleich zu einer Referenzperiode betrachtet.

Der Einfluss des Klimawandels auf das Hochwasserrisiko in Europa wurde anhand der gleichen drei Projektionen untersucht, die bereits in der Fließgeschwindigkeitsstudie verwendet wurden (Kapitel 7). Die Veränderungen zwischen der Referenzperiode (1961-1990) und der Szenarioperiode (2040-2069) wurden für drei verschiedene Hochwasserindikatoren verglichen: (i) der 100-jährliche Hochwasserabfluss, (ii) der Q1, und (iii) die Anzahl der Tage im Jahr, in denen der bordvolle Abfluss überschritten wird. Die Übereinstimmung zwischen den Szenarien ist für den Q1 größer als für den 100-jährlichen Abfluss. Alle Projektionen zeigen einen Anstieg der Hochwasserabflüsse in Teilen des Mittelmeerraumes, obwohl in dieser Region der mittlere jährliche Niederschlag sinken wird. Jedoch ändert sich der Niederschlag in den einzelnen Jahreszeiten unterschiedlich stark und in unterschiedliche Richtungen. So wird der Anstieg des Hochwasserrisikos in den betroffenen Gebieten des Mittelmeerraums durch die erhöhten Niederschläge im Herbst und Winter verursacht. Des Weiteren wird ein Anstieg des Hochwasserrisikos für Teile von West-, Ost- und Mitteleuropa vorhergesagt, allerdings mit unterschiedlich stark ausgeprägter Magnitude und räumlicher Ausdehnung. Die Projektionen zeigen übereinstimmend einen Rückgang des 100-jährlichen Abflusses sowie des Q1 in Teilen von Ost- und Mitteleuropa. Des Weiteren wird ein Rückgang der Hochwassermagnitude in der Ägäis und in Teilen der Iberischen Halbinsel erwartet. Die Zahl der Tage, in denen der bordvolle Abfluss überschritten wird ändert sich nur um ± 1 Tag im größten Teil von Mittel- und Südeuropa. Daraus lässt sich schließen, dass sich die Dauer der Hochwasserereignisse nicht zwingend ändert, auch wenn die Magnitude des Hochwasserindikators erhöht oder abgeschwächt wird. Die drei Projektionen zeigen übereinstimmend einen Rückgang des überbordvollen Abflusses in weiten Teilen Osteuropas, jedoch in unterschiedlichen

Gegenden und mit unterschiedlich starker Ausdehnung. In zwei der Projektionen wird ein Anstieg des überbordvollen Abflusses in Teilen Skandinaviens und des Baltikums erwartet.

Welchen Einfluss hat die Methode, mit der Klimazeitreihen für verschiedene Szenarien abgeleitet werden, auf die Berechnung von Hochwasserindikatoren?

Die Zeitreihen des Klimas der Szenarioperiode mit denen WaterGAP angetrieben wird, kann durch verschiedene Methoden erstellt werden. Zwei Methoden wurden ausgewählt und der Einfluss auf die Berechnung der oben beschriebenen Hochwasserindikatoren verglichen: (i) die direkte Anwendung der Ergebnisse der Klimamodelle der Referenzperiode (1961-1990) und des Szenariozeitraums (2040-2069), und (ii) die mittleren Klimaveränderungen zum Szenariozeitraum, der auf das gemessene Klima der Referenzperiode skaliert wird ("delta change Methode"). Die Wahl der Methode beeinflusst die Ergebnisse der Hochwasserveränderungen immens (Kapitel 7). Die größten Unterschiede wurden auch hier bei den Veränderungen des 100-jährlichen Abflusses festgestellt. Hier wurden für verschiedene europäische Regionen gegensätzliche Ergebnisse berechnet. Der Einfluss auf die Änderungen des Q1 war jedoch verhältnismäßig gering. Das zeigt, dass der Q1 sowohl gegenüber der Wahl der Methode zur Zeitreihenaufbereitung als auch gegenüber der Wahl des Szenarios (s.o.) robuster ist. Das ist darauf zurück zu führen, dass der Q1 nicht aus Hochwasserspitzenabflüssen abgeleitet wird, so wie es beim 100-jährlichen Abfluss der Fall ist, sondern statistisch aus der gesamten Abflusszeitreihe ermittelt wird. Die Hintergründe für die unterschiedlichen Ergebnisse der Methodenwahl beim 100-jährlichen Hochwasser können nicht verallgemeinert werden, da dies davon abhängig ist, ob die Hochwasser aus Schneeschmelze oder aus extremen Niederschlägen entstehen. Eine Analyse von drei ausgewählten Messstationen, an denen gegensätzliche Änderungen der 100-jährlichen Hochwasser berechnet wurden hat gezeigt, dass die direkte Anwendung der GCM-Zeitreihen eine stärkere Niederschlagsvariabilität sowohl während der Referenzperiode als auch während der Szenarioperiode aufweist. Die "delta change Methode" hingegen, gibt Änderungen in der Niederschlagsvariabilität in der Szenarioperiode nicht zufriedenstellend wieder. Jedoch wird durch diese Methode die Schneedecke in Gebirgen und deren Änderung besser repräsentiert als durch die direkte Anwendung der GCM Ergebnisse.

Schlussbemerkungen und Ausblick

Als abschließendes Fazit kann gezogen werden, dass die Zielvorgabe der Doktorarbeit, "die (Weiter-)Entwicklung eines globalen hydrologischen Modells, um damit den Einfluss des Klimawandels auf zukünftige Hochwassergefährdung weltweit beurteilen zu können", erfolgreich umgesetzt wurde. Allerdings wurden durch die Untersuchungen, die in Kapitel 7 beschrieben werden, weitere Forschungsmöglichkeiten im Bereich der Hochwasserszenarienanalyse aufgedeckt. Vor allem das treibende Klima beeinflusst die Ergebnisse der Hochwasseranalysen. Von daher ist es sinnvoll zukünftig weiter an einer Optimierung der Klimazeitreihe zu arbeiten, so dass sowohl die räumlichen und zeitlichen Veränderungen (extremen) Niederschlags, als auch die Schneedecke und ihre Änderung im Szenariozeitraum gut wiedergegeben werden. Eine Option wäre die Anwendung von

Klima aus Regionalen Klimamodellen. Des weitern würde eine Analyse der saisonalen Änderungen der Hochwassermagnitude weitere interessante Erkenntnisse bringen. Auch die Wahl oder Entwicklung weiterer Hochwasserindikatoren kann den Informationsgehalt der WaterGAP Auswertungen verbessern.

Abstract

Floods are one of the most frequent and most costly natural catastrophes. Major floods worldwide generated costs over US\$ 200 Billion in the 1990s alone, whereas the summer flood in Europe in 2002 caused economic losses exceeding 20 Billion Euro. Available research suggests that the expected future increase in heavy rainfall and the decrease of the snow cover in many regions worldwide alters future flood risk. Numerous hydrological studies dealing with flood risks have been performed on catchment scale. To date, only two studies investigated climate change effects on floods risks on European scale and there is a lack of models that are able to perform worldwide calculations of flood risks. This gap is bridged by the central theme of this dissertation: The (further) development of a global scale hydrological model to assess climate change effects on flood hazards worldwide. The model should be suitable to define regions on large scale, in which considerable changes in floods might be expected based on different climate change scenarios. The global hydrological model WaterGAP has been improved to comply with the objective of this dissertation. The spatial resolution of WaterGAP has been increased to enhance the information density of the model input, which leads among other things to a more realistic representation of the river network. Further the model results can be assessed with a higher level on detail. But it is also important to look into the model to examine whether the flood related hydrological processes are represented well. Therefore the representation of the snow dynamics as well as the river flow velocity within WaterGAP have been assessed in detail. This included the validation of the model results as well as the investigation of climate change impacts on snow cover and river flow velocity. It has been found that WaterGAP is able to reproduce the snow related hydrological processes well and calculates flow velocities satisfyingly. It is expected that climate change causes a significant decrease of the snow cover magnitude and extent in most regions of the world until the end of the 21st century. Changes in either direction are expected from the climate change impact on river flow velocity in Europe. The improved model version has been applied to investigate the climate change impact on floods in Europe. It has been found that an increasing flood risk can be expected in parts of the Mediterranean, north and south Scandinavia and in different regions of central Europe with varying extent and location. The flood risk is predicted to decrease most pronounced in parts of the Mediterranean as well as in eastern Europe. However, the results vary between different flood indicators, different scenarios, calculated by different GCMs and between the method that is chosen to derive the time series of the forcing climate. Further research should be carried out on the selection or development of flood indicators and on the choice and preparation of the forcing climate.

Chapter 1

Introduction

1.1 Motivation

Floods are among the most frequent and most costly natural catastrophes. Major floods worldwide generated costs over US\$ 200 Billion in the 1990s alone whereas the summer flood in Europe in 2002 caused an economic loss exceeding 20 Billion Euro (MunicRe 2009). This demonstrates how vulnerable our present society is to the destructiveness of such extreme events.

It is commonly agreed that an enhanced climate variability is induced by climate change (e.g. IPCC, 2007a; Beniston et al., 2007). Available research suggests that the significant future increase in heavy rainfall events in many regions results in increased flood risk (Kundzewicz et al., 2007). However, changes of flood hazards cannot merely be related to expected changes in extreme precipitation. Floods are oftentimes induced by snow melt in watersheds, in which a considerable amount of precipitation is stored as snow.

The magnitude of the climate change impact on river discharge depends partly on the characteristics of the river basin (Leander and Buishand, 2007; Nijssen et al., 2001; Arnell and Reynard, 1996). Hydrological models are therefore required, to assess the complex hydrological processes within the catchments. Numerous hydrological studies dealing with flood risks have been performed on catchment scale (e.g. Graham et al., 2007; Menzel et al., 2006; Pinter et al., 2006; Booij, 2005; Dale, 2005; Menzel and Burger, 2002b) or have investigated a number of large catchments located throughout the world (Kleinen and Petschel-Held, 2007; Milly et al., 20002). However, the application of different hydrological modes, scenarios and model interpretations do not allow a consistent view over large areas on continental or even global scale. To date, there are only few studies that investigate climate change impacts on floods on global or European scale. Hirabayashi et al. (2008) calculated future changes in floods on global scale with a General Circulation Model and they expect an increase of flood hazards over many regions of the world, except parts of North America and Europe. Within two studies, climate change effects on floods have been investigated with hydrological models on European scale (Dankers and Feyen, 2008; Lehner et al., 2006). In both studies, regions with increasing but also decreasing future flood magnitudes have been found. However, the direction of change is contradictory over large areas and no clear conclusion can be drawn. The absence of flood related climate impact studies on large scale shows that there is a lack of validated models available in the literature for making worldwide calculations of flood risks (Alcamo et al., 2005, p.346).

This gap is bridged by the central theme of this dissertation: The (further) development of a global scale hydrological model to assess climate change effects on flood hazards worldwide.

1.2 Background

Lehner et al. (2006) performed a first approach to simulate floods in Europe with the global hydrological model WaterGAP (Alcamo et al., 2003a; Döll et al., 2003). The authors point out however, that their study "serves as an initial, interim assessment until better information becomes available" (Lehner et al., 2006). The analyses for the Lehner-study have been performed at the Center for Environmental System Research (CESR) of the University of Kassel (Germany), where the WaterGAP model has been developed. Based on the experience that the authors gained from their flood analyses with WaterGAP, four determining factors have initially been considered to be crucial for the simulation of floods with WaterGAP:

- The spatial model resolution,
- the simulation of snow accumulation and melt,
- the lateral routing of discharge through the river network, and
- the climatic driving forces especially precipitation and temperature.

The relation of these four factors in relation to flood modeling is explained in the following:

Spatial Model Resolution

Lehner et al. (2006) points out that "the analysis of possible impacts of global change on flood and drought frequencies is generally limited by the quality of the applied input data." The spatial model resolution should be fine enough to capture the spatial variability of physiographic features, such as soil characteristics, land cover or elevation. However the spatial resolution should also be selected reasonably to avoid an over parameterization of the conceptual approaches applied within WaterGAP (see chapter 2). The quality and most notably the spatial resolution of the input data increased since the time when the WaterGAP version applied for the Lehner-study has been developed. To date, most data sources for the static model input are available in a spatial resolution between 5 arc-minutes and 1km covering Europe or even all continents (see Table 2.2). Further do new generations of Regional Climate Models (RCMs) produce climate time series in up to 12 km spatial resolution on European scale (Christensen and Christensen, 2007), which are well suitable to drive a spatially adapted hydrological model. For these reasons, it has been decided to increase the spatial resolution from 0.5° (original WaterGAP version) to 5 arc-minutes globally. The enhanced spatial resolution of the model input consequently leads to a spatially more differentiated representation of the different hydrological variables calculated by WaterGAP. Further a considerably more realistic representation of the river network is obtained. This generally improved the models ability to simulate vertical and lateral processes, also applying for floods.

Hydrological Processes in Snow Cover

Floods in snow dominated watersheds are regularly caused by snow melt in spring. The representation of this process in a global hydrological model is crucial, because wide areas of the Northern Hemisphere are snow covered during winter and more than one-sixth of the world's population live in glacier- or snowmelt-fed river basins (Kundzewicz et al., 2007). The snow cover is particularly susceptible to climate change impacts. A contraction of global snow cover has been observed (Lemke et al., 2007) which is expected to continue in the future (IPCC, 2007a). Snow pack decreases generally due to temperature rise, which causes less snow melt and consequently lower flood peaks in spring. Further, snow melt starts earlier within the year and leads to a temporal shift of the snow melt peak (Kundzewicz et al., 2007).

The representation of the snow melt peak in a hydrological model and the assessment of climate change impacts on the snow cover requires an optimal simulation of the snow related hydrological processes, i.e. snow accumulation and melt. In the original WaterGAP version (as applied by Lehner et al., 2006) an overestimation of the peak flow occurred in a number of snow affected river basins, due to the simplicity of the snow related hydrological processes represented in WaterGAP (Lehner et al., 2006; Schulze et al., 2005). Therefore it has been considered to revise the snow module for improving the representation of the snow melt peak in spring by WaterGAP.

Influence of lateral routing on flooding

The formation of floods is a complex combination of extreme precipitation or temperature rise (leading to snow melt) or a combination of both, the retention of the water in different storages and finally the flowing through the river networks. Therefore regions that are affected by floods are not necessarily concordant with the region in which the initiating effect occurred. A flood peak caused by extreme rainfall in the upstream part of a watershed, naturally reaches the downstream part of the watershed temporally delayed. The same effect applies for catchments with their headwaters in snow covered areas in which snow melt occurs. A number of effects influence the magnitude of the flood wave in the downstream area, such as retention in lakes and wetlands and the amount of water supplied by tributaries.

The lateral transport of water through the river network is a particularly important process for the routing of discharge. This applies for average flow conditions as well as for low or high flows. The flow velocity varies with the actual river discharge (Leopold and Maddock, 1953). Therefore it is meaningful to route the water within a hydrological model with a variable flow velocity.

Future changes in extreme precipitation and temperature

It is commonly agreed that all land regions will warm in the 21st century (IPCC, 2007a; Christensen et al., 2007). It is very likely that hot extremes, heat waves and heavy precipitation events will become more frequent during the 21st century as a consequence of the warming climate (IPCC, 2007a, p.46). Kundzewicz et al. (2007, p.202) points out that the impacts of changes in climate variability need to be integrated into impact modeling efforts. Global scale hydrological models are well suitable to be driven by the output of

General and Regional Circulation Models (GCMs, RCMs) on continental or global scale to assess the impact of climate change on hydrology. The most crucial climatic factor for flood formation is the representation of extreme rainfall. The expected changes in heavy precipitation are well studied (e.g. Sillmann and Roeckner, 2008; Beniston et al., 2007; Meehl et al., 2007) and according to the findings of the Intergovernmental Panel of Climate Change (IPCC) (IPCC, 2007b, p.8), it is very likely that the observed trend of increasing frequency of heavy precipitation events continues until the end of the 21st century. For Europe extreme precipitation is projected to increase in those regions that are relatively wet under present climate conditions such as middle and northern Europe (Sillmann and Roeckner, 2008; Beniston et al., 2007). An increase in the frequency of heavy precipitation is likely in many other regions of the world, such as North America, South East Asia or New Zealand (Christensen et al., 2007, p.859). However, this trend may be offset in areas of significant decrease in mean rainfall, such as Southern Australia or parts of the Mediterranean (Sillmann and Roeckner, 2008; Christensen et al., 2007).

1.3 Scope of the thesis

WaterGAP has been further developed within the scope of this thesis to comply with its central theme: The assessment of climate change effects on flood hazards worldwide.

The model should be suitable to define regions on large scale, in which considerable changes in floods might be expected based on different climate change scenarios. However, it is also important to look into the model to examine whether the flood related hydrological processes are represented well. Therefore representation of the snow dynamics as well as the river flow velocity within WaterGAP has been assessed in detail. This included the validation of the model results as well as the investigation of climate change impacts on snow cover and river flow velocity.

The following research questions have been identified under consideration of predefined flood related topics:

- How can the simulation of snow dynamics and the representation of snow melt induced peak flows be improved? How does climate change affect the snow cover of snow dominated regions of the world?
- How can the lateral transport of the water through the river network be improved? Does climate change affect the flow velocity of European rivers?
- How can floods be simulated on global scale and which climate change impacts on flood risks can be expected in Europe? Which impact has the method of deriving future climate time series on the flood calculations?

1.4 Thesis outline

The thesis is composed of six chapters, beside the general introduction and summary. The contents of Chapters 3 and 5 are based on already published papers, Chapters 4, 6 and 7 are in preparation for publication. Thus, each chapter forms a largely independent study with a corresponding introduction as well as a methodology description. Redundancies

between the chapters, such as descriptions of the WaterGAP model and forcing data are summarized in Chapter 2.

Chapter 2 provides an introduction to the global hydrological model WaterGAP, which has been applied for all hydrological simulations of this dissertation. Further, the most recent improvements of hydrological processes are summarized and the development of the new WaterGAP version, with enhanced spatial resolution, is described.

Chapters 3 and 4 focus on the snow cover. An improved method to simulate snow accumulation and melt is introduced in Chapter 3 as well as the validation of modeled snow cover and discharge in snow dominated catchments. Chapter 4 investigates the climate change effects on the snow cover of the Northern Hemisphere and in different mountain regions worldwide.

An approach to simulate variable flow velocity with WaterGAP is introduced in Chapter 5. The validation of the modeled flow velocity is presented in Chapter 6. This chapter further contains analyses related to the modeled flow velocity in European rivers of the present time and expected changes for three different scenarios.

Chapter 7 describes the application of WaterGAP to simulate floods on European scale. Further, expected changes in flood hazards until the 2050s for three different scenarios are presented. In addition, the impact of two different methods to derive climatic time series for the analyses of changes in flood frequencies have been compared.

Chapter 8 summarizes the results from the previous chapters and answers the research questions defined in Section 1.3. Furthermore, the main findings of this thesis are concluded and an outlook is given for further research.

Chapter 2

WaterGAP - Model History and Recent Developments

2.1 WaterGAP - Overview and Model History

The water model WaterGAP (**Water Global Assessment and Prognosis**) has been developed to simulate the distribution and availability of water on global scale. WaterGAP consists of two main components: a global hydrology model to simulate the continental water cycle (Section 2.4) and a global water use model (Section 2.6) to estimate water withdrawals and water consumption for agriculture, industry and domestic water use. WaterGAP can be applied to compute historical developments as well as future projections of different hydrological variables, water availability and water use.

WaterGAP has been developed since 1996 at the Center for Environmental Systems Research (CESR), located at the University of Kassel (Germany) and has been described in literature since the early years of this century (Alcamo et al., 2003a; Döll et al., 2003). The model has been further developed continuously during the last years. The model version WaterGAP2.1f (Hunger and Döll, 2008), which has been applied for simulations performed for this thesis (see Section 2.3), has been evolved in cooperation with the Institute of Physical Geography of the University of Frankfurt/Main.

WaterGAP calculates discharge on the river basin scale reliably and is well applicable for global assessments related to water security, food security and freshwater ecosystems (Döll et al., 2003). Kaspar (2004) performed a comprehensive sensitivity and uncertainty analysis, focusing on climate change impacts on long-term average discharge and low flow conditions. He found that all examined uncertainties are smaller than the differences obtained by using different climate models. Thus, WaterGAP is well applicable to study climate change effects on water availability on global scale. In addition to the hydrology model of WaterGAP, water use models for the sectors irrigation (Döll and Siebert, 2002), livestock (Alcamo et al., 2003a), domestic and industry (Flörke and Alcamo, 2004; Alcamo et al., 2003a) have been developed and further improved during the last years (see Section 2.6).

WaterGAP has been applied in a number of international projects such as the *Global Environmental Outlook 4* (GEO4) (Rothman et al., 2007), the *Millennium Ecosystem Assessment* (Alcamo et al., 2003b), the *European Outlook on Water Use* (Flörke and Alcamo, 2004) or at present within in the EU funded projects *SCENES* and *WATCH*. Within the

scope of these projects, WaterGAP has been applied on global or European scale to assess the current state and future scenarios of water availability, water demand and different water related indicators as for example water stress.

WaterGAP 2.1*x* (hereafter referred to as "WaterGAP2"), has been applied in all studies cited so far. WaterGAP2 has a spatial resolution of 0.5° globally. The model has been reengineered during the last few years and its spatial resolution has been increased to 5 arc-minutes (1/12°) globally, establishing the model version WaterGAP3.1 (hereafter referred to as "WaterGAP3").

2.2 Development of WaterGAP3

2.2.1 Background

In most studies carried out during the last years by the application of WaterGAP2, the current and future situation of average long term water availability and water use as well as related indicators have been investigated on the global or European scale. WaterGAP2 is well suitable for the application of those studies, as already mentioned above. During the last years, the fields of applications for global and continental scale models have been extended. They have been applied in studies about extreme discharges (Dankers and Feyen, 2008; Lehner et al., 2006) or for modeling water quality (Bouwman et al., 2005; Meybeck, 2003; Vörösmarty and Meybeck, 2004). Recent project goals and project partners in continental or sub-continental scale studies require a higher level of detail of the performed studies. By enhancing the spatial resolution of a hydrological model the locations of first, second and third order streams are represented more accurately. Further, all physiographic input information have a higher level of detail. This allows the development and application of new indicators and facilitates the usage or integration of project specific information from case study regions in the different WaterGAP sub models. As an example, regional information about the number of tourists can be used to improve the domestic water use calculations in the related region. Or detailed information about the types and size of wetlands is suitable to perform regional studies about (changes in) flood inundation frequencies. A global scale hydrological model with an enhanced spatial resolution is also well applicable to compare different regions worldwide consistently. Global scale studies can be performed as well. However, it should be deliberated on whether the advantage of the enhanced spatial resolution for a global scale study is worth the considerably increased time required for computing and data pre- and postprocessing.

The central theme of this PhD-work has been the development of a WaterGAP version that is suitable to study climate change effects on floods on large scale. The idea behind the development of a WaterGAP version with an enhanced spatial resolution for this purpose is that it (i) improves the representation of the river lengths through an enhanced river network and the usage of an individual meandering information per grid cell (see Table 6.1 and Section 6.2.1) and (ii) it leads to a higher level of detail of the static input maps and therefore allows an improved representation of the vertical and lateral hydrological processes. This has been achieved by developing WaterGAP3, which has a spatial resolution of 5 arc minutes, which is a 36-fold increase in spatial resolution compared to WaterGAP2.

At CESR different global scale water models are (further) developed. In addition to the

above mentioned WaterGAP hydrology and water use models, the global water quality model WorldQual is currently designed. All water models provide output at a spatial resolution of 5 arc-minutes and have a consistent land-sea mask. This allows an easy soft-linking of the models as is shown in Figure 2.1.

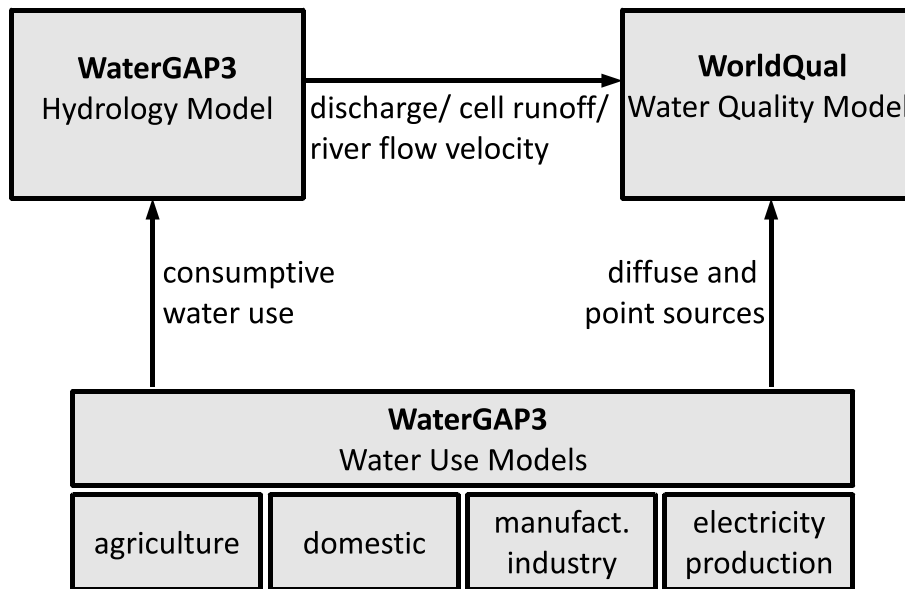


Figure 2.1— Soft-linking between the three global scale water models that are developed at CESR

2.2.2 Technical Realization of WaterGAP3

During the last years the quality of datasets, which can serve as input for WaterGAP, has improved significantly. This comes along with an enhanced spatial resolution compared to the datasets available in the early 1990s, when the development of WaterGAP begun. The main datasets used to derive WaterGAPs input maps (e.g. climate, soil properties, topography), are available in high spatial resolution (see Table 2.2), allowing the preparation of the required input maps for WaterGAP3. This improves the representation of different physiographic parameters compared to the spatial resolution of 0.5° (Figure 2.2 (top)).

However, the crucial factor for the WaterGAP3 development was the availability of a drainage direction map in 5 arc-minutes spatial resolution (DDM5) to route the water through the river network as described in Sections 2.4.2 and 6.2.4. A DDM5 covering the whole globe has been developed as part of the HydroSHEDS dataset¹(Lehner et al., 2008), which is based on elevation data of the Shuttle Radar Topography Mission (SRTM, Farr et al., 2007). The DDM5 pictures the river system more realistically than the DDM30 (Figure 2.2, bottom).

The increased spatial resolution of WaterGAP3 consequently produces model output

¹The DDM5 has been developed in cooperation with Bernhard Lehner from the WWF, Washington DC, USA (by now McGill University, Montreal)

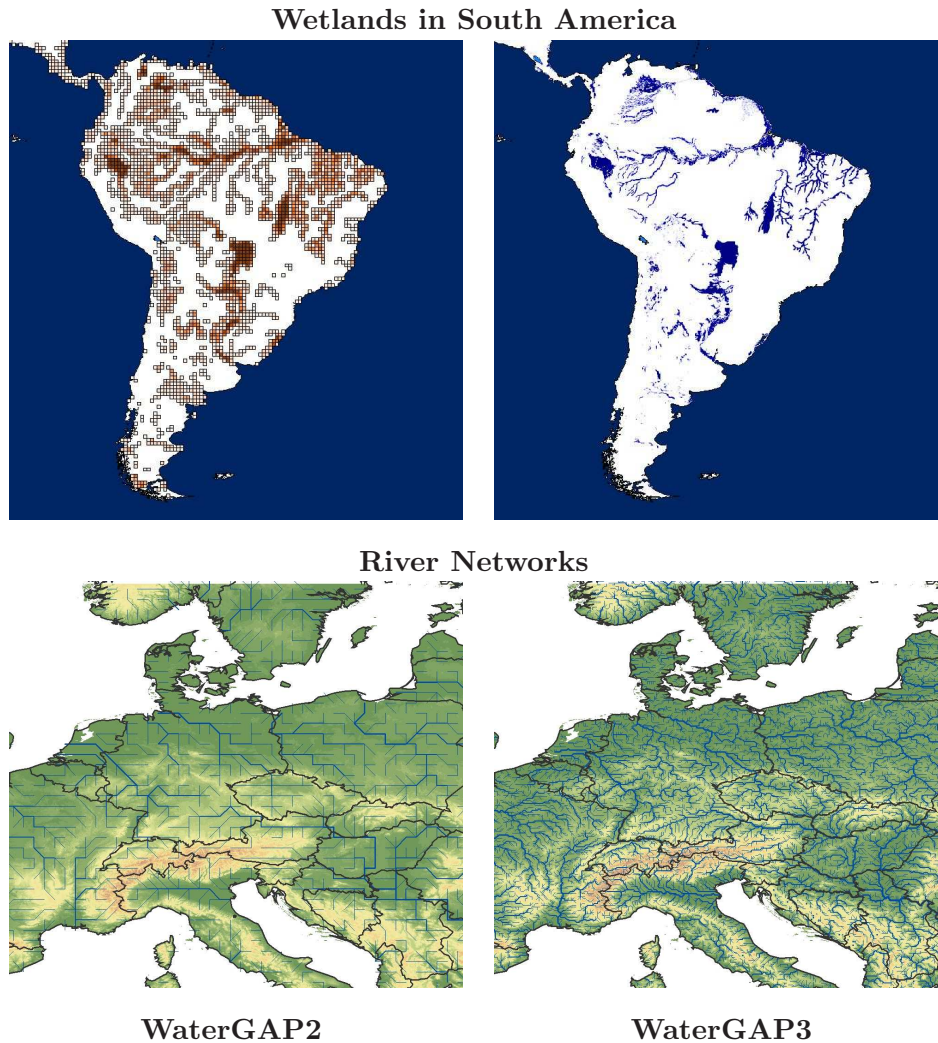


Figure 2.2— Wetland distribution in South America (top) and the river networks (bottom), each for WaterGAP2 and WaterGAP3.

with a higher level of detail. Figure 2.3 shows exemplarily the snow cover (top) and the river availability (bottom) in Central Europe of two arbitrary chosen months. The WaterGAP3 snow cover shows a more detailed snow cover distribution in the Alps and also depicts snow in low mountains more clearly than the WaterGAP2 snow cover. The WaterGAP3 river discharge is also pictured more precisely, due to the high resolution river network.

Beside the availability of improved datasets, the computing power and memory capacities of present-day computers have enhanced exponentially during the last decade. This allows the computation of global terrestrial hydrology on a 5 arc-minute grid. The single continents are computed separately for different technical reasons. First, the file sizes of output files that are required for post-processing work are considerably smaller and consequently easier to handle than files, covering the whole globe. Second, the calibration process requires a considerable amount of time during model development process and a

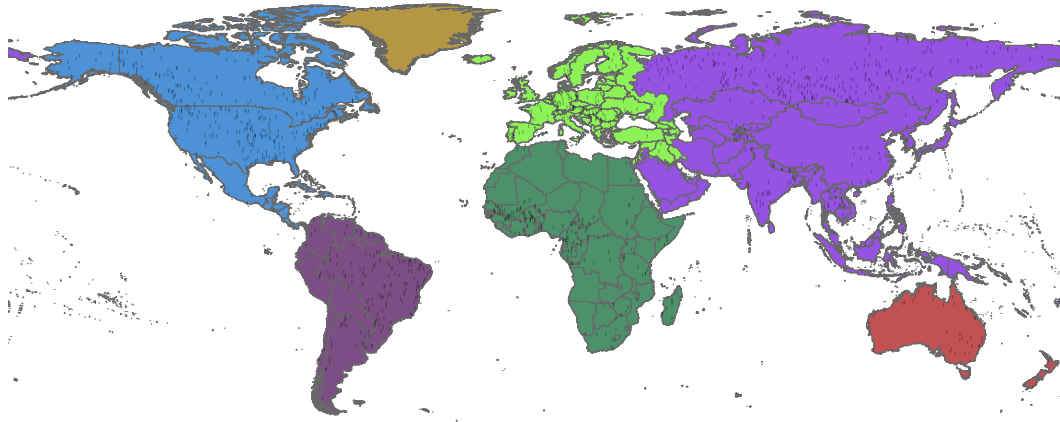


Figure 2.4— Division of continents within WaterGAP3 and the location of calibration stations (state January 2009).

processes, without any need for communication. The WaterGAP program, written in C++, has been parallelized by using the Message Passing Interface MPI-2 Snir et al. (1996). MPI-2 is most appropriate for distributed-memory architectures (Leopold et al., 2006) such as the Linux cluster of the University of Kassel, which is mainly used to run WaterGAP3. The watersheds are distributed among the different processes by the standard master/slave structure. Here the master process coordinates the distribution of the watersheds to the slaves, which compute the water balance of the single watersheds as described in Section 2.4.

2.3 Model versions applied in this thesis

WaterGAP3 has been developed within the period of this PhD-work. Therefore it has been applied for the more recently performed investigations about current state and climate change impacts on river flow velocity (Chapter 5) and simulations about current and future floods as described in Chapter 7 of this thesis.

WaterGAP2 has been applied to develop the improved snow algorithm (Chapter 3) and to perform investigations about recent and future snow cover in different climatic regions of the world (Chapter 4), because these analyses have been performed at an earlier stage of the PhD-work. For the same reason, first investigations related to the variable flow velocity (Chapter 5) have also been based on WaterGAP2.

2.4 Simulation of Hydrological Processes within WaterGAP

The major vertical and lateral hydrological processes of both WaterGAP2 and WaterGAP3 are computed on a daily time step for each individual grid cell as shown schematically in Figure 2.5. The hydrological processes are summarized in Sections 2.4.1 and 2.4.2. These model descriptions refer to both, WaterGAP2 and WaterGAP3. Differences between the

two WaterGAP versions are explicitly pointed out. Kaspar (2004) and Döll et al. (2003) describe the simulation of the different hydrological processes within WaterGAP in detail.

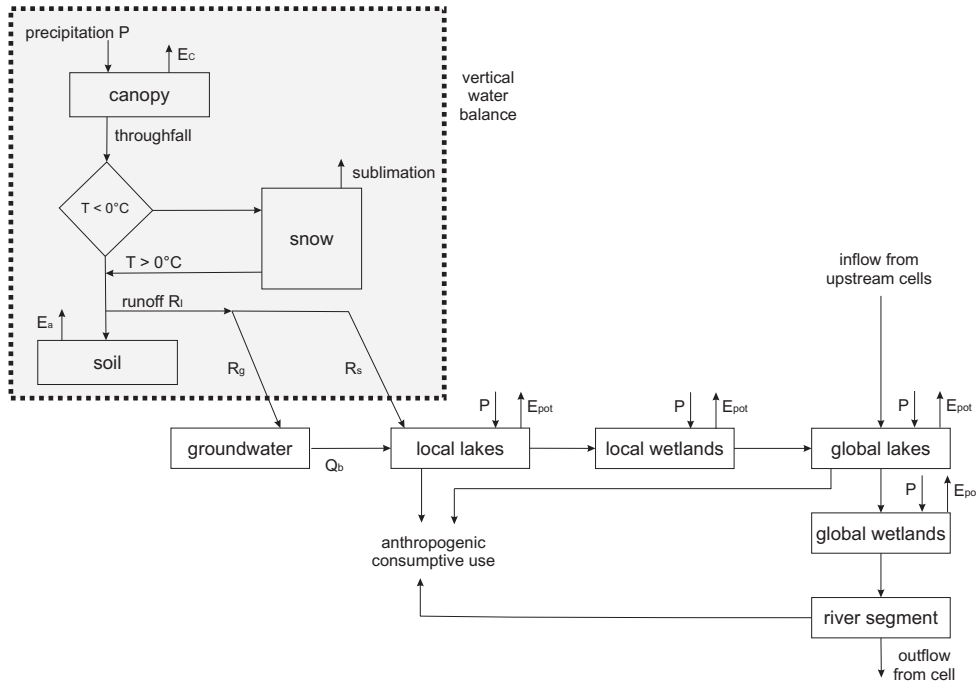


Figure 2.5— Schematic representation of the vertical and lateral water balance considered in WaterGAP, including human water use. E_{pot} : potential evaporation, E_a : actual evaporation, E_c : evaporation from the canopy, R_l : runoff from land, R_g : groundwater recharge, R_s : surface runoff. (after Döll et al. (2003), modified)

2.4.1 Vertical Hydrological Processes

WaterGAP calculates daily vertical water balances for the land areas and for the open water bodies of the individual grid cells. The proportion of open water area per grid cell has been derived from the Global Lakes and Wetlands Dataset (GLWD) (Lehner and Döll, 2004). The vertical water balance of land areas is described by a canopy water balance (representing interception) and a soil water balance. The canopy water balance determines which part of the precipitation is intercepted by the canopy and evaporates, and which part reaches the soil. If temperature falls below 0°C , precipitation is stored as snow. The snow related processes are calculated by a simple degree-day algorithm, which is described in detail in Section 3.2. The total runoff from land area is divided into surface runoff and ground water recharge, using information on cell-specific slope characteristics, soil texture, hydro-geology, and the presence of permafrost and glaciers (Döll and Flörke, 2005). The water balance for the freshwater areas of the individual grid cells determines runoff from open water bodies from the difference between precipitation and evaporation. Evaporation from lakes, reservoirs and wetlands is assumed to equal potential evaporation.

2.4.2 Lateral Hydrological Processes

The total simulated runoff of a grid cell is composed of the runoff from land and from open freshwater bodies. The runoff produced inside one cell and the simulated inflow from upstream cells is transported through a series of storages representing groundwater, lakes and reservoirs, wetlands, and rivers. The grid cell specific consumptive water use of the different sectors described below, can optionally be taken out of the related grid cell. Finally, the resulting cell outflow is routed along the drainage direction map to the next downstream cell. The optimized routing algorithm and the calculation of the dynamic flow velocity, applied in WaterGAP3, are described in Chapter 5.

2.4.3 Recent Developments

As already mentioned, comprehensive descriptions of the representation of vertical and lateral processes within WaterGAP can be found in Döll et al. (2003) and even more detailed in Kaspar (2004). However, these descriptions refer to WaterGAP 2.1d and the model has been further developed since then, i.e. a number of processes have been improved. A few developments have been included into both model versions (WaterGAP2.1f and WaterGAP3) and some were implemented into WaterGAP3 only. The main differences between the hydrological processes within WaterGAP2 and WaterGAP3 are listed in Table 2.1. If not other mentioned, the descriptions of the processes in the following apply for both, WaterGAP 2 and WaterGAP3.

Table 2.1— Differences between WaterGAP 2.1f and WaterGAP 3.1 features

features	WaterGAP2	WaterGAP3
spatial resolution	0.5°	5 arc minutes
temporal resolution	forcing data	
	monthly	daily or monthly
input data	drainage direction map	
	DDM30	DDM5
	digital elevation map	
	GTOPO30	SRTM30
evapo-(transpi)ration	canopy evaporation (max LAI)	
	based on land cover specific leaf mass	based on literature values for different land cover types
	potential evapotranspiration (α-coefficient for Prestley-Taylor-function)	
	distinction between arid and humid areas	based on Köppen climate zones
lateral processes	river flow velocity	
	constant	variable

Snow Accumulation and Melt

An improved snow modeling routine has been implemented into WaterGAP, which has been developed within the scope of this PhD-work (see Chapter 3). The snow dynam-

ics are modeled on sub-grid scale, which improved the representation of the snow cover within a grid cell as well as the snow melt in spring. The approach has initially been integrated into WaterGAP2 and the snow related studies have been performed with this WaterGAP version (see Chapters 3 and 4). The new snow modeling routine has later been implemented into WaterGAP3 as well.

Evapotranspiration

The approach to estimate the α -factor, which is needed to calculate the potential evapotranspiration with the Priestley-Taylor equation, has considerably been improved by Weiß et al. (2009). In WaterGAP2 versions, two α -coefficients have been distinguished only, based on either humid or arid areas of the world. An individual α -coefficient for each Köppen-climate zone has been defined within the new approach, which has been implemented into WaterGAP3.

Hunger and Döll (2008) optimized the simulation of evaporation from lakes and wetlands by making evaporation a function of the water level (water storage), which reflects the dependence of surface area, from which evaporation occurs, on the amount of stored water. They further calibrated WaterGAP2.1f against data of additional discharge observation stations and found that the usage of additional discharge information improves model results, especially in arid and semi arid regions.

Leaf Area Index (LAI)

Further the method to estimate the maximum leaf area index has been improved. In WaterGAP2, the maximum leaf area index has been derived from the land cover type and the leaf mass (see Kaspar (2004, p.13) for a detailed description). Within the scope of the WaterGAP3 development, LAI values from literature (Schulze et al., 1994) were applied to parametrize the maximum LAI per land cover type and to model the daily LAI as a function of daily climate. Maximum LAI is highest during the growing season. The growing season starts within WaterGAP2, when temperature is above 5°C and the monthly precipitation is more than half the monthly potential evapotranspiration. In WaterGAP3 however, the temperature has to be above 8°C and the precipitation sum has to exceed 40mm until the plants start growing.

River Flow Velocity

Within the scope of this PhD-work, a variable flow velocity algorithm has been implemented into WaterGAP3 (see Section 6), which calculates the river flow velocity dynamically as a function of actual discharge, river bed roughness and river slope.

2.5 Model Input and Driving Forces

2.5.1 Static Input Maps

A number of static input maps are required to parametrize the hydrological processes within WaterGAP. The static input maps and its data sources are summarized in Table 2.2. A comprehensive overview about the usage of the dataset within WaterGAP are given in Kaspar (2004). Further information can be found in the descriptions of single hydrological processes ((e.g. Verzano and Menzel, 2009; Verzano et al., 2009; Hunger and Döll, 2008; Döll and Flörke, 2005; Döll et al., 2003)) as well as in Chapters 3, 4 and 6.

2.5.2 Climate Time Series - Historic Simulations

For historic WaterGAP2 simulations, the CRU TS 2.1 (Mitchell and Jones, 2005) dataset is applied. A combination of the datasets CRU TS 2.1 and CRU TS 1.2 (Mitchell et al., 2004) is used to drive WaterGAP3. The CRU TS 1.2 dataset has a spatial resolution of 10 arc-minutes. However this dataset covers Europe only. Therefore, the higher resolved CRU TS 1.2 dataset is used in the covered grid cells, whereas in all other regions CRU TS 2.1 is applied. For the usage in WaterGAP3, both climate datasets have simply been disaggregated to a spatial resolution of 5 arc minutes.

Both CRU datasets provide monthly values for precipitation, temperature, cloud cover and the number of wet days per month, but WaterGAP requires daily climate input. Therefore, temperature and cloudiness are downscaled by a cubic-spline-function between the monthly averages, which are assigned to the middle of each month. Precipitation is first distributed equally over the number of wet days per month. Then, the number of wet days is allocated over each month by applying a Markov Chain. The calculation of pseudo-daily input from monthly climate is described in detail by Kaspar (2004).

2.5.3 Climate Time Series - Future Projections

WaterGAP simulations of future projections (scenarios) are usually driven by the respective scenario of temperature (T) and precipitation (P), calculated by General Circulation Models (GCM) or other climate models. Other variables, such as the number of rain days or cloud cover, are taken from the historic reference period.

For most climate change studies performed with WaterGAP, T and P of the scenario period has been provided as 30-year average monthly values for both the reference period (usually 1961-1990) and the scenario period (e.g. 2050s (2040-2069) or 2080s (2070-2099)). There is always a bias between the simulated GCM data of the reference period and the observed climate (i.e. the CRU dataset). This inconsistency needs to be considered when assessing changes between the reference period and scenarios. Therefore, a delta change method has been applied, which scales the scenario data in consideration of the difference between observed and simulated climate of the reference period (Henrichs and Kaspar, 2001; Lehner et al., 2006). The delta-change method adds the 30-year monthly differences for temperature (Eq. 2.1) or ratios for precipitation (Eq. 2.2) of the GCM data to each month of the CRU dataset for the reference period (1961-1990). An exception to this rule occurs when present-day precipitation is close to zero ($< 1\text{mm}$). In this case the respective

Table 2.2— Data sources for static input maps used in WaterGAP 2.1f and WaterGAP 3

Name	Content	Source	spatial resolution	WaterGAP versions
Global Lake and Wetland Database (GLWD)	location and size of lakes, reservoirs and wetlands worldwide	Lehner and Döll (2004)	30 arcseconds and polygons	2.1f and 3.1
FAO Soil Map of the World	digital soil map and derived soil properties	FAO (2003)	5 arcminutes	2.1f and 3.1
HydroSheds	river network and drainage direction map	Lehner et al. (2008)	from 3 arcseconds to 5 arcminutes	3.1
DDM30	river network and drainage direction map	Döll and Lehner (2002)	0.5°(30 arcminutes)	2.1f
Glacier	World Glacier Inventory	NSIDC (1999, updated 2007)	-	2.1f and 3.1
Permafrost	Circum-Arctic Map of Permafrost and Ground-Ice Conditions	Brown et al. (1998)	- (polygon)	2.1f and 3.1
LAI	Worldwide historical estimates of Leaf Area Index	Scurlock et al. (2001)	-	3.1
Soil water storage	soil water retention properties	Batjes (1996)	-	2.1f and 3.1
Corine Land Cover (CLC)	Land Cover	EEA (2004)	1 km (Europe only)	3.1
Global Land Cover Characterization (GLCC)	Land Cover	USGS (2008)	1 km	3.1
IMAGE2.2 Land Cover	Land Cover	Alcamo et al. (1998)	0.5°	2.1f
GTOPO30	Global Digital Elevation	USGS (2006)	30 arcseconds	2.1f
SRTM30	Global Digital Elevation	Farr et al. (2007)	30 arcseconds	3.1

precipitation rise is added.

$$T_{scaled_future} = T_{CRU,reference} + (T_{meanGCM,future} - T_{meanGCM,reference}) \quad (2.1)$$

$$P_{scaled_future} = P_{CRU,reference} \cdot (P_{meanGCM,future} / P_{meanGCM,reference}) \quad (2.2)$$

with:

T : average monthly temperature [°C]

P : average monthly precipitation [mm]

$scaled_future$: monthly value in 30-year time series representing scenario climate

$CRU,reference$: monthly value in observed 30-year time series (1961-1990)

$meanGCM,future$: monthly average of future climate as computed by GCM

$meanGCM,reference$: monthly average of reference period climate (1961-1990) as computed by the GCM

Following this method, 30-year monthly time series of temperature and precipitation can be constructed for the scenario period. With this procedure, data describing the long-term average future trend in climate were combined with data describing current climate variability.

Alternatively, the direct GCMs model output, aggregated to daily or monthly values, can be used to force the future simulations of WaterGAP. This method is applied for the simulation of future floods (Chapter 7).

2.6 Water Use

Anthropogenic water use affects the hydrological system and the water extraction from the river system can optionally be considered by the Hydrology Model of WaterGAP (see Figures 2.1 and 2.5).

Four (WaterGAP2) or five (WaterGAP3) different water use submodels of WaterGAP compute water withdrawal from the hydrological system as well as consumptive water use. Water withdrawal is the amount of water that is taken from the terrestrial water cycle to meet the demands of the respective water use sector. Consumptive water use is defined as water that has been withdrawn and which mainly evaporates during its use, i.e. it is lost for the terrestrial water system. The remaining water returns back to the river system as the so called return flow. The different water use sectors are summarized below:

- Irrigation:

Water that is used for irrigation is computed on a monthly time scale for the grid cells covering an area, which is assumed to be equipped for irrigation (Siebert et al., 2005), as well as in dependency of meteorological conditions. In the WaterGAP versions used for this PhD thesis, rice and non-rice crops are distinguished. More information about the irrigation water model can be found in Döll and Siebert (2002).

- Livestock:

The livestock submodel computes water demand for ten different varieties of livestock

for each grid cell worldwide on an annual time scale by multiplying the number of livestock per grid cell by their water consumption per head and year. Water withdrawal for livestock is assumed to equal consumptive water use.

- Domestic:

This model computes water demand for households and small manufacturing industries on a yearly time scale. First, the domestic water use intensity [$\text{m}^3/\text{cap-year}$] is calculated for each country worldwide. Then this value is multiplied with the total population per country. Based on a population density map, the country values are allocated to the individual grid cells (Alcamo et al., 2003a).

- Industry(WaterGAP2):

The WaterGAP2 version used for this thesis calculates industrial water use for the sectors manufacturing industry and electricity production as described in Alcamo et al. (2003a).

- Industry (WaterGAP3):

WaterGAP3 applies an improved model version for industrial water demand. The original industrial water use model has been split into two models computing water demand for manufacturing industry and electricity production (see below).

- Manufacturing Industry:

This sub-model computes water withdrawal and consumption of six manufacturing sectors to assess the great diversity of industrial processes (Flörke and Alcamo, 2004).

- Electricity Production:

This model calculates the water requirements for thermal power plants. Tower cooled and once-through-cooled power plants are distinguished (Flörke and Alcamo, 2004).

Chapter 3

A New Approach to Simulate Snow Accumulation and Melt within WaterGAP ¹

3.1 Introduction

The storage of precipitation as snow is a crucial process within the hydrological cycle. Snow melt in spring induces drastically increased river discharge or even floods in snow affected watersheds. Since the 1960s a decrease of the Northern Hemisphere snow cover of roughly 10% has been observed (IPCC, 2001, p.123), caused by climate change.

The physical processes in the snow cover are complex and have been studied in detail in numerous local and regional scale studies (see examples in Marsh, 1999). Especially in high mountains the characteristics and magnitude of the snow cover varies on small scale, caused by the heterogeneous topography and related microclimate. Complex small scale snow hydrological models are required to simulate the snow processes in such areas. However, detailed and data demanding approaches to simulate snow dynamics or runoff processes in mountains can not be incorporated into large scale hydrological models. Thus, ways have to be found to model snow dynamics and discharge with robust and simple approaches, which require only few data but which are able to reproduce hydrological processes best possible. The feasibility of modeling reliable snow dynamics with a conceptual approach has been proven by numerous applications of the conceptual HBV-model (Bergström, 1992) in snow affected regions. The most important dynamical variables in conceptual snow modeling routines are precipitation and temperature. These climatic standard parameters are available in historical and recent climatic datasets based on measurements and are calculated by General Circulation Models (GCMs), which is essential for the simulation of future scenarios.

In WaterGAP 2.1e and earlier versions, snow cover is assumed to be homogeneous within a 0.5° grid cell. This frequently leads to an underestimation of discharge during winter

¹based on K. Verzano (published as K. Schulze) and P. Döll (2004): Neue Ansätze zur Modellierung von Schneeakkumulation und -schmelze im globalen Wassermmodell WaterGAP, in: Neue methodische Ansätze zur Modellierung der Wasser- und Stoffumsätze in großen Einzugsgebieten. (ed. by Ludwig, R., Reichert, D. and Mauser, W.), Proceedings of the 7th "Workshop zur großskaligen Modellierung in der Hydrologie", Munich, Germany, November 2003, pp. 145-154, Kassel University Press, Kassel, Germany.

months and an overestimation of the discharge peaks due to snow melt in spring, especially in mountain regions. This effect occurs, because the mean temperature of a 0.5° grid cell is often below the threshold temperature during winter and consequently all precipitation is stored as snow. In reality however, the lower parts of an area covered by a 0.5° grid square might have temperatures above the melting point already and snow starts melting from low to high altitudes. During spring, when the mean temperature of an individual cell rises above 0°C , the model assumes that all stored snow melts simultaneously, which leads to an overestimation of the related discharge peaks.

The snow algorithm of WaterGAP has been reworked to improve the simulation of the snow cover and the snow melt induced flood peak in spring, which is explained in detail in Section 3.2. The improved snow algorithm has been validated at gauging stations of 50 snow dominated watersheds of the Northern Hemisphere (Section 3.3.1). Further, WaterGAPs ability to simulate the spatial extent of the Northern Hemisphere snow cover is verified by comparing model results to satellite derived data (Section 3.3.2).

3.2 Methodology

3.2.1 Snow Modelling Within the WaterGAP Model

Sub Scale Modelling

Snow cover can be very heterogeneous on local scale, especially in mountainous regions. This cannot be incorporated by homogeneous snow cover on a 0.5° grid cell. In mountains, each grid cell covers a comparably wide range of altitudes. Due to the adiabatic lapse rate, snow can be found in high altitudes, whereas there is less or no snow in lower elevations at the same time. To improve the representation of the snow cover within a 0.5° grid cell, each grid cell is divided into 100 sub-grid squares. Based on the digital elevation dataset GTOPO30 (U.S. Geological Survey, 2003), each sub-grid square is assigned its individual elevation. The temperature for each sub-grid square is calculated based on the mean temperature of the 0.5° grid cell and the application of a constant adiabatic lapse rate of $-0.6\text{ K}/100\text{ m}$ (Semádeni-Davies, 1997; Dunn and Colohan, 1999). Snow accumulation and melt are then calculated for each individual sub-grid square on a daily time step as described in the following section. Finally, the 100 individual snow cover and snow melt values are aggregated to single values for the respective 0.5° cell.

Figure 3.1 presents the altitude dependent distribution of Snow Water Equivalent (SWE) and temperature on January 30, 1990 for an exemplary grid cell, located in the European Alps. The 100 sub-grids are ranked according to their individual altitude (370 - 2351 m).

Snow Accumulation and Melt

Snow accumulation and snow melt is modeled within WaterGAP by using a simple temperature-index-approach (Eq. 3.1). Snow accumulates when the air temperature drops below the threshold value of 0°C . For temperatures below the threshold snow storage is reduced by sublimation only (Kaspar, 2004). Snow starts melting if the air temperature exceeds 0°C (T_{melt}). The melting rate is expressed by the land cover dependent degree-day factor C_{melt} : melt rates under closed canopies are assumed to be smaller

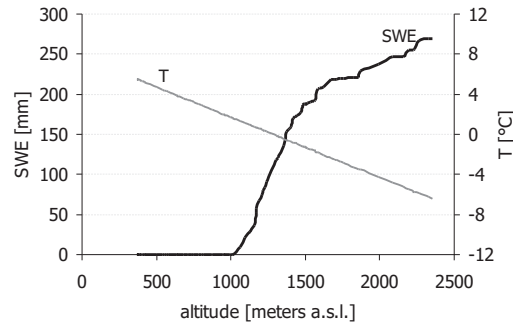


Figure 3.1— Example for the altitude dependent, subscale distribution of temperature T and SWE within one 0.5° grid cell. T is linearly distributed over the individual elevation intervals.

($2\text{mm} \cdot ^\circ\text{C}^{-1} \cdot \text{day}^{-1}$) than over open land ($4\text{mm} \cdot ^\circ\text{C}^{-1} \cdot \text{day}^{-1}$). This is in accordance with values applied by Semádeni-Davies (1997) and SMHI (1996). The snow melt rate increases with increasing actual air temperature T_{act} .

$$\text{snowmelt} = C_{melt} \cdot (T_{act} - T_{melt})[\text{mm}] \quad (3.1)$$

Other energy fluxes, like energy transport from soil or rain into the snow cover are not considered. This would require an extensive number of data, which are not available on global scale. Thus, if rain falls on an existing snow cover, the model forces the water to percolate through the snow into the soil while no additional snow melt occurs.

3.2.2 Investigated River Basins

It is difficult to find data which can be used to validate the modeled SWE of continental or global scale hydrological models. A large number of SWE point measurements exist, but these data cannot be used to validate the spatially averaged snow cover of a 0.5° grid cell. Thus, discharge hydrographs of snow influenced watersheds are used, since they imply the modelled goodness of snow simulation. To validate the effect of the sub grid implementation, gauging stations of 50 snow dominated watersheds have been selected for further investigations (see Figure 3.4 and Table 3.1). The drainage area of the selected gauges ranges from 10.7 to $1589 \cdot 10^3 \text{ km}^2$. The selected catchments are located throughout the Northern Hemisphere and represent a variety of different topographical characteristics. A few watersheds are located in comparably plain regions, such as the Pechora watershed in western Russia, others are catchments in high mountains (e.g. the Rhone catchment in the Swiss and French Alps).

Table 3.1— Characteristics and MMEs of the 50 watersheds that were selected for this study

Nr.	River	Station	Country	Area [10 ³ km ²]	data years	MME without sub grids	MME with sub grids
1	Yongding	Guanting	China	42.6	30	-3.4	-3.4
2	Luanhe	Luanxian	China	46.5	30	0.6	0.6
3	Jinghe	Zhang- jiashan	China	42.6	30	0.4	0.39
4	Yellow River	Sanmenxia	China	681	30	0.49	0.49
5	Chindwin	Hkamti	Burma	27.6	11	0.77	0.77
6	Bheri River	Jamu	Nepal	13.5	17	0.72	0.74
7	Arun River	Turkeghat	Nepal	27.2	11	-0.16	-0.39
8	Ishikari	Ishikari- Ohashi	Japan	13.4	27	0.52	0.6
9	Selenga	Chutic	Mongolia	89.8	9	-0.57	-0.54
10	Orkhon	Orkhon	Mongolia	39.8	9	0.31	0.3
11	Brahmaputra	Pandu	India	411	8	0.49	0.48
12	Amnokgang	Kumchang	N.- Korea	18.7	9	0.15	0.13
13	Anadyr	Novy Eropol	Russia	45.9	20	0.8	0.82
14	Vitim	Bodaibo	Russia	186	20	0.77	0.78
15	Indigirka	Vorontsovo	Russia	30.8	27	0.86	0.87
16	Olenek	8km upstr. of mouth of Pur river	Russia	178	11	0.8	0.8
17	Kuskokwim	Crooked Creek.	USA	82.6	20	0.48	0.5
18	Yukon	Kaltag	USA	756	8	0.72	0.66
19	Columbia	The Dalles	USA	618	30	0.1	0.29
20	Snake River	Clarkston	USA	268	29	0.2	0.46
21	Humboldt	Imlay	USA	42.3	20	-0.5	-0.22
22	Missouri	Culbertson	USA	239	19	-0.79	-0.78
23	Colorado	Lees Ferry	USA	288	30	-0.43	-0.12
24	Green	Green River	USA	108	20	0.37	0.37
25	Yukon	Dawson	Canada	260	15	0.89	0.87
26	Mackenzie	Norman Wells	Canada	1,589	14	0.79	0.78
27	Liard River	Lower Crossing	Canada	104	23	0.11	0.38

continued on next page

<i>continued from previous page</i>							
Nr.	River	Station	Country	Area [10 ³ km ²]	data years	MME without sub grids	MME with sub grids
28	Liard River	Fort Liard	Canada	224	16	0.52	0.66
29	Slave River	Fitzgerald	Canada	598	25	0.62	0.7
30	N. Saskatchewan	Prince Albert	Canada	133	30	-0.12	0.14
31	Saskatchewan	The Pas	Canada	351	18	-0.39	-0.09
32	Kazan River	above Kazan Falls	Canada	71.4	16	-0.39	-0.39
33	Columbia	Intern. boundary	Canada	158	30	-0.65	-0.19
34	Rhone	Beaucaire	France	99.5	30	0.36	0.37
35	Rhone	La Murlatiere	France	48.8	30	0.41	0.46
36	Segre	Seros	Spain	13.8	30	-1.34	-1.2
37	Vaenern-Goeta	Vaenersborg	Sweden	47.1	30	0.48	0.48
38	Po	Piacenta	Italy	39.3	30	0.56	0.62
39	Po	Pontelagoscuro	Italy	74.0	30	0.29	0.42
40	Adige	Boara Pisani	Italy	12.8	29	-2.12	-1.06
41	Tana	Polmak	Norway	14.2	30	0.82	0.82
42	Gloma	Langnes	Norway	41.6	30	0.67	0.73
43	Siret	Lungoci	Romania	36.0	21	0.6	0.64
44	Oulujoki	near the mouth	Finland	25.3	30	0.13	0.13
45	Kenijoki	near the mouth	Finland	54.1	30	0.76	0.76
46	Vuoksi	Tainionkoski	Finland	62.6	30	0.14	0.13
47	Aare	Untersigenthal	Swiss	19.0	30	-0.11	0.44
48	Rhone	Chancy	Swiss	10.7	18	-1.62	-0.2
49	Northern Dvina	Ust-Pinega	Russia	353	27	0.77	0.77
50	Pechora	Ust-Tsilma	Russia	250	30	0.88	0.87

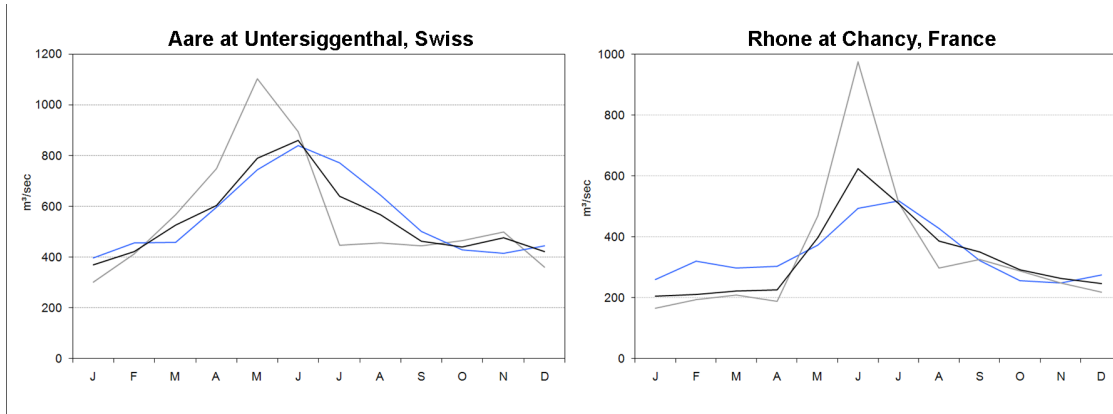


Figure 3.2— Long term average monthly discharge of the Aare at Untersiggenthal (1961-1990) and the Rhone at Chancy (1961-1978). The figure compares the measured discharge (blue line) with WaterGAP simulated discharge before (gray line) and after (black line) the implementation of the new snow routine.

3.3 Results

3.3.1 Simulation of discharge hydrographs

We compared long-term average monthly discharge modeled by WaterGAP to respective measurements of the 50 selected watersheds (GRDC, 1999) before and after implementing the new snow modeling routine (Table 3.1). Due to the simulation of snow dynamics on sub-grid scale, the snow melt induced discharge peaks are generally lower than in earlier WaterGAP versions, especially in mountainous regions. The snow in lower altitudes starts melting earlier than in high elevated sub grids. In the original snow routine, the snow of the whole grid cells starts melting, once the melting temperature is exceeded. This causes an overestimation of the snow melt peak in spring. The new snow routine leads to higher discharge levels during the summer months, because snow melt continues on sub grids with high elevations, so that the hydrographs are more balanced. Figure 3.2 shows the results of two watersheds, representing the typical effect of the sub grid implementation. The Monthly Modelling Efficiency (MME, synonymical to Nash-Sutcliffe Coefficient) has been enhanced in both examples due to the improved representation of the discharge peak in spring. At the Aare at Untersiggenthal (Swiss), the MME increased from -0.12 to 0.52 and the MME of the Rhone at Chancy (France) has been improved from -1.62 (original snow routine) to 0.12 (new snow routine).

The MME varies strongly between the 50 selected river basins (Figure 3.3 and Table 3.1). In 36% of the 50 gauging stations a good MME larger than 0.6 is achieved after model improvement. But still about one third of the studied catchments have a unsatisfying MME below 0.2. Low Nash-Sutcliffe-Coefficients are mainly caused by the overestimation of discharge peaks in spring by WaterGAP, even after the implementation of the sub grids. This large gap between data and model typically in one or two months per year reduces the MME significantly and occurs mainly in high mountainous regions such as the Rocky Mountains (e.g. Columbia and Colorado sub catchments) or inner Alps (Adige and Rhone) (see Figure 3.4, top). Still, the number of catchments with low MMEs has decreased and more gauging stations show comparably high MME values. The average

MME of the 50 gauging stations increased from 0.13 to 0.25 (Figure 3.3). The results improved even more to an average MME of 0.31 after calibrating WaterGAP with the new snow routine implemented (WaterGAP2).

The model results have improved in 24 of 50 investigated watersheds, due to the new snow

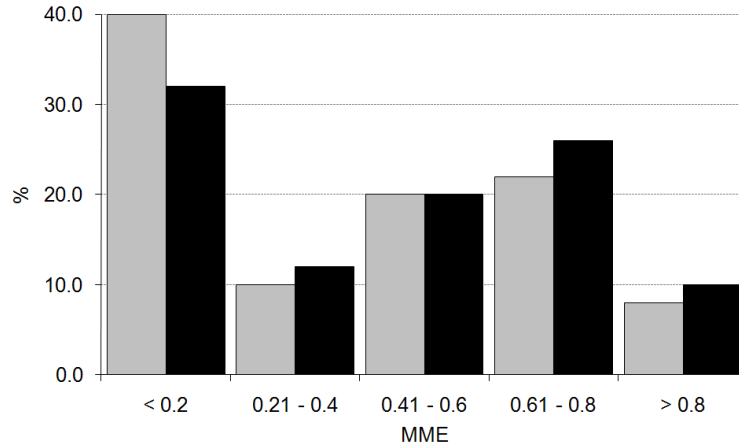


Figure 3.3— MME of 50 river basins before (grey) and after (black) implementation of sub grids into the snow routine.

modeling routine. The most significant improvements occur in mountainous areas worldwide, especially in the Alps and large parts of the Rocky Mountains (figure 3.4, bottom). These are discharge regimes of catchments with high relief energy, which are particularly affected by the sub-grid variability. The MME of four catchments has decreased. The most significant negative effect can be found in the Arun river basin in the Himalaya (Δ MME -0.23). Here, the spring discharge peak has already been underestimated in earlier WaterGAP versions and is underestimated even more after the implementation of the sub-grids. The hydrological regime of the Arun River is strongly influenced by glaciers, which is not considered by WaterGAP. For catchments with small relief energy, the implementation of sub grid variability shows only a minor effect on simulated hydrographs (MME \pm 0.01).

3.3.2 Northern Hemisphere Snow Cover

The application of satellite derived data is a well established method to monitor and investigate global snow cover. The International Satellite Land Surface Climatology Project (ISLSCP) Initiative 2 dataset (Armstrong et al., 2003) provides monthly Northern Hemisphere snow cover in 0.5° spatial resolution for 1986-1995. This dataset is well suitable to validate snow cover modeled by WaterGAP, due to the consistent spatial resolution. The ISLSCP dataset is comprised from weekly snow observations. A grid cell is defined as snow covered for one week, if 50 percent or more of the grid cell is observed to be snow covered at the last day of the respective week on which the observer could see the land surface, i.e. no clouds obstruct the view. The dataset provides no information, which day of the week is used to map the snow cover for the respective cell. Therefore we were not able to use exactly the same definition to derive snow cover maps from WaterGAP results. To be as close to the ISLSCP definition as possible, a WaterGAP

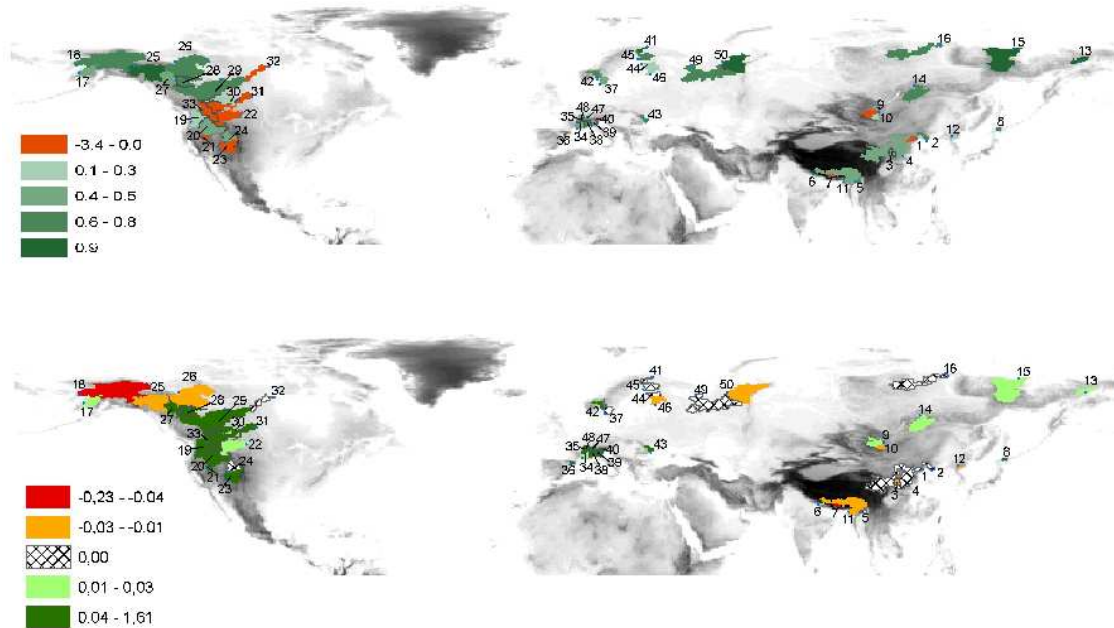


Figure 3.4— Snow dominated river basins chosen for testing the subscale approach. The top figure shows the monthly modeling efficiency of river discharge after the implementation of the sub grid routine. The bottom figures shows the MME changes that were induced by the sub grid implementation. The numbers refer to the catchments listed in Table 3.1.

grid cell is defined as snow covered for one month if at least 50 percent of its area is snow covered at least one day of this month. Consequently one source of error are short duration snow cover events, which are mapped by WaterGAP but not necessarily by the ISLSCP data set.

The spatial extent of the snow cover is well reproduced by WaterGAP throughout the year, especially in wide parts of Northern America and Russia (Figure 3.5). In fall, the modelled snow cover extent spreads out faster in southern direction than it is shown by the observed data. This is probably caused by single days with snow cover, which are considered by WaterGAP but not by the satellite data. The model has problems to match the observed snow cover especially in middle and south-eastern Europe as well as in the Hindu Kush-Himalayas region (Figure 3.5). This caused by the complex terrain, which leads to a heterogeneous snow cover on small scale. The spatial model resolution (0.5°) does not consider small scale climatic effects and local conditions affecting the snow cover, as already described above.

Beside the subjective visual comparison of modeled and observed snow cover extent, model performance is assessed more objectively by calculating the Figure of Merit in Space (FMS) from satellite derived and modeled snow cover of the Northern Hemisphere. The FMS has been applied in a number of studies, mainly in air quality modeling (Rowland and Thompson, 1972; Klug et al., 1992; Straume, 2001; Chang and Hanna, 2001). The FMS is defined as the ratio between the overlap of modeled (A_m) and observed (A_o) area and the union of A_m and A_o (Eq. 3.2). The resulting FMS values range between 0 (no agreement) and 1 (100% agreement).

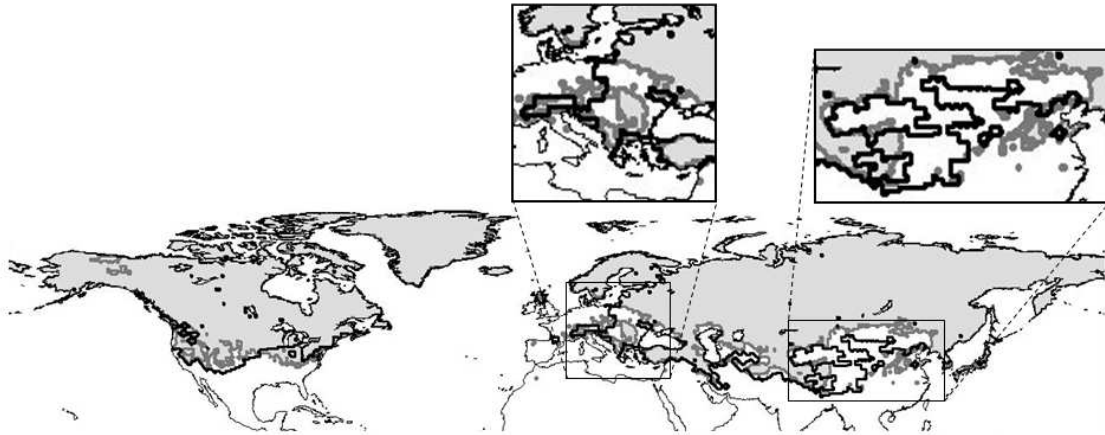


Figure 3.5— Global snow cover in January 1990. The grey area indicates the snow cover modeled by WaterGAP, the black line indicates the ISLSCP satellite data.

$$FMS = \frac{A_m \cap A_o}{A_m \cup A_o} \quad (3.2)$$

The FMS has been calculated for each month of 1990 as exemplary year, representing the typical model behaviour. Figure 3.6 shows that the agreement between the two snow cover extent data sets is generally good during the winter months ($FMS > 0.8$) and around 0.5 during the summer months. In summer, the snow covered areas A_m and A_o are comparably small, which makes the indicator sensitive to mismatches between A_o and A_m . Snow patterns generally occur in the same regions of the world, even though this is not seen by the indicator as long as the snow covers do not overlap. The total monthly areas of Northern Hemisphere snow cover extent match well throughout the year, including the summer months (Figure 3.6). The figure also shows that WaterGAP typically overestimates the snow covered area in fall compared to the satellite data, for the reasons described above.

3.4 Discussion

A new approach to simulate snow accumulation and melt on sub grid scale within WaterGAP has been introduced within this chapter. Each 0.5° grid cell of WaterGAP has been divided into 100 sub grids, each with individual elevation and temperature. The the simulation of snow accumulation and melt on sub grid scale has improved the modeled discharge of snow dominated watersheds on average. Largest improvements occur in mountainous watersheds due to the heterogeneous topography. This is not surprising, because the effect of the topography dependent sub scale simulation is largest in regions with high relief energy. The simulation of the snow melt peak in spring has been improved at most investigated gauging stations in mountainous regions due to the new snow routine. This enhanced WaterGAPs ability to simulate snow melt induced floods, which is especially important for the central theme of this thesis.

However, the model has problems in representing discharge hydrographs of high mountainous regions and in regulated catchments, which could not be solved by a sub grid sim-

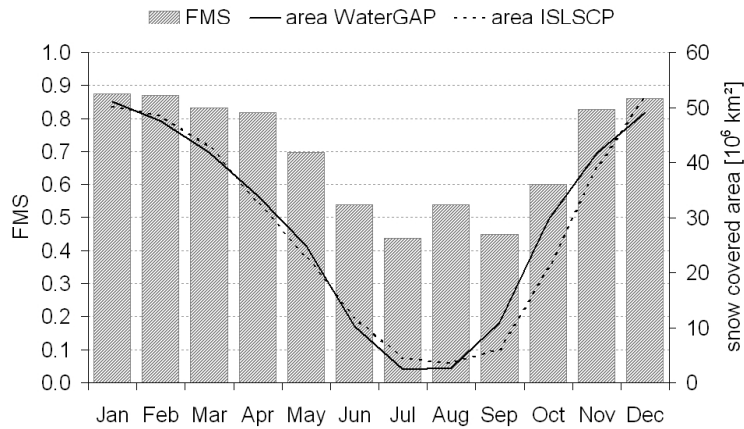


Figure 3.6— The bars indicate the Figure of Merit in Space of the snow covered areas of the Northern Hemisphere in 1990 based on WaterGAP calculations and the ISLSCP data set. Further the modeled (continuous line) and satellite derived (dashed line) snow covered area is shown.

ulation of the snow dynamics. Models with high resolution in space and time are required to simulate snow cover and river runoff of mountainous catchments satisfactorily. Snow dynamics especially in mountains is affected by the local exposition and radiation. These parameters are not taken into account by WaterGAP. Summer discharge of high mountain watersheds is frequently influenced by glacier melt, which is not considered by WaterGAP as well and leads to an underestimation of summer discharge in the affected catchments. The coarse climate input data in 0.5° spatial resolution are an additional source of error. The simple elevation dependent temperature scaling approach approximates the real temperature distribution only. Climate in mountains is by far more heterogeneous in reality. Considerable discrepancies between modeled and measured discharge regimes occur in regulated catchments. River regulation is not considered within WaterGAP and the model treats reservoirs equal to natural lakes.

The sub grid implementation shows no or marginal effects in regions with large natural lakes, such as in Finland or Sweden. The balancing effect of the lakes is higher than the impact of the sub grid implementation. In numerous watersheds investigated, winter discharge is underestimated. This can be ascribed to the uncorrected precipitation applied, where measurement errors underestimate precipitation falling as snow.

The Northern Hemisphere snow cover is represented well by WaterGAP. The modeled snow cover extent has been compared to satellite derived data and best results are found in regions with a high density of climate measurement stations. This is connected to reliable climate used to force WaterGAP (Mitchell et al., 2004), which is especially true for North America and parts of Europe. The model results also match the satellite data well in spacious plain areas such as Northern Russia. The largest discrepancies between observed and modeled snow cover extent occur in heterogeneous regions, such as high mountains, and in regions with comparably imprecise climate data, such as the Hindu Kush-Himalaya region and eastern Asia.

It can be concluded that WaterGAP is well suitable to reproduce snow dynamics and snow cover extent on large scale. The model results should be interpreted on large spatial units

such as mountains or on sub-continental scale. Thus WaterGAP is especially applicable in studies about climate change impacts on snow cover and discharge in large snow affected watersheds. The new implemented snow routine improved WaterGAPs ability to simulate snow melt induced floods in catchments that are located completely or with their headwaters in mountains.

Chapter 4

Snow Hydrological Conditions in Mountains and Cold Regions: Current State and Future Projections

4.1 Introduction

The Northern Hemisphere snow covered area is projected to contract until the end of this century (IPCC, 2007a). Most studies on this scale analyze historic or recent changes of snow and ice cover based on satellite data (e.g. Brown et al., 2000; Déry and Brown, 2007; Lemke et al., 2007). A few of studies apply GCMs to investigate future projections of snow cover changes. Meehl et al. (2007) project widespread reductions in Northern Hemisphere snow cover over the 21st century based on multi model simulations. Hosaka et al. (2005) investigate changes in snow cover between the late 20th and late 21st century for the A1b scenario calculated by an atmospheric general circulation model (AGCM). They find that the snow accumulating season starts later and ends earlier in most snow regions with generally decreasing snow cover and SWE. ACIA (2005) compares different model simulations of Arctic snow cover for the B2 scenario. Not astonishing, they find a substantial decrease of snow cover in over most of the Arctic until the end of the 21st century with largest reductions in spring (-3.1 - -6.8% between 1981-2000 and 2071-2090). But the report also points out the large range of GCM results and the differences in the GCMs abilities to simulate terrestrial snow cover .

Snow however, is an important hydrological parameter and consequently incorporated in many hydrological models. Continental and global scale hydrological models are spatially well adapted to be driven by climate scenarios from GCMs, thus enabling large scale investigations about climate change impacts on important hydrological parameters. An additional advantage of these models is their ability to compare the hydrological characteristics of typical landscape units (such as mountains) in different climate zones with a consistent approach. Mountains are especially sensitive to climate warming and global hydrological models are well suitable to compare climate change impacts to snow cover in different mountain regions worldwide.

For global scale models however, data for model calibration and validation are limited. This is especially true for mountain regions. Therefore, detailed and data demanding approaches to simulate snow dynamics or runoff processes in mountains can not be incorporated in large scale hydrological models. Thus, ways have to be found to model snow dynamics and discharge with robust and simple approaches which require only few data but which are able to reproduce hydrological processes best possible.

The present study uses a model based approach to assess snow cover worldwide with special focus on mountains located in different climatic zones worldwide and the Northern Hemisphere snow cover. Snow cover during the period 1961-1990 (reference period) is assessed and the susceptibility of the snow cover in these regions to climate change impacts is investigated. Climate data for the A1b and B1 scenarios for the 2080s from two GCMs (ECHAM5 and HadCM3) were used to force the future simulations. Within the scope of this study, we developed a new global map of mountains in 0.5° spatial resolution and selected seven mountain regions for our investigations. Different characteristics of the snow cover in the selected mountains are compared with a consistent approach by applying the global scale hydrological model WaterGAP (Alcamo et al., 2003a; Döll et al., 2003). Strongly connected to alterations of the Northern Hemisphere snow cover is the discharge of rivers draining into the Arctic Ocean. We investigate the current state and future changes in discharge of the nine largest Arctic rivers, since changes in Arctic river discharge might impact the sensitive freshwater balance of the Arctic Ocean.

The chapter is organized as follows. The global map of mountains is described in Section 4.2 and the forcing data are introduced. The snow related hydrological characteristics of mountains and selected rivers within the seven investigated mountains during the period 1961-1990 are presented in Section 4.3. In this section, we also validate the modeled discharge of nine large Arctic Rivers. In the proximate Section 4.4, the climate change impacts on snow cover in the focus regions as well as on discharge in Arctic rivers are presented. The chapter finishes with a summary and concluding remarks.

4.2 Material and methods

4.2.1 Definition of mountains

To our knowledge, no universally valid and objective definition of mountains is available. A consideration of mountains from a global viewpoint inevitably leads to a collection of characteristics which are difficult to arrange into a simple set of rules. For example, the distinction between mountains and their forelands is frequently based on the selection of a contour line, with areas above this line being classified as mountains. However, this neglects climatic effects of decreasing snow- and timberlines between equatorial areas and high latitudes (Troll, 1973) and no differentiation is made between high plateau areas and steep slopes - see Gerrard (1990) and Meybeck et al. (2001) for extensive discussions. It is therefore clear that any attempt to distinguish mountain areas is arbitrary (Barry, 1992). A global mapping of mountains and a consideration of their water resources however requires a distinction between mountains and their surroundings, even though a generalised view unavoidably leads to a loss of some individual characteristics. On the other hand facilitates an operational definition the comparison of data and modelling results between different mountain ranges. Meybeck et al. (2001) defined common criteria at the global

scale based on a classification of both relief patterns and elevation classes. According to their typology are mountains characterised by a relatively high relief roughness (maximum minus minimum elevation per grid cell divided by half the cell length in ‰) which at least exceeds 20‰ to differentiate mountains from plateaus, and by a mean elevation > 500 m as a criteria to distinguish mountains from hills. They excluded high plateaus (such as the South American Altiplano or the high interior of the Tibetan Plateau) from their typology, i.e. these are not classified as mountains or mountainous areas.

In contrast to the characterization presented in Meybeck et al. (2001), we selected a somehow different procedure for the categorization of mountains. Since focus of our work is on the importance of snow for the hydrological conditions of cold regions, we include high plateaus into our consideration because their specific weather and climate definitely makes them part of cold regions. Secondly, we applied a different spatial subdivision of mountains. Meybeck et al. (2001) derived their information regarding altitude and relief roughness from a Digital Elevation Model (DEM) with a 0.5° (30 arc-minute) spatial resolution. In the first instance, we also applied an aggregated DEM of the same (relatively coarse) resolution, but when we considered the mean elevation of each grid cell only, some areas, which were known as mountains, fell out of the definition since the mean elevation of the grid cell was below the selected threshold. This is mainly caused by the existence of adjoining mountain tops, valleys and foreland regions within one 0.5° grid cell. We were far more successful when implementing subscale information within each grid cell. Based on the GTOPO30 dataset (U.S. Geological Survey, 2003) with an original spatial resolution of 30 arc-seconds, the altitudes of 100 sub-grid cells were assigned to each aggregated 0.5° square. This gives sufficient information on the distribution of elevation classes within one 0.5° grid square; the spatial location of each sub-grid cell within the square is here not required. Based on this procedure, mountains have been classified by the following scheme:

$$elevation_{10} \geq 1000m \text{ AND } elevation_{90} - elevation_{10} \geq elevation_{10} \cdot 0.3 \quad (4.1)$$

$$elevation_{50} \geq 1000m \quad (4.2)$$

where the individual subscripts of "elevation" are the corresponding percentiles of all sub-grid elevation data within each 0.5° grid cell. Condition (4.1) defines those grid cells as mountains that show at least 10% of their sub-grid elevation data to be equal to or higher than 1000 m a.s.l (the elevation limit has been set to 1000 m following Viviroli and Weingartner (2004)). In addition, condition (4.1) ensures that a certain relief is present. Thus, it defines those regions as mountains which include both steep slopes and elevations above 1000 m. Since high plateaus do not show the required relief for an application of condition (4.1), we additionally defined condition (4.2) which says that more than 50% of the elevation data within a 0.5° grid cell need to be equal to or higher than 1000 m. This condition applies to the spacious, high plateaus on earth.

Figure 4.1 shows the spatial extent of mountain areas on the globe which have been defined according the above given definition (note that we excluded Greenland and Antarctica). For further investigations in this study, we selected a total of seven mountains or sub-regions within extended mountain chains. The latitudinally extensive Rocky Mountains have been further subdivided into a northern region which can be roughly assigned to the Koeppen-type D-climate and a central region which is about to be associated with

the Koeppen-type B-climate. From the Andes we selected those parts which belong to the Koeppen-type A-climate, i.e. the tropical domain, with their limits (arbitrarily) set between 11.5° N and 17.0° S. Furthermore, we selected the Scandinavian Mountains, the European Alps, the Hindu-Kush-Himalayas (only those parts which drain south), and the Altai (see Figure 4.1). When we follow our definition of mountains and high plateaus and

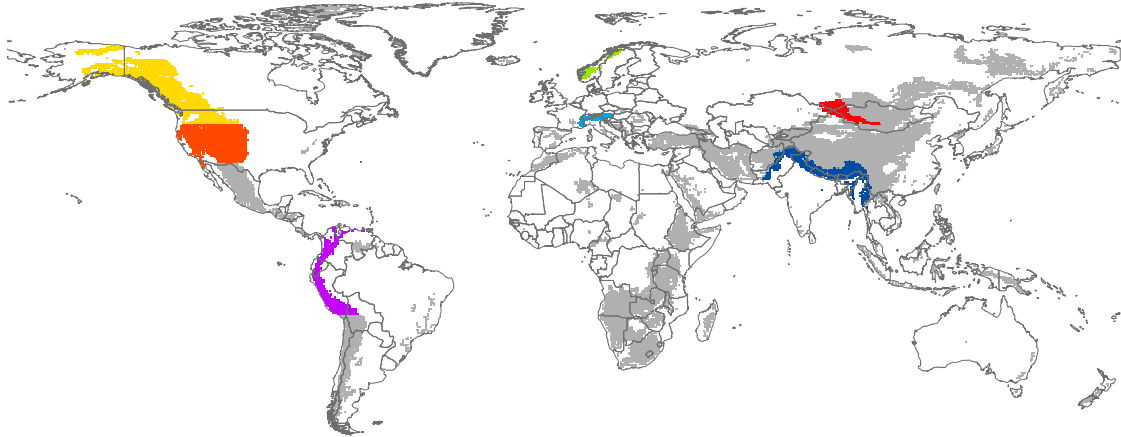


Figure 4.1— Global map of mountains and high plateaus (shaded areas), classified according to the definition developed within this study. The coloured areas have been selected for further analysis.

sum up the respective areas, a total of approx. $33.3 \cdot 10^6 km^2$ results which is ca. 25% of the global land area excluding Antarctica and Greenland. (Meybeck et al., 2001) give exactly the same areal extent for their definition of mountains, which however includes elevations above 500 m a.s.l. (given they exceed the predefined relief roughness) and excludes high plateaus.

4.2.2 Definition of arctic regions

In contrast to the arbitrary and complicated delimitation of mountains from their surroundings, arctic regions are defined here as those catchments which drain into the Arctic Ocean. For this study, we selected the nine largest rivers which flow into the Arctic Ocean, i.e. the Yukon, Mackenzie, and Nelson (N-America) as well as the Severnaya Dvina, Ob, Yenisey, Lena, Kolyma, and Indigirka (Asia).

4.2.3 Forcing data

To simulate present-day and future hydrological conditions, WaterGAP requires current and scenario-specific meteorological time series with monthly values. For the reference period (1961-1990) the CRU dataset (Mitchell and Jones, 2005) has been applied to force WaterGAP. For the scenario simulations we used future global patterns of temperature and precipitation provided by the coupled atmosphere-ocean GCMs ECHAM5/MPIOM model of the Max Planck Institute of Meteorology in Germany (Röckner et al., 2003; Jungclaus et al., 2006), and HadCM3 of the British MetOffice Hadley Centre (Gordon et al., 2000). GCM computations for the two SRES emission scenarios A1b and B1

were selected. The GCM results were introduced within the 4th assessment report of the Intergovernmental Panel on Climate Change (IPCC, 2007a). The GCM results have been downscaled from their original resolutions to a $0.5^\circ \times 0.5^\circ$ degree grid by PINGO grid interpolation (Waszkewitz et al., 1996) and are provided as 30-year average monthly precipitation and temperature for both the reference period (1961-1990) and the 2080s (2071-2100). The time series of future climate were derived with a delta change approach as described in Section 2.5.3.

4.3 Results current situation

4.3.1 Results for Mountain Regions

Hydrological characteristics of mountain regions

In most mountain and arctic regions, the presence of snow controls the hydro-climatic situation over a great part of the year. The delayed and long-lasting process of snow melt guarantees a relatively well-balanced discharge regime of rivers in the spring and summer melting season, even if only a small part of their catchment includes high mountain or arctic areas (Figure 4.2). For the typical mountain weather conditions, this results in high melt water runoff during dry conditions when net radiation and air temperature are high, while, during cooler periods, rainfall compensates for reduced or discontinued melt rates and sustains streamflow at a balanced level (Menzel and Lang, 2005). Furthermore, because of the relatively high albedo of snow, changes in mountain or arctic snow cover are associated with a feedback to climate, a process that has not yet been very well investigated. For example, a climate-induced decrease in snow cover will reduce surface albedo, which leads to an amplification of the initial warming. In mountains, all these factors and processes may vary considerably with space and time. The temporal variability of snow cover and its spatial heterogeneity across mountains results in complex dynamics of hydrological processes and marked differences between the hydro-climatic characteristics of the various mountain ranges. The many different conditions and processes in the context of the presence of snow in mountains and arctic regions can not be treated collectively in this paper. Therefore, focus is on the consideration of snow cover, its amount and duration as well as its impact on discharge regimes.

Snow Cover

In the following, investigations are focused on the seven selected mountain ranges. First, we analyze altitudinal variations of air temperature and typical snow parameters from sub-grid information. For each of the squares that divide a 0.5° cell into 100 sub-units (see section 3.2.1), monthly values of temperature, SWE as well as annual snow cover duration was calculated over the period 1961-1990. Then we averaged each of the three variables for altitudinal belts covering 100m difference in altitude over each single mountain range and plotted T, SWE and snow cover duration over the related altitude (Figure 4.3). This allows a comparison of mountains in different climatic regions worldwide. We focus on T and SWE values for representative months for maximum snow cover. This is usually January

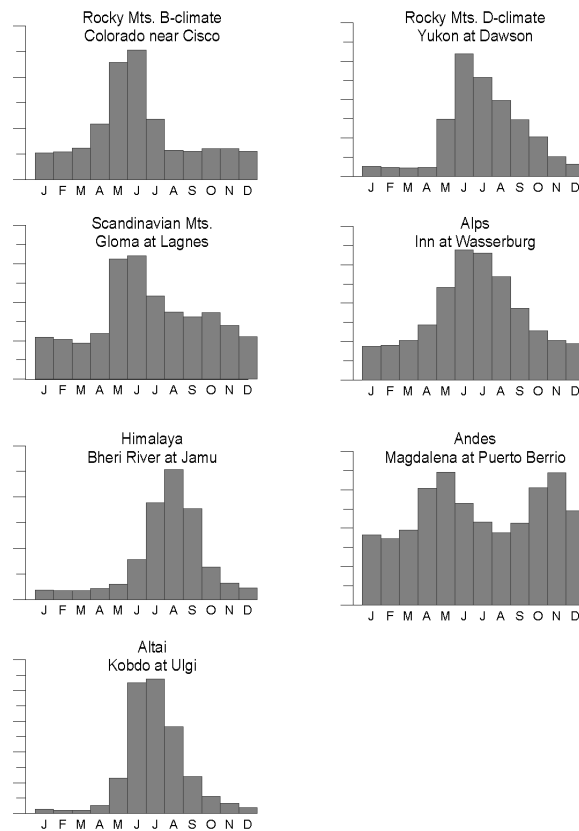


Figure 4.2— Typical discharge regimes (mean monthly discharges) of mountains. The examples come from seven different mountain ranges which have been selected for a detailed analysis in this paper.

for most mountains of the Northern Hemisphere and April in the Hindu Kush-Himalaya and Andes. It should be kept in mind that average results for large mountain areas are shown, modeled with a global hydrological model. It is commonly known that snow cover can be very heterogeneous on small scale and is highly influenced by local climate and topography. Neither our goal nor our ability is to model exact SWE values. We rather want to show the order of magnitude of the SWE values to compare snow conditions in different mountains worldwide.

Snow cover in mountains of the B, C and D climates of the Northern Hemisphere typically occurs during the Northern Hemisphere winter, which is true for the Rocky Mountains, Scandinavian Mountains, Alps and the Altai. The Andes are tropical mountains and the climate varies greatly depending on location and altitude. We investigate the equatorial part of the Andes, adjacent to tropical climate (A-climate). Here, the snow line lies above 4500 m all year long and the inter-annual SWE variability is much smaller than in the other mountains. Highest SWE values can on average be found between March and May in the Andes. The southerly directed part of the Hindu Kush-Himalaya region is monsoon influenced and a large amount of the annual precipitation falls during the summer months. The winter months are cold and dry and SWE maxima are on average found between March and May as well.

Figure 4.3 shows temperature, SWE and the number of snow days per year (day with

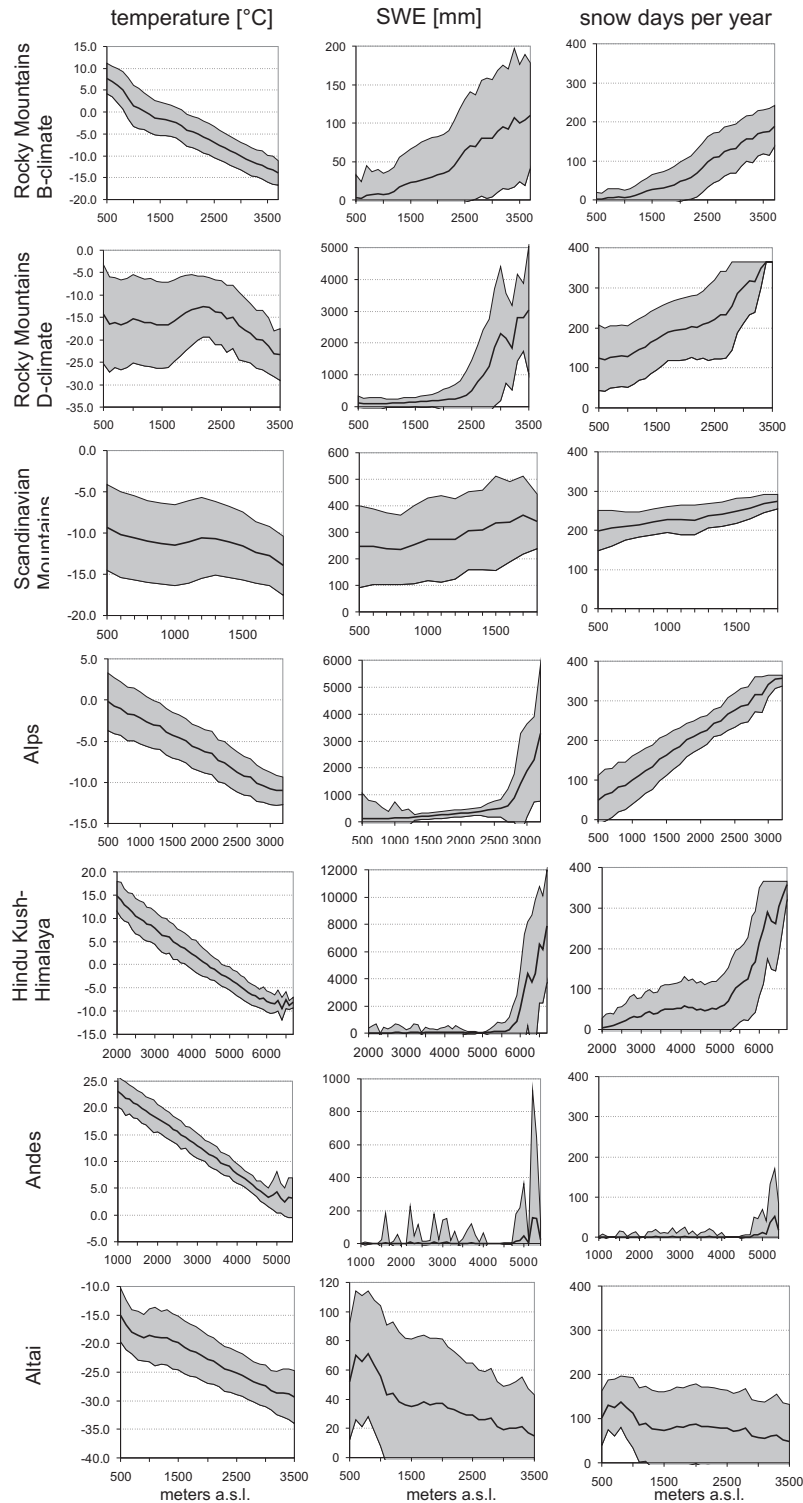


Figure 4.3— Average January or April temperature and SWE 1961-1990 (depending on annual SWE maximum) and annual number of snow days over the altitude [m a.s.l.] of seven selected mountain ranges. The black line shows the average values for the whole mountain, the grey area indicates the standard deviation. We show results for altitudinal belts that include more than 5 sub grids.

SWE > 20mm) for each of the seven mountains selected for this study. The B-climate part of the Rocky Mountains is quite dry with an average January temperature below -6.9°C ($\pm 3.5^{\circ}\text{C}$) in altitudes > 2500m. The average SWE hardly exceeds 100mm. However, snow cover remains more than three months in altitudes >2500m due to the cold temperatures. The northerly located and wetter D-climate regions of the Rocky Mountains show a significant increase in SWE in altitudes > 2300m. SWE values below 2000m are about factor 5-7 and above 2500m even more than factor 20 higher compared to the B-climate areas of the Rocky Mountains (Figure 4.4, middle). Snow cover remains on average more than six months in altitudes larger 1600m.

The mean January temperature in the Scandinavian Mountains is around -10°C at 500 to 1200 m a.s.l.. The temperature decline with increasing altitude is smallest compared to the other mountains. Temperature decreases to -13.9°C ($\pm 3.6^{\circ}\text{C}$) on 2800m only. Snow cover remains more than 200 days in wide parts of the Scandinavian Mountains and average SWE values lie between 250 and 350 mm between 500 and 1500m a.s.l..

Average January SWE values in the Alps are on average below 500 mm in altitudes up to 2500m and SWE strongly rises in higher located areas. The snow duration increases almost linearly from 50 (± 62) days at 500m to 292 (± 44) days in altitudes larger 2700 m. The high standard deviations for SWE in altitudes below 1400 m result from differences between the northern and southern Alps and a high year to year variability, since temperatures are close to 0°C in these altitudes. The SWE values in the Alps are high compared to the other investigated mountains (Figure 4.4, middle). The average SWE magnitudes are in the same order of magnitude as in the D-climate part of the Rocky-Mountains over all altitudes.

In the investigated part of the Hindu Kush-Himalaya region, average SWE > 500 mm can be found in areas higher than 5800m all over the year. SWE increases strongly with increasing altitude. There are conspicuous SWE values > 6000 mm above 6500 m a.s.l. In these altitudes snow remains on average more than 300 days per year or is even permanent in high altitudes. Accordingly, snow is stored in glaciers in reality. However, the current WaterGAP version does not consider glaciers and related processes and SWE simply accumulates over the year in the affected sub-grids, which implies a high uncertainty of these SWE values.

The SWE figure of the Andes is quite heterogeneous. This is caused by the complex climate of these mountains. Snow occurs on high mountain tops only and the snow line differs immensely over the whole mountain range. Thus, a clear picture cannot be drawn. Mean SWE values > 50 mm are found in areas above 5000m only and remain comparably low (Figure 4.4, middle).

The SWE gradient of the Altai differs from the trend found in the mountains discussed before. Here, the comparably thin average SWE decreases with increasing altitude from approx. 70mm at 800 m a.s.l. to 15 mm at 3500m. There is little precipitation in high altitudes of the Altai caused by the already dry climate and intensified by the extremely cold temperatures that allow a low humidity only.

Runoff in Mountain Catchments

Due to the relatively coarse resolution of WaterGAP, it is difficult to find data which can be used to validate the modeled SWE. A large number of SWE point measurements exist,

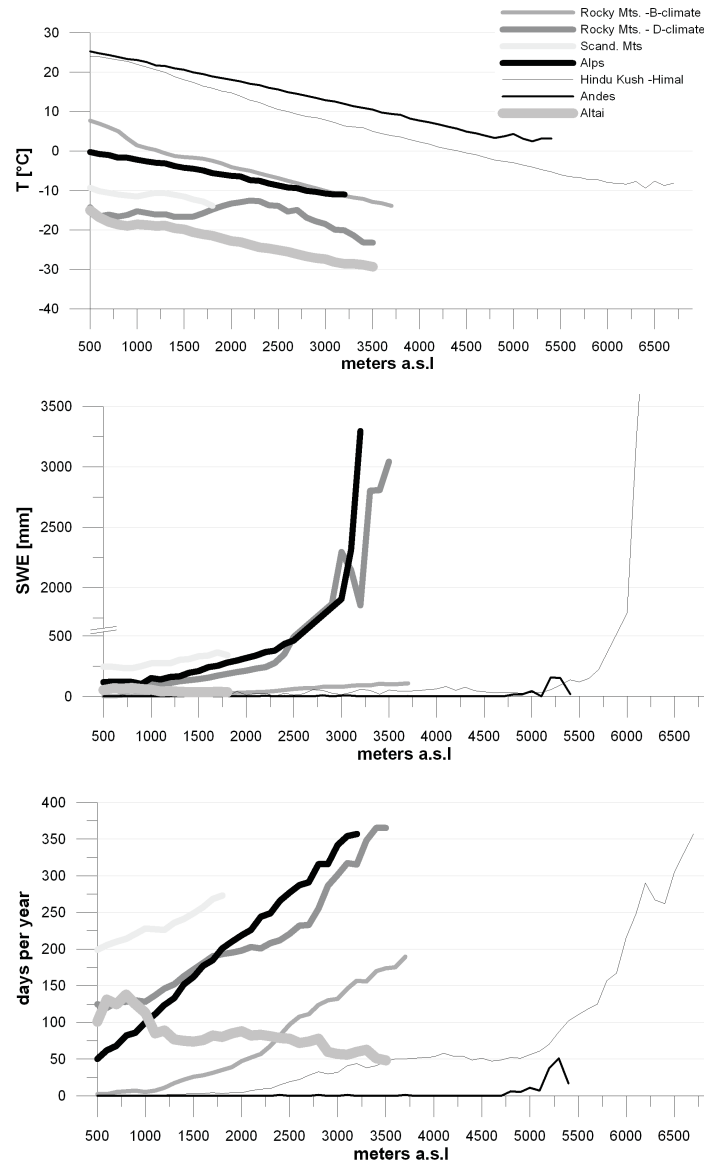


Figure 4.4— Intercomparison of average temperature, SWE and snow days per year for 1961-1990 between the different mountains.

but these data cannot be compared to spatially averaged SWE values. Spatial SWE information with a large spatial extent are available from satellite derived data. Armstrong et al. (2005) provide a comprehensive dataset with gridded monthly SWE data for 1978 - 2005, which would be well suitable from its temporal scale and spatial resolution to serve as validation data source for WaterGAP results. However, this dataset is designed for continental-scale time-series studies of snow cover and water equivalent and SWE is undermeasured in mountainous and forested areas, areas near coastlines and in areas containing melting, shallow or intermittent snow (Armstrong et al., 2005). We compared parts of the dataset to WaterGAP results and found the dataset not suitable to serve as reliable data source for the given reasons.

However, discharge can be used as an indirect validation of the simulation of snow dynamics, because it comprises the hydrological processes of the related watershed. We selected 16 rivers that are located completely or with their headwaters in snow dominated parts of the mountain ranges. We simulated monthly discharge between 1961 and 2002 for each catchment and compared it to the discharge data. The time series that were actually used for comparison are shorter for most gauging stations, limited by the data availability (Table 4.1). The impacts of snow melt on discharge of the single watersheds differ between the mountain ranges, the related snow cover and time of the year. The fraction of snow melt in discharge is large in mountains with high SWE and seasonal snow melt, such as the Alps the Scandinavian or the Rocky Mountains. However, the volume of snow melt water in the Magdalena River located in the North Andes is marginal only. Anyhow, exemplary rivers of all mountains are listed in Table 4.1 to assess the quality of the WaterGAP at the selected gauges. We calculated the Nash-Sutcliffe-Coefficient (NSC) based on monthly discharge data as well as the total volume error. WaterGAP is generally produces reliable results for the selected river basins. However, the quality criteria differ between the single catchments. Lowest NSC values occur in strongly regulated watersheds, such as the Colorado or Columbia rivers in the B-climate part of the Rocky Mountains.

4.3.2 Northern Hemisphere

Snow cover

WaterGAP is well applicable to simulate the spatial extent of the Northern Hemisphere snow cover, which is discussed in Section 3.3.2. The model shows errors in matching the observed snow cover in Europe and the Hindu Kush-Himalayas region (Figure 3.5), which is likely to originate from the heterogeneous snow cover in these regions. However, the snow cover is well reproduced by WaterGAP throughout the year in wide areas of the Northern Hemisphere, especially in large parts of North America and Asia.

Freshwater inflow into the Arctic Ocean

Wide-ranging areas of the D and E-climate zones of the Northern Hemisphere are snow covered for the best part of the year. Snow melt runoff in spring is an important component in the hydrological system of this region and snow melt runoff provides a considerable volume of freshwater that drains into the Arctic Ocean. Snow melt induces a strong increase in discharge of the affected rivers in spring and summer and approximately 60% of their annual river discharge occurs between April and July (Lammers et al., 2001). The freshwater inflow from rivers draining North America and Eurasia are by far the largest single source of freshwater for the Arctic Ocean (Arnell, 2005). The average annual freshwater inflow for the period 1961-1989 from rivers into the Arctic Ocean is $4804 \text{ km}^3/\text{year}$ (Lammers et al., 2001; Arnell, 2005), whereas sea ice melt as second highest freshwater source, is estimated to be $2500 \text{ km}^3/\text{year}$ only (Zhang et al., 2003; Arnell, 2005).

Long term average monthly discharge has been calculated with WaterGAP for the nine largest rivers draining in the Arctic Ocean (Table 4.2) and has been compared to discharge measured at gauges closest to the mouths these rivers. The total upstream area of the investigated gauges covers $12.5 \cdot 10^6 \text{ km}^2$, which is about 56% of the total area draining into the Arctic Ocean. WaterGAP is able to reproduce the long term average annual discharge

Table 4.1— Characteristics and quality criteria of catchments located in the selected mountains.

Mountain ^a	River	Station	Period	Catchment Area [10 ³ km ²]	Mean Q_{month} [m ³ /sec] data	Mean Q_{month} [m ³ /sec] WaterGAP	Vol. Error [%]	NSC
1	Columbia Riv.	The Dalles	1961-2002	614	5136	5089	-0.85	0.20
1	Colorado Riv.	Lees Ferry	1961-1984	290	370	392	5.90	-0.17
1	Colorado Riv.	near Cisco	1961-2002	62.4	192	195	1.59	0.51
2	Yukon Riv.	Dawson	1961-1980	264	2260	2281	0.86	0.71
2	Teslin Riv.	near Whitehorse	1961-1996	36.5	905	849	-6.29	0.42
3	Gloma	Langnes	1961-2000	40.2	682	677	-0.59	0.54
4	Rhone	Beaucaire	1961-1979	95.6	1657	1725	4.31	0.47
4	Rhone	La Mulatiere	1961-1972	50.2	973	983	1.17	0.50
4	Inn	Wasserburg	1961-2002	12.0	358	353	-1.38	0.67
5	Karnali Riv.	Chisapani	1962-1993	42.9	1353	1323	-2.21	0.66
5	Bheri Riv.	Jamu	1963-1992	12.3	298	295	-0.92	0.71
5	Narayani	Devghat	1963-1993	31.1	1560	1550	-0.57	0.50
6	Magdalena	Puerto Berrio	1969-1984	74.4	2481	2479	-0.10	0.30
7	Kobdo	Ulgi	1976-1984	22.1	52	52	0.69	0.29
7	Katun	Malyi Yaloman	1961-1971	36.8	475	454	-4.28	0.62
7	Buqtyrma	Lesnaya Pristan	1961-1987	10.7	199	199	-0.08	0.49

^a1: Rocky Mts. (B-climate), 2:Rocky Mts. (D-climate), 3: Scand. Mts., 4:Alps, 5:Hindu K. - Himal., 6: Andes, 7: Altai

well. The total volume error lies between -3.7% and 1.0% compared to the measured data (Table 4.2). Thus, WaterGAP is well applicable for studies investigating changes in the total annual freshwater inflow into the Arctic Ocean (see Section 4.4.3). In this study we focus on annual discharge, because WaterGAP generally overestimates winter discharge

Table 4.2— Characteristics of major rivers draining into the Arctic Ocean

River	Station	Period ^a	Catchment Area [10 ³ km ²]	Mean Q_{annual} [km ³ /year] data	Mean Q_{annual} [km ³ /year] WaterGAP	Vol. Error [%]
Yukon Riv.	Pilot Station	1976-2002	831	203	198	-2.0
Mackenzie Riv.	Arctic Red River	1973-2002	1,660	287	284	-1.3
Nelson River	Kelsey Generating Station	1961-2002	1,010	68	67	-1.5
Severnaya Dvina	Ust-Pinega	1961-1998	348	101	100	-1.7
Ob	Salekhard	1961-1999	2,950	404	409	1.0
Yenisey	Igarka	1961-1999	2,440	662	639	-3.4
Lena	Stolb	1961-1994	2,460	481	477	-0.5
Kolmya	Kolymaskaya	1978-1998	526	101	99	-2
Indigirka	Vorontsovo	1961-1994	305	52	50	-3.7

^aonly years with complete data records were considered

and underestimates discharge in summer and spring of the Arctic rivers (Figure 4.5) caused by river freezing, which is not considered within the WaterGAP version applied in this study.

4.4 Scenarios based on GCM output

It is commonly known that climate change effects are not uniform and that the magnitude of temperature rise differs globally. We assessed the climate change impact on snow cover of the Northern Hemisphere as well as for the studied mountain regions based on the SRES scenarios A1b and B1 for the 2080s calculated by the GCMs ECHAM and HadCM (Section 4.2.3). The GCM results agree in terms of the average global trend of important climatic variables like temperature, but the magnitude of changes varies considerably between the models. For precipitation, even the direction of changes shows contradictory results in some areas, for example in the Andes. Thus, follow-up hydrological simulations, as changes in runoff or snow cover, might even proceed in opposed directions for the same scenario (Alcamo et al., 2007; Verzano and Menzel, 2008).

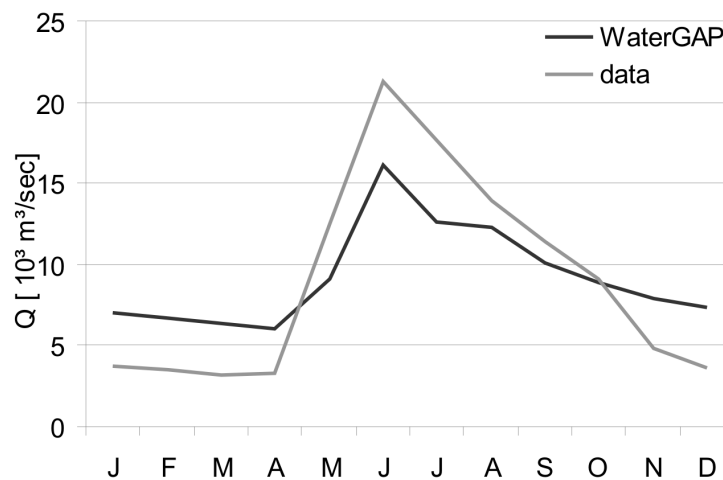


Figure 4.5— Simulated and measured average monthly discharge of the Mackenzie River at Arctic Red River (Canada) showing the typical winter discharge underestimation of WaterGAP results.

4.4.1 Climate change impacts on mountain snow cover

The magnitude and duration and extent of snow cover varies significantly between mountains in different climatic zones worldwide (Section 4.3.1). But which mountain regions are especially sensitive to climate change and how large is the magnitude of projected snow cover contractions? For the seven large mountains investigated in this study (Figure 4.1) we compared temperature and SWE for a month representing maximum snow cover during the year. We chose January for the Rocky Mountains, Scandinavian Mountains, Alps and Altai and April for the Hindu-Kush Himalaya and the Andes as described in Section 4.3.1. It is commonly known that mountains are particularly heterogeneous regions, and SWE varies depending on spatial local climatic conditions and altitude. However, average climate and snow hydrological values are applicable to indicate the typical characteristics of the mountain ranges and to study differences of climate impacts between scenarios, GCMs and different mountain regions.

During the winter months, the average temperature is projected to increase in all selected mountains and for all combinations of scenarios and GCMs (Figure 4.6, top). The model mean of both scenarios projects lowest temperature changes for the D-climate part of the Rocky Mountains with +3.8°C for the A1b scenario and +2.3°C for B1. The scenarios also agree in the region of highest temperature changes, which are the Scandinavian Mountains with +5.7°C and +3.5°C (A1b and B1 respectively) closely followed by the Altai (A1b: +5.5°C, B1: +3.4°C). One can also see that there are mountains with average temperatures close to 0°C (Rocky Mountains B-climate and Alps) or even above (Hindu Kush-Himalaya and Andes). Snow cover of these mountains is especially sensitive to temperature rise. However, changes in precipitation also play an important role in the formation of snow cover. Precipitation is projected to increase during both scenarios in all mountains except Alps and Andes. In the Alps, an average annual precipitation decrease ranging between -5% and -12% is projected (HadCM B1 and Echem A1b). The GCMs show contradictory results for the Andes - Echem projects a precipitation increase between 5% (B1) and 12%

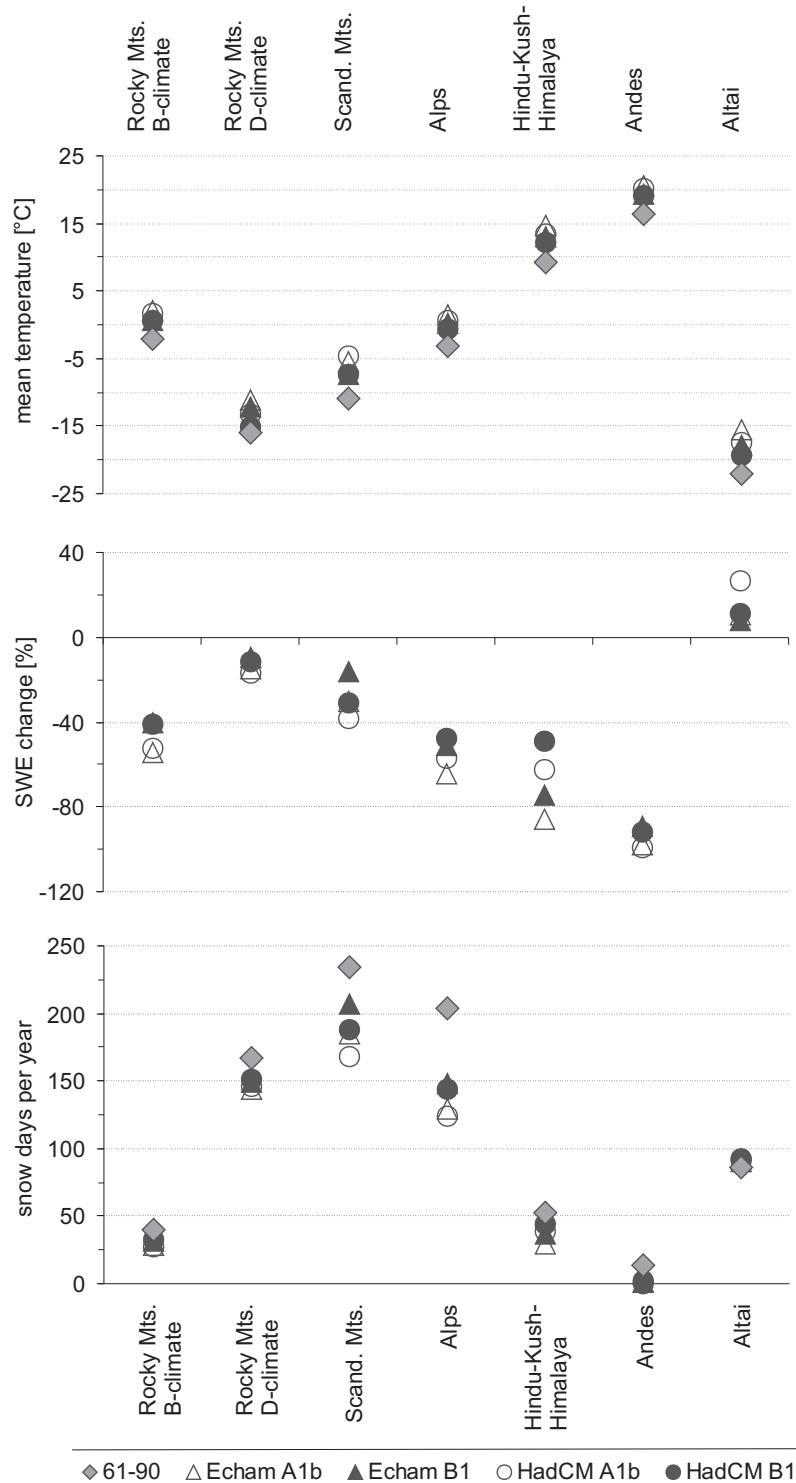


Figure 4.6— Climate change impacts on temperature and snow characteristics for different mountain regions for the reference period 1961-1990 (top and bottom graph) and for the 2080s. The top and middle graphs show average temperature and SWE for January (Rocky Mts., Scandinavian Mts., Alps and Altai) and April (Hindu Kush-Himalaya and Andes) as representative months with maximum snow cover. The bottom graph shows the mean number of snow days per year. SWE and snow duration have been calculated with WaterGAP.

(A1b), whereas HadCM computed a precipitation decrease of -4% and -5% (A1b and B1). At a first glance on Figure 4.6 (middle), it is conspicuous that the average SWE decreases in all mountains except the Altai. Here SWE is projected to increase between 8% and 26%. But one should keep in mind that the Altai has a comparably low snow cover (Figure 4.4) and the SWE increases absolutely between 3mm and 10mm only. The SWE rise is caused by a projected annual precipitation rise between 2mm and 18mm. The future temperature rise does affect snow cover and the number of snow days per year only marginal due to the extremely cold temperatures.

Future changes in snow cover differ between the B- and D-climate parts of the Rocky Mountains. The temperature increase affects SWE of the northern part of the mountains less than the southern part caused by the cold temperatures in the subarctic and boreal climate. In the B-climate part, SWE is projected to decline between roughly 40% for B1 and on average 54% for the A1b scenario.

In the Scandinavian Mountains we find the largest range of projected annual snow day reduction compared to the other mountains. The average annual number of snow days decreases from 235 days during the reference period to between 168 and 206 days (A1b HadCM and B1 Echem) during the 2080s. Still, the number of snow days remains the highest compared to the other mountains (Figure 4.6, bottom).

The Alps will suffer from the strongest change in the number of snow days caused by the temperature increase and concurrent precipitation decrease. As consequence, the total annual number of snow days will decrease from 204 days (1961-1990) to slightly below 130 days for A1b and on average 148 days for B1. The different GCM driven results agree in projecting a significant SWE decrease by roughly 50% to 60%. The snow cover is expected to decrease drastically from low to high latitudes (see Figure A.1)

The magnitude of SWE change in the Hindu Kush-Himalaya differs between the underlying GCM input. All calculations show a strong SWE decline. However, both scenarios driven by Echem5 climate show a stronger SWE decrease compared to the HadCM driven SWE results. WaterGAP calculates a SWE reduction of 49% to 86% compared to the average SWE of 48mm during the reference period. Snow cover varies strongly over the altitudes in the Hindu-Kush Himalaya (Figure 4.3) and climate change will affect in particular snow in lower altitudes (Figure A.1).

The Andes as tropical mountains already have the lowest snow cover compared to the other mountains of this study. During the reference period, snow occurs on high mountain tops only (Figure 4.4) and the average SWE is very low consequently. Mean SWE in April is projected to decrease from 4mm to less than 0.4 mm on average and the annual number of snow days will decrease from 14 days during the reference period to less than 2 days during the 2080s. Hence, only very high mountain tops are projected to be snow covered a few days per year, with a strongly reduced snow cover magnitude.

4.4.2 Climate change impacts on Northern Hemisphere Snow Cover

Based on the climate change scenarios described above, global snow cover for the 2080s has been modeled with WaterGAP. We defined grid as snow dominated if they are snow covered at least 100 days within one year. We assume that in these areas ecology as well as human life is well adapted or even dependent on extensive snow cover during the winter months.

Snow dominated areas have been calculated with WaterGAP for the reference period (1961-1990) and for A1b and B1 scenarios for the 2080s each based on Echem and HadCM climate. All scenario simulations project in agreement a shrinking of the snow dominated area until the 2080s especially in north-eastern Europe, northern USA and the Canadian west coast (Figures 4.7 and A.2). The same effect has been found by Hosaka et al. (2005), who investigated changes in Northern Hemisphere snow cover for the A1b scenario. It can also be seen that snow cover in mountainous regions throughout the Northern Hemisphere decreases significantly until the end of the 21st century, which has been discussed in detail in Section 4.4.1. However, the magnitude of snow decline differs between scenarios and underlying GCMs. The snow dominated area is projected to shrink from 35.0 10^6 km² during the reference period about 14.0% to 15.1% during the A1b scenario and about 9.6% to 10.8% for B1. The lower values in both scenarios are the snow cover declines derived from Echem driven WaterGAP calculations. Snow cover change of the same range was reported by ACIA (2005, chap. 6.4.3) for the period 2071-2090 (B2 scenario - results from five GCMs).



Figure 4.7— Snow dominated area of the reference period (1961-1990, white area with black border) and the A1b scenario for the 2080s (gray area with gray border) as calculated by WaterGAP based on Echem climate.

4.4.3 Climate Change impact on Arctic River discharge

A number of large rivers are located in the snow dominated part of the Northern Hemisphere (D- and E-climates) and climate change affects the volume of river discharge, i.e. freshwater, that drains into the Arctic Ocean. The Arctic Ocean is susceptible to

changes in the freshwater balance, because this alters the ocean salinity and thus the sea ice formation and thermohaline circulation. Peterson et al. (2002) already proved an annual discharge increase of 7% between 1939 and 1999 for the six largest Eurasian rivers. Koenigk et al. (2007) report a rise in Eurasian river runoff into the Arctic Ocean of 5000 m³/sec between 1960 and 2000. This is in accordance with Wu et al. (2005), who found an enhanced total river runoff into the Arctic of 10,000 m³/sec between 1960 and 2001, based on HadCM3 calculations. However, a decrease in Canadian river discharge since 1964 has been reported by Déry and Wood (2005).

In Section 4.3.2 we showed that WaterGAP results are well suitable for studies about changes in long term average inflow into the Arctic Ocean. Arnell (2005) modeled changes in freshwater inflow into the Arctic Ocean for the 2080s based on the SRES scenarios A2 and B2 (IPCC, 2001) of six climate models and two emission scenarios. He found that total freshwater inflow increases up to 31% for A2 and up to 24% for the B2 scenario. For IPCC (2007a) new GCM results were produced, which we used as forcing data for WaterGAP. We computed changes in river discharge for the nine largest Arctic rivers, covering 56% of the total area draining into the Arctic Ocean for the 2080s and compared it to the reference period 1961-1990. Our results show in agreement with the studies cited above an increase of total discharge of these nine rivers. The increase for the A1b scenario is projected to be 19% (Echam driven) and 25% (HadCM driven) and for B1 9% and 15% for Echam and HadCM driven results, respectively. Our results for the Echam A1b driven calculations are somewhat lower than the results presented by Koenigk et al. (2007), who found an increase of 31% until 2100, though for total river runoff draining into the Arctic Ocean.

The magnitude of river discharge change differs between the nine watersheds (Table 4.3). Largest changes are found for the Yukon in Alaska and the Indigirka and Kolmya Rivers in Eastern Siberia. The projected changes for A1b are higher than for B1. However, for the Siberian Rivers, the results for the two different GCMs vary significantly. For the Kolmya River Echam driven results show an discharge increase of 17% (A1b) and 5% (B1), whereas HadCM based calculations project by far higher changes (68% and 46%, A1b and B1). We find an agreement in all combinations of scenarios and GCMs that discharge of the Ob watershed is least affected by climate change. Here we find even a slight decrease in river discharge for the B1 scenario. A discharge decrease is also found for three of four scenario runs for the Canadian Nelson River, which is in accordance with the results found by Déry and Wood (2005) for the last decades of the 21st century.

4.5 Summary and Conclusions

In the study presented in this chapter, the current and future situation of snow related hydrological processes have been investigated with a global view, focusing on seven large mountains of the world as well as the Northern Hemisphere snow cover. In addition to climate change impacts on the snow cover in the focus regions, expected future alterations on river discharge in the nine largest Arctic rivers have been investigated, covering 56% of the total area draining into the Arctic Ocean. The application of the global scale hydrological model WaterGAP allowed a consistent comparison of snow cover between the single focus regions.

Table 4.3— Change in annual river discharge (Q_{annual}) of the nine largest Arctic Rivers until the 2080s compared to 1961-1990.

River	Station		Mean Q_{annual} 1961-1990 (WaterGAP) [km ³ /year]	Change in Q_{annual} between 1961-1990 and the 2080s [%]			
				A1b Echam	A1b HadCM	B1 Echam	B1 HadCM
Yukon Riv.	Pilot	Sta- tion	203	32.6	41.3	26.1	20.1
Mackenzie Riv.	Arctic River	Red	289	14.4	12.1	5.6	4.2
Nelson River	Kelsey Generating Stat.		69	6.2	-13.6	-8.9	-8.5
Severnaya Dvina	Ust-Pinega		99	19.1	12.4	9.8	16.1
Ob	Salekhard		408	5.7	4.9	-0.2	-3.3
Yenisey	Igarka		567	16.9	19.2	10.5	11.4
Lena	Stolb		481	27.4	41.8	13.9	28.8
Kolmya	Kolymskaya		111	16.8	68.4	5	46.4
Indigirka	Vorontsovo		52	42.4	69.2	21.4	50.3

The investigated mountain areas were derived from a new global map of mountain areas that has been developed within the scope of this study. As could be expected, all investigated mountains will be affected by climate change, with drastic impacts on their future snow cover, which is projected to decrease significantly in most mountains. Mountains of the lower latitudes will obviously suffer from a stronger decrease in snow cover than those located in the northern regions of the globe. Most affected are the Alps, the Andes and the Hindu Kush-Himalaya region. In these mountains an average decrease of the SWE over 40% is expected, in the Andes even over 80%. This goes along with a significant rise of the snow line. In contrary to the other selected mountains, the snow cover magnitude of the Altai is expected to rise due to increasing precipitation and the extremely cold temperatures, which are despite climate warming far below the 0°C threshold. The A1b scenarios of both GCMs (Echam and HadCM) project a stronger temperature increase in all mountains and a connected decrease of the snow cover magnitude in the affected areas. Changes in snow cover of the mountains affect related hydrological conditions, and consequently the water services of mountains, e.g. for human water use, electricity production, or tourism, will change. Alterations in mountain hydrology will in any case impact large regions that belong to watersheds having their headwaters in mountains, since mountains often serve as water towers for downstream regions. It would be reasonable to carry out further studies, which compare climate and global change impacts on mountain hydrology of different mountains worldwide, to define particularly sensitive mountain areas and to assess the consequences of changes in mountain hydrology to adjacent regions.

The snow dominated areas of the Northern Hemisphere, defined as having at least 100 snow days per year, are expected to shrink especially in mountain areas, north-eastern

Europe, northern USA and the Canadian west coast. This is shown in agreement by both GCMs and scenarios. The alteration of the snow cover does also affect the discharge of large rivers located in the snow dominated area of the Northern Hemisphere. They drain into the Arctic Ocean and the total freshwater inflow provided by the nine largest rivers is projected to increase between 9% and 25%, depending on forcing GCM and scenario. This is likely to alter the freshwater balance of the Arctic Ocean with possible impacts on sea ice formation and the thermohaline circulation. Within the scope of this study, the alterations of the freshwater inflow into the Arctic Ocean could just be touched and average annual values of only nine rivers were investigated. However, discharge and thus the freshwater inflow into the Arctic Ocean vary significantly within a year. Further research should be carried out, investigating the climate change effects on seasonal discharge of Arctic rivers and connected impacts on the Arctic freshwater balance.

Chapter 5

Simulating River Flow Velocity on Global Scale: a Pre-Study¹

5.1 Introduction

River flow velocity is crucial to simulate discharge hydrographs and the residence time of water in the hydrological system. If a single or a limited number of catchments are modeled, complex flow velocity equations can be parameterized with observed catchment-specific values. This is not possible at larger scales. Hence, for a global approach, a simplified methodology is needed. In state-of-the-art global hydrological models, either no lateral routing and thus no river flow velocity is used (Arnell, 1999; Yates, 1997) or just simple approaches like constant river flow velocity (Döll et al., 2003), simple functions of discharge (Vöröshmarty et al., 1989) or of topography (Hagemann and Dümenil, 1998) are applied to simulate flow velocity or retention time in rivers, respectively. In general these models are designed to model mean long-term discharges and for these cases it is sufficient to use simple approaches. However, to model flood events or water quality, it is necessary to use a more sophisticated approach.

In this work a simple algorithm to model flow velocity based on a limited number of parameters is presented. The approach allows simulating spatially and temporally variable river flow velocities based on parameters derived from globally available data and discharge time series, that might be provided by measurements or by spatially distributed hydrological models. It was tested against independent flow velocity measurements at several river cross sections. The longterm objective of these efforts is to improve flow routing in the Global Hydrology Model WaterGAP (Döll et al., 2003; Alcamo et al., 2003a), which was designed to assess and predict water availability at the global scale with a spatial resolution of 0.5 by 0.5 degrees.

¹based on K. Verzano (published as Schulze, K.) , M. Hunger and P. Döll (2005), Simulating River Flow Velocity on Global Scale *Advances in Geosciences*, **5**, 133-136

5.2 Methodology

To determine river velocity at the global scale, an approach had to be found, simple enough that the required parameters could be derived from data globally available and sophisticated enough to deliver realistic flow velocity values for a large variety of environmental conditions. The Manning-Strickler formula (Eq. (5.1)), one of the best known and most often used equations to calculate river flow velocity, is considered to meet these demands.

$$v = n^{-1} \cdot R^{2/3} \cdot S^{1/2} \quad [m/s] \quad (5.1)$$

In (5.1), v is the flow velocity [m/s], n is the river bed roughness $[-]$, R the hydraulic radius [m] and S the river slope [m/m].

The hydraulic radius (R) of a specific river cross section is temporally variable due to river stage dynamics. It depends on the shape of the river bed profile and the actual water level. Assuming that the river bed is shaped as a rectangle it can be calculated as a function of river depth (D , [m]) and width (W , [m]).

$$R = \frac{D \cdot W}{2D + W} \quad [m] \quad (5.2)$$

Continuous data on river width and depth is lacking at the global scale. Based on the close relationship between channel form and discharge (Q , [m^3/s]), Leopold and Maddock (1953) introduced equations, which estimate these parameters as a function of discharge:

$$W = a \cdot Q^b \quad [m] \quad (5.3)$$

$$D = c \cdot Q^f \quad [m] \quad (5.4)$$

Equations (5.3) and (5.4) can be found in recent hydrology textbooks (e.g. Mosley and McKerchar 1993, (p. 8.4.); Dunne and Leopold 1978, (p. 637)) and are frequently applied. Allen et al. (1994) carried out a regression analysis with a dataset of 674 river cross sections across the USA and Canada to quantify the best-fit coefficients (a , c) and exponents (b , f) in the equations, valid for bankfull discharge (Q_b):

$$W = 2.71 \cdot Q^{0.557} \quad [m] \quad (5.5)$$

$$D = 0.349 \cdot Q^{0.341} \quad [m] \quad (5.6)$$

During regression analysis, Allen et al. (1994) obtained high coefficients of determination (r^2) of 0.88 and 0.75 for width and depth.

In this approach of modeling river velocity, it is assumed that the hydraulic radius of a non-bankfull river follows the same geometric rules as bankfull discharge. Hence (5.5) and (5.6) are used to calculate the hydraulic radius in (5.2) for all discharges. Assuming that major rivers tend to have a nearly flat river bed and their width exceeds their depth by far, the assumption of a rectangular cross section is considered as acceptable for bankfull discharge. For less than bankfull discharge, which is the normal case, width and depth are scaled, but their ratio remains the same. Under natural conditions, in a flat and broad river bed, depth would decrease faster than width with falling discharge. Hence the model tends to overestimate the ratio of depth to width. As the hydraulic radius and thus

river velocity are especially sensitive to changes in depth with this first approach velocity results for less than bankfull discharge will be overestimated which has to be kept in mind regarding the results.

River slope values ($S, [m/m]$) are determined for each cell of a global 0.5° grid by GIS analysis of a digital elevation model with a resolution of 3 arc minutes ($10 \cdot 10$ values per grid cell). The 0.5° grid has been chosen for compatibility reasons with regard to the spatial resolution of WaterGAP. One cell's outflow level is estimated as mean of the five lowest elevation values at the respective cell. The slope of a river segment is calculated as elevation difference between up- and downstream cell outflow levels, divided by the product of their horizontal distance and a meandering factor which was arbitrary estimated at 1.3 as global average. The estimation of the meandering factor is based on a visual analysis of a map of actual river courses and an abstracted 0.5° drainage direction map that connects up- and downstream cells with a straight line. Although the meandering factor varies spatially it is assumed that the approximation reflects reality better than using the distance between neighboring cell centers only.

Values of Manning's roughness ($n, [-]$) vary between 0.015 and 0.07 in natural streams for flows less than bankfull discharge and reach up to 0.25 for overbank flows (Fread, 1993, p. 10.25). There is very few local data and no way to assess river roughness at the global scale. Therefore three options to estimate river roughness globally were identified.

1. use of roughness as tuning factor (based on discharge or velocity data) and regionalize in basins without validation data;
2. use of constant river roughness;
3. use of topographic and/or geologic information to estimate river roughness for each grid cell.

For the model-tests performed, roughness was determined by tuning or set constant.

5.3 Results

5.3.1 Testing the Approach

The modeling approach was tested for single river cross sections by comparing the results to an independent set of measured river velocity data. While the USGS (United States Geological Survey) provides an extensive dataset of surface water measurements for the United States of America (USGS), it turned out to be difficult to find stream flow and velocity data for other parts of the world. Thus only U.S. data could be used to validate the modeling approach. A subset of the USGS data was generated that includes 16 gauging stations representing a variety of climatic and topographic conditions as well as different basin sizes between Alaska and Florida (see Table 5.1). The validation dataset covers the period from 1970 to 2004 and contains a total of 4500 measurements of actual flow velocity and discharge.

Manning's roughness (n) was adjusted for each station to maximize modeling efficiency (Nash-Sutcliffe coefficient, NSC) which relates the goodness-of-fit of the model to the variance of the measurement data.

Table 5.1 — Gauging stations used for model testing with optimized roughness and modeling efficiency (NSC)

River / Site	State	Basin area [1000km ²]	No. of measuram.	Slope (from WGHM) [m/m]	Roughness adj.	Mean velocity (NSC) mod.	meas.	NSC
Kuskokwim/Crooked Creek	AK	80.5	134	0.0001	0.021	1.01	0.94	0.7
Yukon/Pilot Station	AK	831.4	107	0.0001	0.036	0.88	0.86	0.57
Connecticut/Thompsonville	CT	24.9	92	0.001	0.063	0.86	0.79	0.58
Apalachicola/Chattahoochee	FL	44.5	168	0.0003	0.06	0.52	0.51	0.49
Ohio/Metropolis	IL	525.8	96	0.0002	0.058	0.87	0.82	0.49
Mississippi/Clinton	IA	221.7	287	0.0004	0.077	0.58	0.57	0.55
Penobscot/West Enfield	ME	17.3	64	0.0011	0.071	0.72	0.7	0.58
Missouri/Culbertson	MT	237.1	104	0.0002	0.028	0.74	0.73	0.6
Roanoke/Roanoke Rapids	NC	21.7	56	0.0008	0.06	0.62	0.6	0.59
Red River North/Grand Forks	ND	68.1	630	0.0001	0.023	0.58	0.56	0.71
Missouri/Nebraska City	NE	1061.9	1843	0.0004	0.031	1.36	1.38	0.59
Humboldt/Imlay	NV	40.2	297	0.0008	0.041	0.37	0.37	0.59
Arkansas/Tulsa	OK	160.8	133	0.0004	0.037	0.78	0.75	0.78
Rogue/Agness	OR	10.2	96	0.0001	0.016	0.76	0.71	0.53
Brazos/Richmond	TX	92.1	188	0.0003	0.039	0.57	0.55	0.69
Sevier/Juab	UT	13.4	214	0.0009	0.035	0.46	0.47	0.74

Table 5.1 shows the modeling efficiency for tuned roughness values at the 16 stations. NSC values vary from 0.49 to 0.78 (the optimum would be 1.0). Taking into account, the only temporally variable input data was discharge (Eqs. 5.5 and 5.6) all modeling results are considered satisfactory. Since it will not be possible to optimize n by measured velocity data in a global application, it was additionally attempted to run the model with just one, average n (0.044) for all stations. Even without adjusting roughness, at 12 of the 16 stations model results proved to be better than a constant velocity of 1 m/sec which has been used in WaterGAP so far (not in the table). Using 1 m/sec constantly would lead to NSC values below zero for all stations (not in the table).

Measured and modeled river velocity from three selected stations are compared in Figure 5.1. It can clearly be seen, that the new approach estimates flow velocity far better than WaterGAPs hitherto used constant velocity of 1 m/sec (bold dashed line). Thus, the figure supports the idea of improving the flow velocity simulation within the global hydrology model WaterGAP.

In general, the modeling approach tends to overestimate flow velocity for low discharges and to underestimate it for high discharges (see Section 5.2). This suggests an imprecise determination of the hydraulic radius (too big for low discharges and vice versa). This is probably due to the approach itself (Eqs. 5.5 and 5.6) which is only valid for bankfull discharge. Discrepancies between modeled and measured velocity could also be due to uncertainties in the regression analysis carried out by Allen et. al. (1994). Further, slope input into the model only represents a mean value for a 0.5° grid cell and is projected to the location of a single gauging station. Even the flow velocity measurements might contain errors because this parameter is not easy to measure.

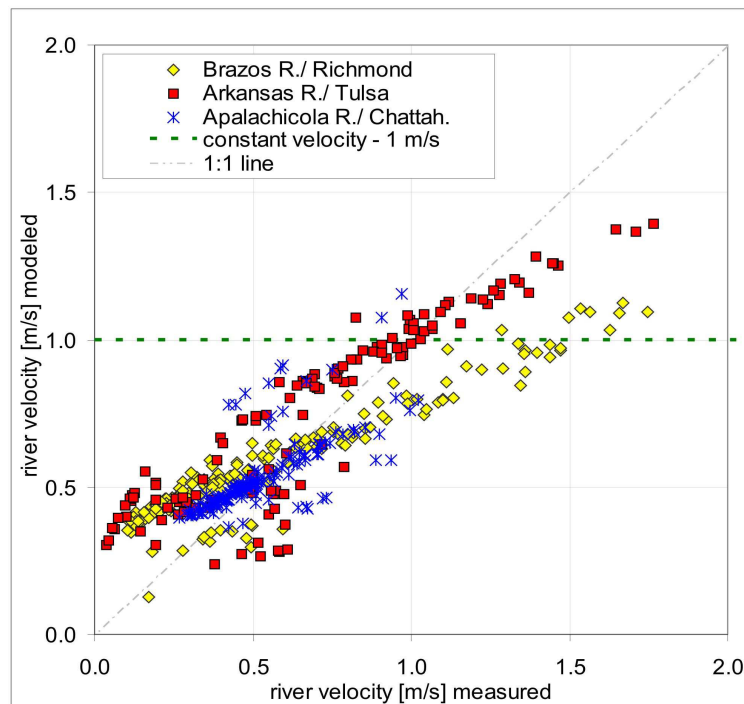


Figure 5.1— Modeled values of river velocity compared to measured values for three selected stations

5.3.2 Integrating the algorithm into a global hydrology model

Despite of the remaining uncertainties the new river flow velocity algorithm was integrated into the Global Hydrology Model WaterGAP for a tentative evaluation. The objective was to gain experience in the technical feasibility on the one hand and to get an impression of model performance in different parts of the world on the other hand.

It turned out that the flow routing time step (two hours in the standard version of WaterGAP with constant velocity) had to be adjusted dynamically. For numerical stability higher flow velocities require shorter routing time steps. To avoid excessive simulation durations, caused by very short time steps, a maximum flow velocity can be defined by the model user.

Preliminary tests of the new approach within WaterGAP were conducted for several river basins around the world. Results are rather encouraging since at least, minor improvements in modeling efficiency could be achieved for all sites tested. However, roughness adjustment and validation of the results could yet only be performed based on monthly discharge values which are, for almost all rivers, not very sensitive to river velocity.

To find out how much effort is adequate to put into the estimation of river roughness (see Section 5.2), its sensitivity to discharge and the mean residence time of water in a river basin need to be investigated in detail using WaterGAP results. Here it has also be taken into account that the influence of other processes within the hydrological cycle might overlap the influence of roughness. For example, routing through lakes and wetlands has a major impact on simulated discharge and residence time, and is not affected by the new flow velocity algorithm.

5.4 Conclusions

The goal was to find an algorithm appropriate to model flow velocity in a large scale hydrological model. In this paper, we present a simple approach which is based on the Manning-Strickler equation and the correlation of river discharge and river width and depth.

- A comparison at 16 selected US gauging stations showed that simulated river velocity fits measured values quite well, indicating a significant improvement over a constant flow velocity.
- Model results are very sensitive to river roughness. The impact of roughness on discharge and residence time will be investigated in more detail using WaterGAP. A method to estimate river roughness globally needs to be defined.
- The approach has been found suitable to be integrated into the global model WaterGAP further investigation. First test runs are encouraging.

The validation of the flow velocity impact on WaterGAP results is not yet finished. Depending on the validation results, the approach might still be modified. As the computation of river width and depth is based on Eqs. 5.5 and 5.6, valid only for bankfull

discharge, further improvements might be achieved by integrating an approach for non-bankfull discharge.

Chapter 6

Modeling Variable River Flow Velocity on Continental Scale: Current Situation and Climate Change impacts

6.1 Introduction

During the last years, global and continental scale hydrological models have frequently been applied to study current and future long term average monthly and annual discharge. These studies have been based on simple approaches to approximate flow velocities. Either a constant flow velocity has been used (Döll et al., 2003), or flow velocities were parameterized as time-independent functions of the topographic gradient (Hagemann and Dümenil, 1998), or as simple functions of discharge (Vöröshmarty et al., 1989). For single watersheds flow velocities were even adjusted manually (Nijssen et al., 1997). Recently, the fields of applications for global or continental scale models have been extended. They are applied for studying extreme discharges (Dankers and Feyen, 2008; Lehner et al., 2006) or for modeling water quality (Bouwman et al., 2005; Meybeck, 2003; Vörösmarty and Meybeck, 2004). For these kinds of studies more sophisticated lateral routing approaches are required to improve the representation of residence time of the water in the river system. The flow velocity equations of local scale models can be parameterized with catchment specific values. At the global scale however, a way has to be found to model flow velocity simple enough to derive the required parameters from data globally available and sophisticated enough to deliver realistic flow velocity values for a large variety of environmental conditions. In a few global scale models, the Manning-Strickler-formula is applied to simulate variable river flow velocities (Arora and Boer, 1999; Schulze et al., 2005; Ngo-Duc et al., 2007), which led to enhanced representations of flow velocities (Schulze et al., 2005) and discharge (Ngo-Duc et al., 2007). Schulze et al. (2005) (see Chapter 5) performed a preliminary study before implementing the Manning-Strickler-formula into WaterGAP by testing the approach with roughly 4500 flow velocity measurements of 16 gauging stations in the US. They concluded that replacing the previously applied constant flow velocity by a variable flow velocity would improve the representation of flow velocities within the

model considerably.

The approach introduced in Chapter 5 (Schulze et al., 2005) has been adapted within the scope of this study and is described in section 6.2. The routine has been implemented into WaterGAP3, which has a spatial resolution of 5 arc-minutes (longitude and latitude) globally. Further, a new method to estimate an individual river bed roughness for each grid cell globally is introduced. The modeled flow velocities are validated by comparing them to a comprehensive dataset of flow velocity measurements collected at US rivers (Section 6.3.2). WaterGAP3 is applied to model current flow velocities and residence time of water in rivers throughout Europe, the focus region of this study. The number of days the water needs from the spring to the mouth at 13 major rivers in Europe is compared and the impact of the dynamic flow velocity on simulated on discharge hydrographs and flood discharge is analyzed (Sections 6.3.3 and 6.3.4). Finally the impact of three climate change projections on residence time and flow velocity for the 2050s in Europe is assessed and discussed (Sections 6.4 and 6.5).

6.2 Methodology

The Manning-Strickler formula is widely applied to calculate river flow velocity (v) as a function of the river bed roughness (n), also named Manning's n , the hydraulic radius of the river channel (HR) and the river bed slope (s).

$$v = n^{-1} \cdot HR^{\frac{2}{3}} \cdot s^{\frac{1}{2}} \quad (6.1)$$

In the following subsections is explained how the single parameters of Eq. 6.1 are derived for the application within WaterGAP.

6.2.1 River Bed Slope

The river bed slope used in WaterGAP is calculated based on high resolution elevation data (SRTM30), the HydroSHEDS drainage direction map (Lehner et al., 2008) and an individual meandering factor for each grid cell. All datasets are consistently based on the SRTM dataset (Farr et al., 2007). The HydroSHEDS dataset provides stream networks on different spatial scales globally. Out of it, the main river sinuosity of each 5 arc-minute grid cell has been calculated from the subjacent 15-arc second stream network. The resulting meandering factors range from 1 to 6.41 globally with an average sinuosity of 1.17. The application of the meandering factor leads to an improved representation of real river lengths compared to those calculated from the direct distance between the raster cells (Table 6.1).

As a first attempt, we calculated the river bed slope from the mean elevations of adjacent grid cells but got far too high slopes for a number of cells and consequently unrealistically high flow velocities. This occurred in particular in low mountain ranges or at the edges of high mountains. We got more realistic results by deriving 25 sub elevations for each 5 arc-minute raster cell from the SRTM30 dataset. Then we calculated the vertical height between the lowest sub elevation of each 5 arc-minute grid cell and its downstream neighbor cell, assuming that the main river flows in the lowest altitudes of the grid cells.

Table 6.1— River lengths [km] of exemplary rivers with and without considering the individual meandering ratio (MR).

River	River Length Derived from:		
	Measured (e.g. EB, 2009)	Direct Cell Distance	Considering MR
Danube	2850	2539	2845
Rhine	1390	1057	1243
Elbe	1091	817	1000
Weser	440	287	351
Rhone	813	692	810
Guadiana	742	621	734
Ebro	910	620	761
Po	652	534	638
Dnjepr	2201	1711	2010
Vistula	1047	921	1098
Glomma	604	522	571
Thames	346	242	292

However, there remains an overestimation of the derived river bed slope in a number of grid cells, especially in the regions mentioned above. If required, the slope of these grid cells can to be adjusted manually. To finally derive the river bed slope (Figure 6.1), the vertical difference has been divided by the product of the direct horizontal distance between the raster cell centers and the individual meandering factor.

Due to the coarse resolution and schematic drainage direction map, negative or zero slopes arise. For such raster cells it is reasonable to adjust slope values based on slopes of adjacent grid cells rather than just to use a pre-defined minimum slope. If the direct downstream neighbor cell does not provide a positive slope, the model is allowed to look in up to 10 downstream cells for a valid slope value. Only if no positive downstream slope is available, the value of this grid cell is set to a minimum slope of 0.0001 m/m.

6.2.2 Hydraulic Radius

The hydraulic radius (HR) changes with actual discharge and is thus the dynamic variable within the Manning-Strickler-formula (Eq. 6.1). Due to our global scale approach, we assume a trapezoidal river channel with a side slope of 0.5. HR of a trapezoidal channel is calculated as a function of river bottom width (W_{bottom}) and river depth (D).

$$HR = \frac{D(2D + W_{bottom})}{W_{bottom} + 2D\sqrt{1 + 2^2}} \quad (6.2)$$

Channel form and discharge are closely related. River top width (W) and D can be approximated with catchment specific coefficients (a , c) and exponents (b , f) (Leopold and Maddock, 1953; Dunne and Leopold, 1978, chap. 16).

$$W = aQ^b \text{ [m]} \quad (6.3)$$

$$D = cQ^f \text{ [m]} \quad (6.4)$$

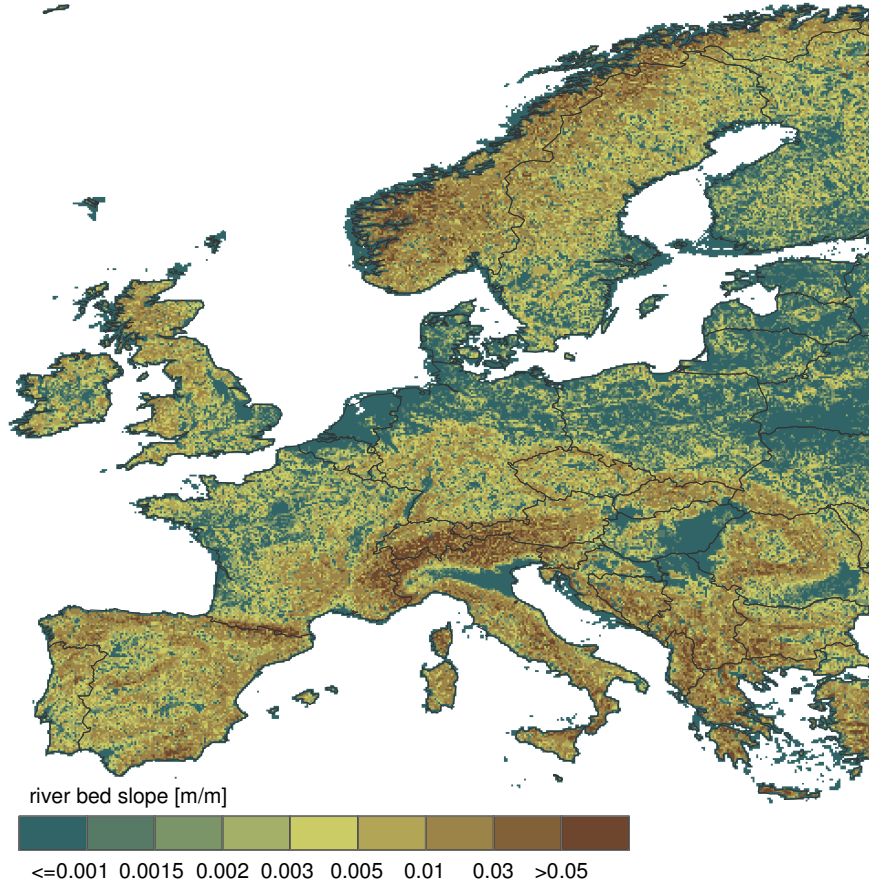


Figure 6.1— Approximated river bed slopes in Europe [m/m]

Allen et al. (1994) applied Eqs. 6.3 and 6.4 to data of 674 river cross sections across the USA and Canada and found empirically the best-fit coefficients and exponents for bankfull flow (Q_{bf}) conditions:

$$W_{bf} = 2.71Q_{bf}^{0.557} \text{ [m]} \quad (6.5)$$

$$D_{bf} = 0.349Q_{bf}^{0.341} \text{ [m]} \quad (6.6)$$

We used the 1.5-year flood return discharge as surrogate for Q_{bf} (Schneider, 2009), calculated the W after Eq. 6.5 and out of it W_{bottom} of the river, which remains constant for each river section.

$$W_{bottom} = W_{bf} - 2 \cdot 2D \text{ [m]} \quad (6.7)$$

To solve Eq. 6.2 for each time step, we had to find a robust approach that delivers realistic river depths from actual discharge. In our analysis we found that Eq. 6.6 is also suitable to approximate D from actual discharge in order to calculate average daily and monthly flow velocities. Of course, the coefficients c and f of Eq. 6.4 can be adjusted individually for single watersheds if required.

6.2.3 River roughness (Manning's n)

For field studies, river bed roughness (n) can be estimated using established lists with photographs of rivers (Barnes, 1967) or it can be used as tuning parameter for small scale hydrological models. On the global scale however, comprehensive datasets with roughness data are not available. Schulze et al. (2005) identified three options to estimate river bed roughness worldwide (see 5):

1. Usage of constant river roughness,
2. usage of roughness as a tuning factor (regionalized in ungauged basins),
3. usage of topographic and/or geologic information to estimate river roughness for each grid cell.

A constant river velocity of 0.035 is used by the global scale approach of Arora and Boer (1999). Schulze et al. (2005) found that flow velocity results can be improved by optimizing roughness values. They tentatively used n as a tuning parameter when validating the approach before implementing it into WaterGAP. Ngo-Duc et al. (2007) derived n for each grid cell as a function of the cross sectional area, the hydraulic radius and the channel slope.

In this paper we introduce a new method to estimate Manning's n for the application in global scale models according to the third point in the list above. Our approach is based on Cowan (1956) who describes the total roughness (n) as the sum of a series of contributions from different spatial characteristics (n_x , see Table 6.2), enhanced by a river sinuosity factor (m).

$$n = (n_b + n_1 + n_2 + n_3 + n_4)m \quad (6.8)$$

Cowan's approach is originally designed for in situ estimations of Manning's n . We use different physiographic parameters and information about rural and urban areas to parameterize Eq. 6.8 with the values given by Cowan (1956) to derive an average n for each 5 arc minute grid cell of WaterGAP. The values used are summarized in Table 6.2.

For the base value n_b , we assume that mountainous rivers are cut into rock ($n_b = 0.025$), and non-mountainous areas are rivers in sand ($n_b = 0.02$). A global 5 arc-minute map of mountains has been derived after the approach introduced in section 4.2.1. Surface irregularities in rivers (n_1), such as eroded banks or exposed tree roots, are very special local conditions and cannot be parameterized in our global approach. Thus we assume "minor" surface irregularities globally ($n_1 = 0.001$). In urban areas rivers are frequently channeled and consequently the channel cross section usually does not vary significantly on small scale. Still, there are quite some exceptions to this assumption and therefore we parameterize n_2 quite carefully with low values: n_2 is set to 0.0 in urban areas (Cowan (1956): "*size and shape of channel cross sections changes gradually*") and $n_2 = 0.005$ in rural areas (Cowan (1956): "*large and small sections alternate occasionally*"). The GRUMP dataset (GRUMP, 2004) is used as the source for urban and rural areas. Enhanced roughness due to obstructions, such as logs, boulders, debris, or bridge piers are considered by n_3 . Here we assume that in urban areas obstructions such as bridge piers occupy 5% to 15% of the cross sectional area ("*minor*": $n_3 = 0.01$). The same value is used for mountainous areas with a river slope $> 2\%$, where we assume a considerable

Table 6.2— Values used to estimate the river roughness for the application in WaterGAP. After Cowan (1956), modified:

n_b	base value	mountain	0.025
		non-mountain	0.02
n_1	surface irregularities		0.001
n_2	variations in channel cross section	urban area	0.0
		rural area	0.005
n_3	obstructions	urban area	0.01
		mountain with river slope > 2%	0.01
		other areas	0.002
n_4	vegetation in river bed		0.005
m	modifying value for meandering	meandering ratio 1.0 - 1.2	1.0
		meandering ratio 1.2 - 1.5	1.15
		meandering ratio 1.5	1.3
		urban areas	1.0

amount of debris and boulder in the channel. For all other areas we apply $n_3 = 0.002$. The amount of vegetation in the river bed (n_4) depends on complex local conditions such as water quality, time of the year and vegetation types in the river. We do not have such information on global scale with the WaterGAP version applied, so we use $n_4 = 0.005$ ("low") globally. We determined the modifying value for meandering (m) from the meandering factor, which has been introduced in Section 6.2.1.

The global roughness values cover a range between 0.033 and 0.0598 with a mean roughness of 0.0359 globally. The resulting roughness values have been analyzed for all European countries except Russia. The average European roughness is 0.0358, slightly lower than the average global roughness. 55% of the 5 arc minute raster cells have a Manning's n between 0.033 and 0.035 (Figure 6.2). For European mountains, roughness values between 0.04 and 0.06 are estimated (Figures 6.2 and 6.3), whereas 30% have a roughness of 0.04 and 41% a roughness of 0.0475. This is in accordance with Chow (1959), who specifies roughness coefficients of 0.04 and 0.05 for mountain streams.

Cowan (1956) points out that his approach is valid for rivers with a hydraulic radius below 4.57 m (15ft) only. For Europe, the hydraulic radius of mean discharge 1961-2002 lies below this threshold in 99.3% of all grid cells. Nevertheless, we do apply the approach for large rivers as well, since we do not exhaust the whole range of possible roughness values of Cowan's approach and keep the roughness values in a comparably small range. Chow (1959) provides a wide range of possible roughness values between 0.025 to 0.1 for "major streams". According to his definition, major streams have a top width at flood stage > 31 m (100ft). 95% of the WaterGAP grid cells with a river top width at bankfull stage above 31 m have a roughness value in the medium range, between 0.033 and 0.04. Due to the spatial scale, many simplifications have to be taken into account to derive a river bed roughness with the approach introduced. However, this approach is easily reproducible, delivers realistic roughness approximations and is well suitable to be applied in

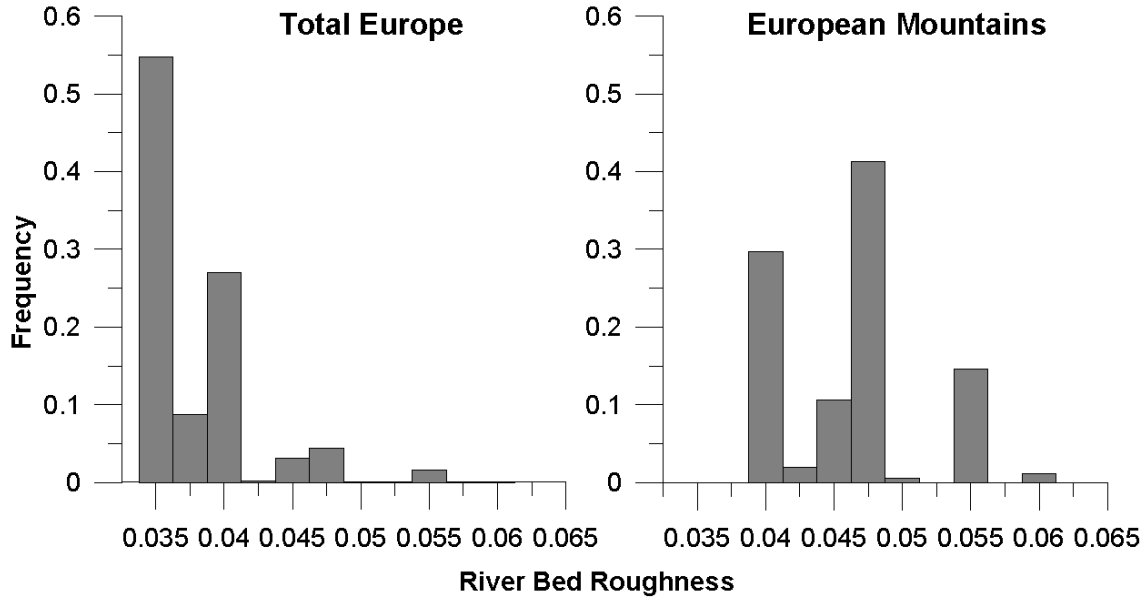


Figure 6.2— Histograms of river roughness in entire Europe (left) and European mountains (right)

sub-continental to global scale studies. In addition, this approach allows the consideration of anthropogenic disturbances of natural rivers.

6.2.4 Lateral Routing

The total runoff produced within each grid cell and the volume of water coming from the cell upstream is transported through a series of linear and nonlinear retention storages representing lakes, reservoirs, wetlands and the river itself (Figure 6.4). The lateral transport within WaterGAP is described in detail in Kaspar (2004) and Döll et al. (2003). Here we adapted this approach to enhance computing time and avoid running into any numerical stability problems (see Section 5.3.2).

Water flow between grid cells is assumed to occur only as river discharge. The total cell discharge is routed according to the newly developed drainage direction map (HydroSHEDS Lehner et al., 2008) to the next downstream cell. The HydroSHEDS scheme describes the estimated flow routing between approximately 180.000 grid cells representing the total land surface of Europe on 5 arc-minute grid cell size. The cells are connected to each other by their respective drainage direction and are thus organized into drainage basins. Each cell can drain into only one of the eight neighboring cells. To ensure computing hierarchy of water flowing downstream we introduced a specific routing order for each grid cell. The resulting cell outflow becomes the inflow of the downstream cell.

Storage change in the river segment (dS_r) can be described with equation of continuity:

$$\frac{dS_r}{dt} = Q_{r,in} - Q_{r,out} \quad (6.9)$$

The storage routing is based on a linear storage discharge relationship as follows:

$$Q_{r,out} = \frac{1}{k_r} S_r \text{ with } k_r = \frac{1}{v} \quad (6.10)$$

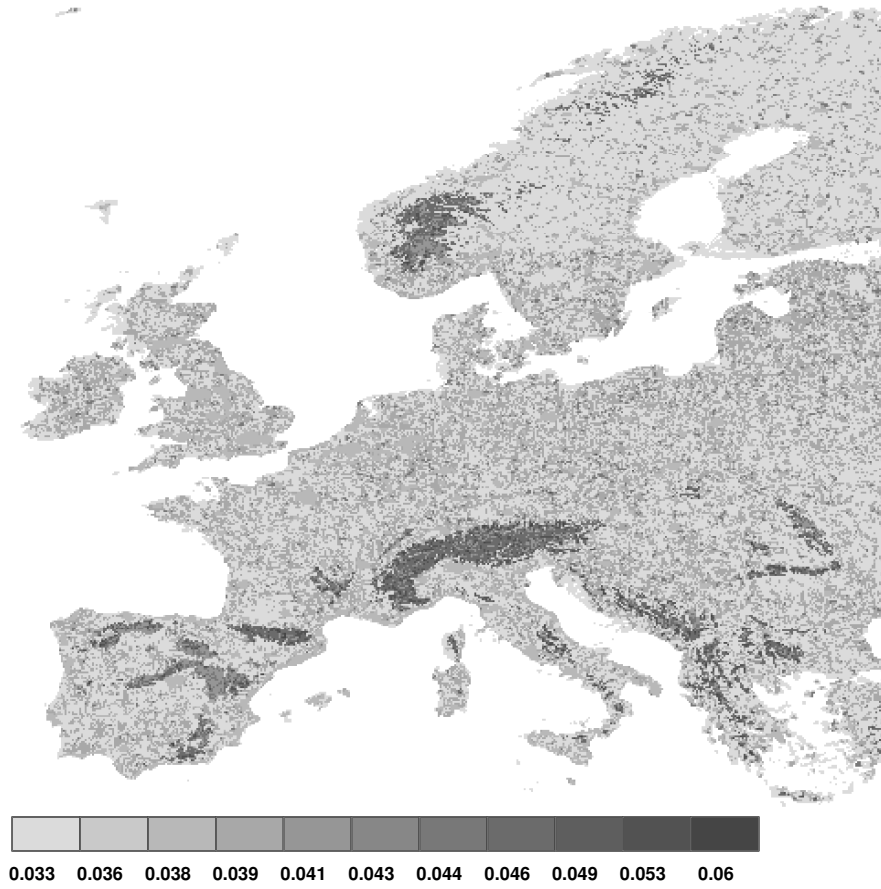


Figure 6.3— Approximated roughness values for Europe.

where $Q_{r,in}$ = river inflow from upstream [km^3/d], $Q_{r,out}$ = river discharge to downstream cell [km^3/d], k_r = storage coefficient in river segment [d], l = river length in grid cell [km], and v = river flow velocity [km/d].

The equation of continuity (Eq. 6.9) can be solved using Eq. 6.10 to give the response of a linear storage (Dyck and Peschke, 1995):

$$S_r = S_{r0} \cdot e^{-\frac{t}{k_r}} + k_r \cdot Q_{r,in} \cdot (1 - e^{-\frac{t}{k_r}}) \quad (6.11)$$

where S_{r0} [km^3] denotes the river storage from the previous time step.

River flow velocity is used as expressed in Eq. 6.1 and the representation of real river lengths is calculated from the direct distance between the raster cells applying the meandering ratio (see section 6.2.1). Eq. 6.11 can be applied for any given time step, so we chose a time step of one day as it is the case for all other temporal resolutions within WaterGAP.

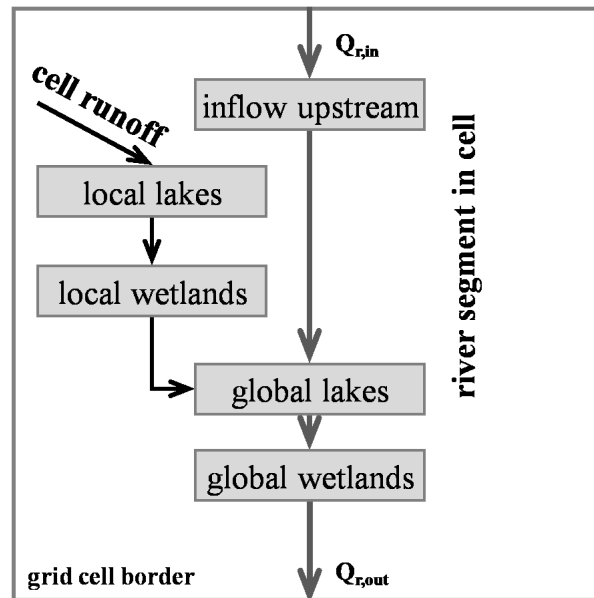


Figure 6.4— Routing scheme of WaterGAP

6.3 Results for the Current Situation

6.3.1 River flow velocity in Europe

The average annual river flow velocity for the period 1971-2000 has been computed for Europe (Figure 6.5). It can be seen that river flow velocities in mountains are significantly higher compared to lower regions, due to the comparably steep river bed slopes (Figure 6.1). Large rivers stick out as well, caused by the positive discharge - velocity correlation. The calculated average European river flow velocity is 0.62 m/sec. This is considerably lower than the constant flow velocity of 1 m/sec, which has been used in previous WaterGAP versions. Merely 19% of the European grid cells have an average flow velocity of 1m/sec or above.

6.3.2 Validation of river flow velocities

The intention was to compare the modeled river flow velocity with measured data. It turned out to be difficult to find substantial datasets with flow velocity data for a variety of rivers in Europe. However, the USGS (United States Geological Survey) provides a comprehensive dataset with flow velocity and stream flow data (USGS). 22 US rivers with catchment sizes between roughly 10,000 and 1,000,000 km² have been selected. The US-dataset has been found very valuable to validate our model, because the watersheds cover a variety of climatic and topographic regions between Oregon and Florida (Table 6.3). Available velocity data for the period 1961 - 2002 have been applied, in total more than 9000 values. The number of available velocity data varies between the sites (Table 6.3).

From the data sample of each gauging station, the average flow velocity and the related standard deviations has been computed and compared to the average modeled flow velocity

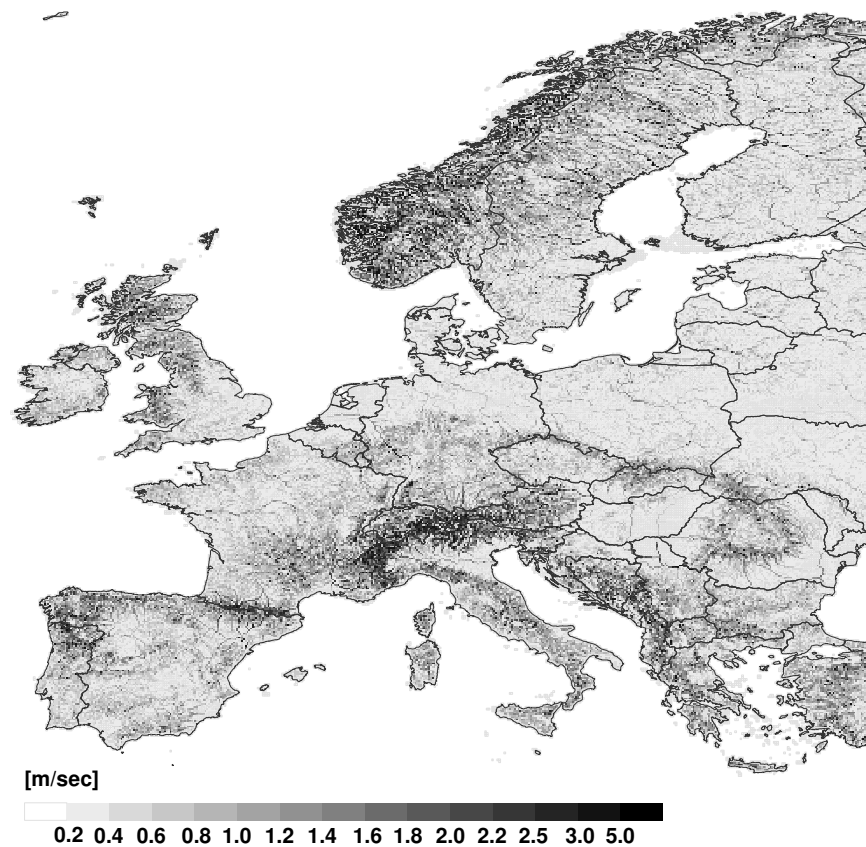


Figure 6.5— Average annual river flow velocities for 1971-2000 in Europe (WaterGAP results)

of the related 5 arc minute grid cell. Only modeled velocity data of days with a measured velocity values have been considered. The simple approach to compute river flow velocities within WaterGAP allows an approximation of real river values only. In addition it should be considered that instantaneous point measurements are compared to the modeled daily flow velocities of a 5 arc minute grid cell, based on pseudo-daily climate data (see Section 2.5). Thus, there is a high uncertainty of the comparison shown in Figure 6.6. It can be seen that the modeled average river flow velocity WaterGAP matches the magnitude of the measurements satisfyingly. However, the difference between modeled and measured velocities varies between the single sites. At nine of 22 sites, the range of the modeled average flow velocity including the error bars (showing the standard deviation) lies within the range of the measured flow velocities (e.g. Red of the North, Sevier, Kansas, Hudson Rivers). At 17 stations, WaterGAP overestimates the average measured flow velocities. This can be attributed to an overestimation of either the discharge or the river bed slope of the respective grid cell, as discussed in Section 6.2.1. Also tidal effects, which influence the flow velocity at gauging stations close to coastal river mouths in reality, are not considered within WaterGAP. The velocity is underestimated by WaterGAP at the remaining five gauging stations (Humboldt, Sevier, Missouri (at Nebraska), White, and Grand Rivers). Figure 6.6 also shows that the range of the velocity measurements is larger than the range of the WaterGAP results. This indicates that flow velocity processes are more complex in

Table 6.3— Gauging Stations with flow velocity data

River	Site	State	Catchment area [10 ³ km ³]	No. of velocity measurements
Red of the North	Grand Forks	ND	75.7	908
Humboldt	near Imlay	NV	42.3	286
Sevier	near Juab	UT	12.1	206
Missouri	near Culbertson	MT	238	99
Missouri	Nebraska City	NE	1,058	4210
Kansas	Desoto	KS	155	216
Wabash	Mt. Carmel	IL	73.8	152
White	DeValls Bluff	AR	59.7	202
Grand	Grand Rapids	MI	13.6	112
Rogue	near Agness	OR	9.13	117
Hudson	Green Island	NV	42.3	31
James	near Richmond	VA	17.1	65
Roanoke	Roanoke Rapids	NC	22.3	83
PeeDee	Peedee	SC	22.7	280
Altamaha	Doctortown	GA	36.4	232
Pearl	near Bogalusa	LA	18.3	314
Escambia	Near Century	FL	10.5	135
Suwanee	Branford	FL	21.2	266
Nueces	near Mathis	TX	43.3	428
Colorado	Wharton	TX	108	182
Neches	Evadale	TX	21.1	341
Green River	Green River	UT	108	271

reality than WaterGAP is able to reproduce with the simple approach applied. However, despite of all errors and uncertainties shown, the variability of average flow velocities between the single rivers and between different discharge levels is reproduced considerably better by applying the variable flow velocity than with a constant flow velocity of 1 m/sec. The average velocity of small catchments (e.g. Humboldt near Imlay or White River at DeValls Bluff) is calculated to be considerably below 1 m/sec, which is also shown by the related measurements. The measured and modeled velocities rise during high discharges in most watersheds oftentimes above 1m/sec. The velocity measurements also show that the average flow velocities of various river types are below 1m/sec, which is reproduced in most cases by WaterGAP.

6.3.3 Effect of the dynamic flow velocity on river discharge

To assess the effect of the variable flow velocity on discharge hydrographs, we computed monthly river discharge with (a) using a constant river flow velocity of 1 m/sec and (b) the newly implemented dynamic flow velocity. Both simulations have been compared to measured discharge of 157 European gauging stations for the period 1961-2002 (if data available, else shorter time series were applied) by computing the Nash-Sutcliffe-Coefficient (NSC). In general, the differences between the two simulations are quite small. The low and medium flows change marginally only. However, the dynamic flow velocity causes

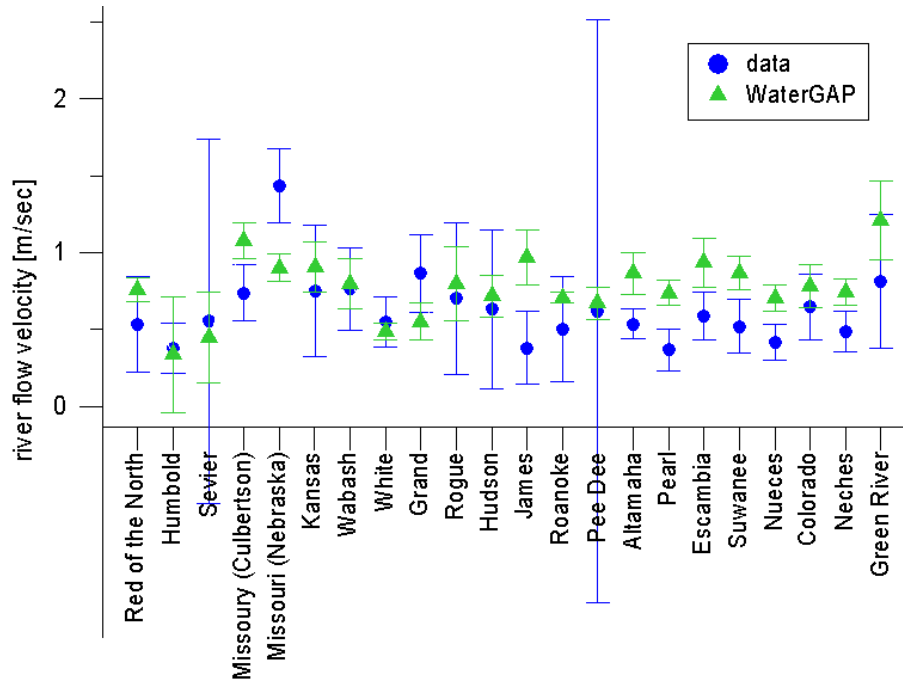


Figure 6.6— Comparison of average simulated and measured river flow velocity at 22 US gauges. The error bars indicate the standard deviations.

slightly heightened discharge peaks in most investigated cases. This leads to a lower NSC at gauging stations, where maximum flow has so far been overestimated with the constant flow velocity (Figure 6.7, top) and to an improved NSC at stations with previously underestimated discharge peaks (Figure 6.7, bottom). This effect is discussed with more detail in section 6.3.4. A clear conclusion, whether the discharge improves or worsens due to the implementation of the variable river flow velocity, cannot be drawn. The NSC improved in 30% of the stations and remained constant or worsened at the remaining stations.

6.3.4 Effect of the dynamic flow velocity on floods

Within the scope of this thesis, WaterGAP has been improved to enhance its capability to simulate floods. Lateral flow processes are crucial for the routing of the flood discharge through the river network. The flow velocity is considerably higher during flood events than at medium flow rates. This effect is not taken into account when applying a constant river flow velocity. The impact of the implementation of the variable flow velocity on large floods has been assessed by comparing the magnitude of the relative change between 100-year flood discharge derived from WaterGAP results with constant and variable flow velocity, respectively, and from measured data. The 100-year flood discharge (see Section 7.2.2, p.97 for details) has been calculated from daily discharge time series of 100 European gauging stations. Only gauging stations with at least 20 years of full daily data records between 1950 and 2002 have been chosen for the comparison, because the calculation of flood discharge requires comparably large sample sized to deliver reliable results. The stations are located throughout Europe (see Figure 6.8). In 46 of the 100

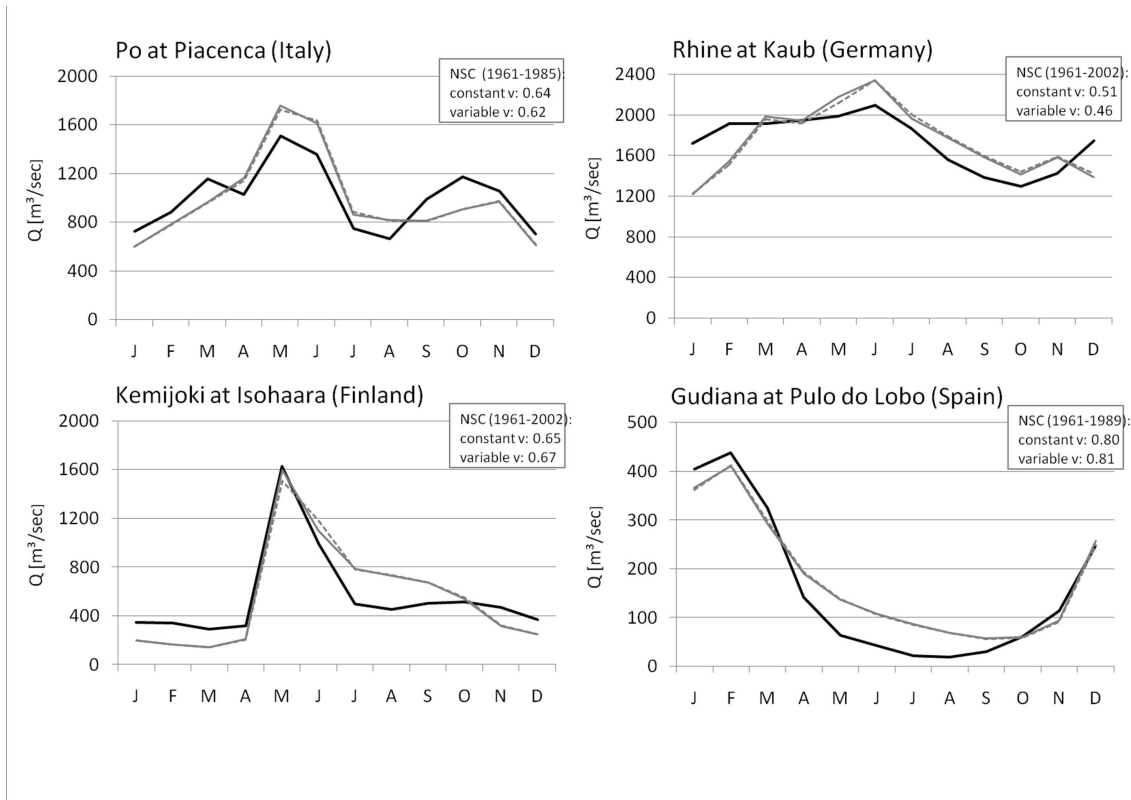


Figure 6.7— Effect of the variable flow velocity on average long term monthly discharges at four European gauging stations. The black line indicates measured values, the solid grey line the simulation applying a variable flow velocity and the grey dashed line, the WaterGAP simulation with constant flow velocity. Further the Nash-Sutcliffe-Coefficients (NSC) for the two WaterGAP hydrographs are shown.

gauging stations, the 100-year flood discharge calculated with the variable flow velocity was worse and at 45 stations better than the flood discharge calculated with constant flow velocity. At 9 stations there was no difference.

The flood peak calculated with variable flow velocity is generally higher than the one that has been derived from the constant flow velocity run. During flood events, the flow velocity is usually considerably higher than 1 m/sec. This leads to accelerated lateral transport from the upper to the lower grid cells within a watershed, causing the enhanced flood peak. Consequently, the flood discharge improved at stations, where flood peaks have been underestimated when applying the constant flow velocity and vice versa. No change between the two WaterGAP runs occurs mainly in Finnish rivers, which are flowing through large lakes (Figure 6.8). Here the balancing effect of the lakes is stronger than the effect caused by the different flow velocity approaches. No clear picture can be drawn, whether there is an improving effect of the variable flow velocity on large or small rivers. The 100-year flood discharge improved at most stations of the Rhine and worsened in other large rivers such as the Elbe or parts of the Danube. In most cases the same effects (improvement or worsening) can be found in all stations of the same river. This is not surprising, since the flood discharge is transported downstream and consequently an

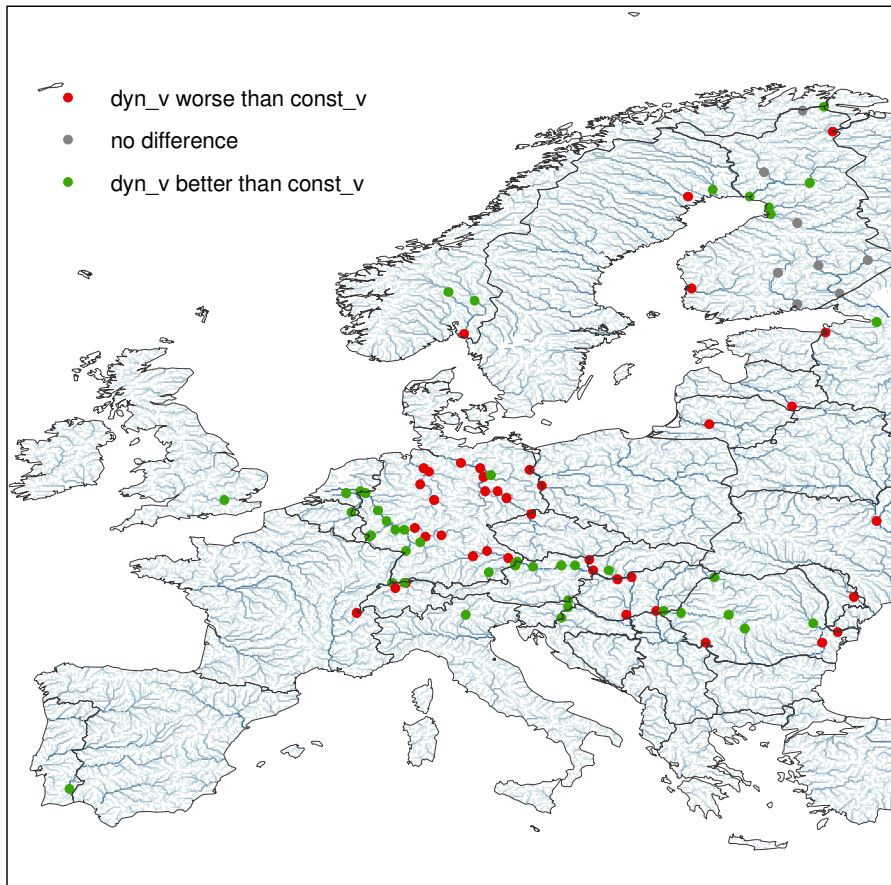


Figure 6.8— The figure compares the goodness of 100-year-flood discharges calculated with constant and variable flow velocity, respectively, being compared to the related flood discharge from discharge measurements.

overestimation of the flood peak at an upstream station can be retrieved at the downstream stations again. An exception is the Danube. Here flood peaks worsen at the German gauging stations of this river, improve at most Austrian gauges and worsen again in the lower part of the river. However, the Danube is considerably longer than all other European rivers and covers different physiographic regions. Therefore the hydrological processes behind the flood formation and WaterGAPs ability to reproduce those differ within the catchment. In general the flood discharges in western Europe and the Mediterranean region improved. With the exception of the Rhine, most flood peaks worsened at most Mid-European gauging stations. No clear picture can be drawn in northern and eastern Europe. WaterGAPs capability to simulate floods is discussed in detail in Chapter 7.

6.3.5 Residence time in rivers

The average annual residence time of the water in rivers can be deduced from the river flow velocity and the distance to the river outlet. In our case, the residence time of each grid cell is defined as the number of days that the water in a river needs to reach the

river mouth. Average values for the period 1971-2000 (Figure 6.9) have been calculated. Retention time in lakes or reservoirs through which a river flows is not considered. Thus, residence times in catchments with large lakes, dams or reservoirs are significantly higher in reality. This applies for example for the Rhine, which flows through Lake Constance, the Rhone, which enters Lake Geneva and for strongly regulated catchments like the Guadiana (Spain).

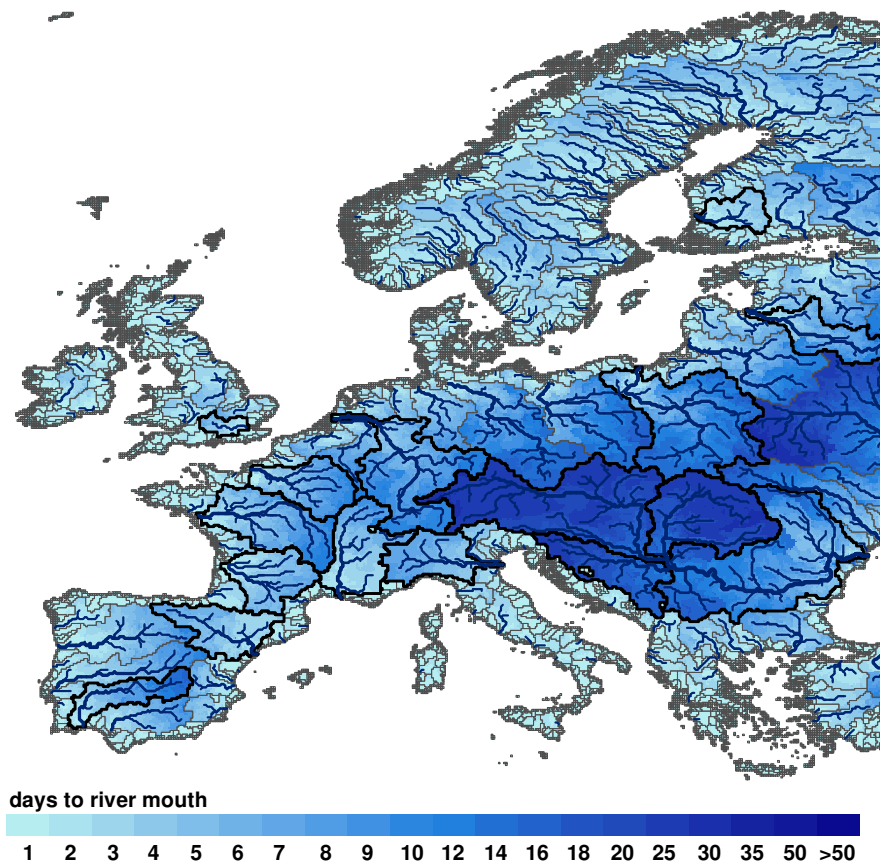


Figure 6.9— Number of days that the water needs on average to reach the river mouth (residence time). The values were calculated from average annual WGHM results 1971-2000. Watersheds that are investigated in more detail are outlined with a bold black line.

We have selected 13 rivers across Europe (Figure 6.9) and compared the theoretically undisturbed flow time from the river source to the mouth between these rivers (Table 6.4). One can see that the water of the rivers Daugava, Vistula, Guadiana and Thames need a comparably long time from the river source to the mouth. This is caused by different reasons. Water of the Polish river Vistula needs approximately 14 days for roughly 1100 km from the river source to the mouth. The river has a catchment area of 194,424 km² and an average discharge of 1080 m³/sec at the river mouth. However, the mean river flow velocity is below 1m/sec in most river reaches. This is caused by the low river bed slope in the whole catchment area. Water of the

Thames River takes seven days to reach the mouth, which is 292 km away from the spring (WaterGAP river scheme). The river has river flow velocities well below 1 m/sec and even below 0.5m/sec in its upper third. The Thames has a comparably small watershed and drains around 13,000 km only. As a consequence, the average discharge in London is with 66 m³/sec comparably low. In addition, southern England is a flat region, leading to low river bed slopes. The Guadiana drains a considerably larger area (66,800 km²) but due to the climatic conditions and water use for agriculture, the river has low average discharge only (80m³/sec), which is very irregular over the year (Figure 6.7). Here the low discharge causes the low flow velocity, especially during summer. So the water takes around 11 days for approx. 740 river kilometers. The real duration is significantly higher, since the river flows through a number of reservoirs. The river Rhine on the other hand flows on average quite fast and water stays only 10 days in the 1250 km river system until it enters the ocean. This is due to the steep slopes in the Swiss part of the Rhine and the comparably large discharge volume. Even after exiting Lake Constance, the residence time of the water amounts slightly more than 8 days for 1000 km.

Table 6.4 also lists the distances from river source to the mouth; measured (e.g. EB, 2009) and from the WaterGAP river network (derived from DDM5 and a meandering factor). The model derived flow lengths are below the literature values in most cases. Here the simplified stream network of the model underestimates the river meandering or ignores river loops. This is especially true for the Ebro and the Seine. In contrast, the simplified river network of the model overestimates the river length of the Danube and the Vistula by 5.4% and 4.8%, respectively. Here the river course is more straight and direct than what the WaterGAP river scheme can picture.

6.4 Climate change impacts on flow velocities and residence time

It is commonly known that climate change alters the hydrological cycle and thus the terrestrial hydrological system. There is high confidence that water availability will increase by mid-century in high latitudes and that, among other regions, the Mediterranean will suffer from a decrease in water resources (IPCC, 2007a, p.49). Changing river discharge impacts the average flow velocity and residence time of the water in the river system. But how strong is this effect and which European regions will especially be affected? To answer this question, we have chosen three climate change projections for 2050 (2040-2069) from the ensemble of GCMs and scenarios analyzed within the Fourth IPCC Assessment Report (IPCC, 2007a).

- **IPCM-A2:** IPSL-CM4, Institute Pierre Simon Laplace, France
A2 scenario: high temperature increase, low precipitation increase or decrease ("dry projection"),
- **MIMR-A2:** MICRO3.2, Center for Climate System Research, University of Tokyo, Japan
A2 scenario: high temperature increase, high precipitation increase or low decrease ("wet projection"),

Table 6.4— Mean residence time in selected European rivers during the reference period and projected future changes due to climate change impacts. The scenario values refer to the whole catchment including all tributaries.

River	Distance from river source to mouth [km] ^a	Approximated time [days] from river source to mouth - reference period ^b	average change [%] of all grid cells in basin between reference period and 2050s		
			IPCM	MIMR	MPEH5
Kokemäenjoki	121 (104)	1	0.1	-1.9	-2.4
Daugava	1020 (998)	11	-0.1	-5	-2.3
Vistula	1047 (1098)	14	1.3	-3.8	-1.2
Rhine	1390 (1243)	10	3.5	-1.5	-0.2
Thames	346 (292)	7	2.8	0.1	0.6
Seine	776 (600)	10	4.3	-0.3	0.2
Loire	1013 (975)	11	7.1	1	2.1
Danube	2850 (2845)	27			
Danube (East)			6.9	0.8	3
Danube (West)			3.2	-1.4	-0.9
Tisza (Danube trib.)			4.4	-0.2	0.4
Sava (Danube trib.)			3.6	-0.7	-0.1
Garonne	575 (505)	5	6.5	0.7	1.1
Po	652 (637)	7	3	-0.2	0.4
Rhone	813 (810)	7	3.2	-0.4	0.1
Ebro	910 (761)	7	4.7	-0.2	-0.1
Guadiana	742 (734)	11	-0.5	-3	-3

^adistances as considered by WaterGAP in brackets.

^bretention times in lakes are not considered

- **MPEH5-B1**: ECHAM5/MPI-OM, Max-Planck Institute for Meteorology, Germany
B1 scenario: small temperature increase, average precipitation change ("intermediate projection").

These scenarios are hereafter referred to as "IPCM-A2", "MIMR-A2" and "MPEH5-A2". The A2 scenario "describes a very heterogeneous world with high population growth, slow economic development and slow technological change" (IPCC, 2007a, p.44). The B1 world is a convergent world with a global population that peaks in mid-century and rapid changes in economic structures toward a service and information economy.

The three projections IPCC-A2, MIMR-A2 and MPEH-B1 cover a wide range of possible futures and the WaterGAP results driven by the GCMs differ in large areas (Figures 6.10 and 6.11). From this follows that the level of confidence is high in regions where all three models agree. This study considers climate change impacts on rivers system only. Alterations in water availability due to human water use e.g. for irrigation, industrial purposes

or households are not considered. The future 30-year time series that have been applied to drive WaterGAP, were derived by the delta change method as described in Section 2.5.3. The projected changes in river flow velocity differ strongly between the scenarios (Figure 6.10). Strongest effects in Northern and Southern Europe are projected by the IPCM-A2 based results. Here, increased river flow velocities by 2% to 10% are projected for large parts of the Scandinavian Mountains, caused by increased water availability. However, the IPCM-A2 driven calculations project a decrease in water resources over middle and southern Europe, which leads to a slower river flow. The MIMR-A2 based calculations show an enhanced river flow velocity over northern Europe and large parts of mid- and southern Europe. A velocity decrease can be seen in a few regions only, which are the northwestern and southeastern part of the Iberian Peninsula, southern Italy and the Aegean Region (Greece and Turkey). MPEH-B1 basically defines the same patterns as MIMR-A2 but with a lower rate of change in most regions. This is caused by the comparable low temperature and precipitation changes in the B1 scenario. However, the MPEH-B1 driven calculations show a stronger decrease in flow velocity in Mid- and Southern France, which leads to an increased residence time in the upper Seine and northern Garonne basins compared to the MIMR-A2 driven WaterGAP results (Figure 6.11). All three projections agree in showing an increased river flow velocity of 2% over parts of the Scandinavian mountains. They show a decreased river flow by at least -2% in Northwestern Spain, in parts of central and south-eastern Spain as well as in some areas of south-eastern Europe. No change, defined as $\pm 2\%$ change, is found in Ireland, Mid- and North Great Britain.

The residence time of the water in the river system, i.e. the number of days that the water needs to reach the river mouth, ignoring retention in lakes, reservoirs and wetlands, is directly derived from the river flow velocity. Thus, the patterns shown in Figure 6.10 are in agreement with those of the changes in residence time of the water in the river system (Figure 6.11). However, the magnitude differs. It turns out that the changes in river flow velocity are somewhat higher than the related changes in the residence time.

Table 6.4 lists the average changes in residence time of the 13 selected watersheds. The Danube is by far the largest watersheds and has therefore been divided into four sub-catchments (see Figure 6.11). Simulations based on all three projections show an average decrease in residence time between -0.1 and -5.0% in the Daugava and between -0.5 and -3.0% in the Guadiana watershed. Here the flow velocity increases on average, which can be seen in Figure 6.10 (lower right). All three projections expect an increasing residence time for the Thames (0.1% - 2.8%), the Loire (1.0% - 7.1%), the eastern part of the Danube (0.8% - 6.9%) and the Garonne (0.7 - 6.5%). In all cases, the lowest increases are based on MIMR-A2 and by far the highest increases are projected by IPCM-A2 except for the Daugava and Guadiana watershed. Here it is the other way round. IPCM-A2 projects least decreases whereas highest increases are projected by the MIMR-A2 based results. The projections show contradictory results for all other selected watersheds. IPCM-A2 shows an increasing residence time in all remaining catchments while MIMR-A2 based calculations predict a decreasing residence time.

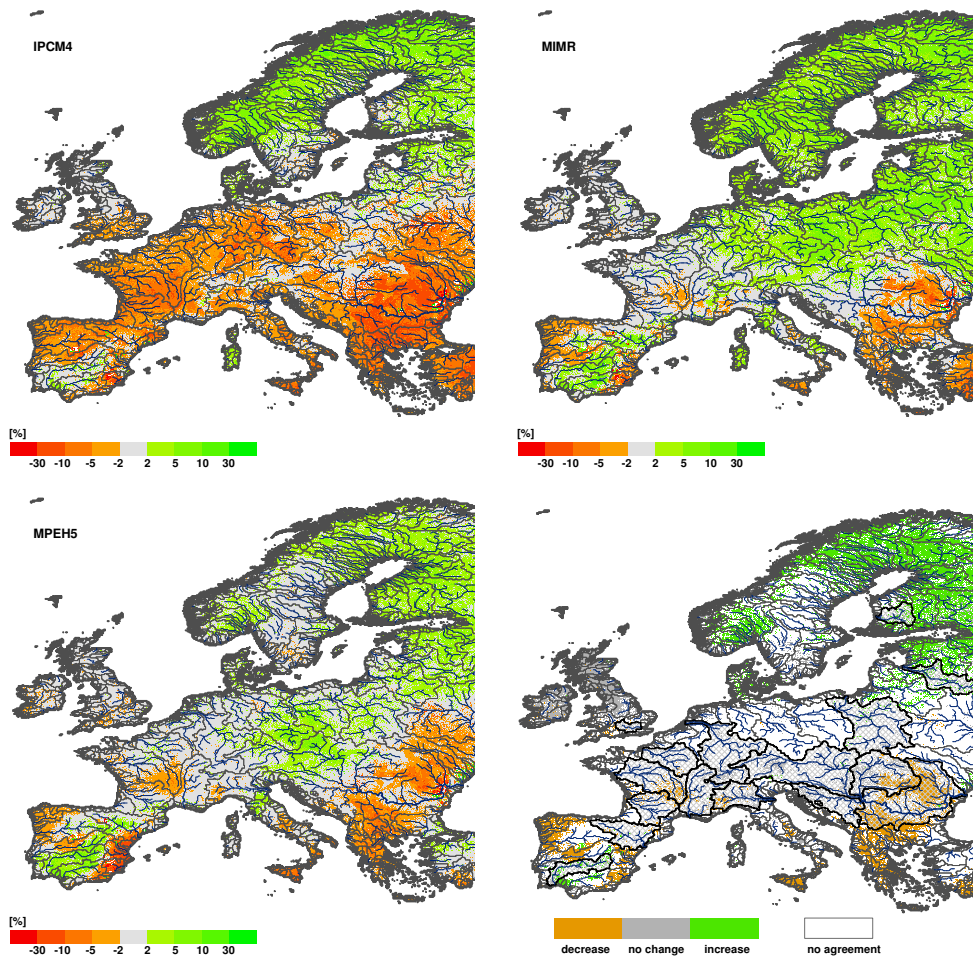


Figure 6.10— Climate change effects on average annual river flow velocity between reference period (1971-2000) and the three scenarios (top and lower left figures). The lower right figure indicates the agreement between the three projections and outlines the selected catchments.

6.5 Discussion and Conclusion

A new approach to model variable river flow velocity with the Manning-Strickler formula on global scale has been introduced. The river bed roughness (Manning's n) is approximated spatially explicit based on topography, location of urban population and an individual meandering ratio per grid cell. The hydraulic radius is estimated from actual river discharge and the river slope is derived by combining a high resolution DEM, a 5 arc-minute drainage direction map and an individual meandering factor for each grid cell. The global scale hydrology model WaterGAP has been applied to model flow variable velocities with the approach introduced. A comparison of the modeled velocity to data derived at 22 of US rivers has shown that WaterGAP matches the level of the measured velocity satisfyingly. The model overestimates the average velocity at most investigated gauging stations. This indicates that the model results are uncertain, especially when interpreting modeled velocities for single grid cells or gauging stations.

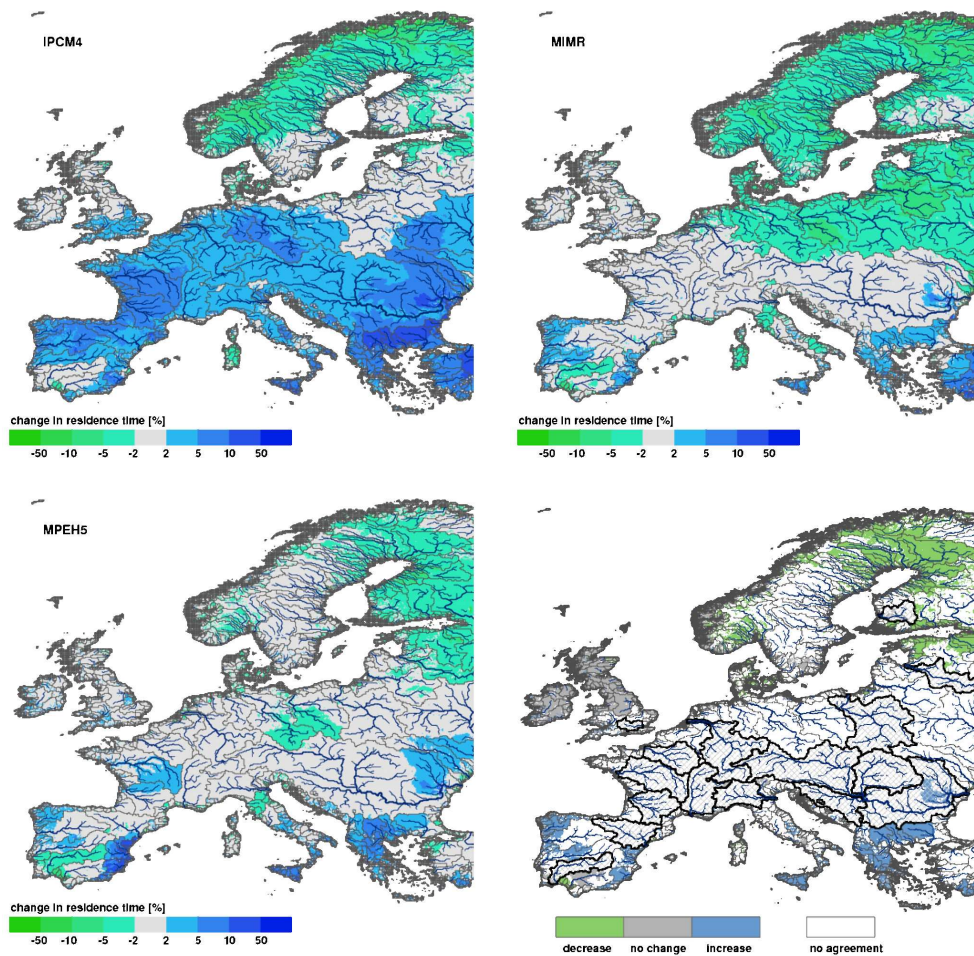


Figure 6.11— Climate change effects on residence time in rivers between reference period (1971-2000) and the tree scenarios (top and lower left figures). The lower right figure indicates the agreement between the three projections and outlines the selected catchments.

Compared to the constant flow velocity, which has been applied in previous WaterGAP versions, the representation of the lateral transport processes in rivers has clearly improved. This is especially true for grid cells covering tributary rivers, which is by far the majority of all grid cells. Here the flow velocity lies significantly below 1 m/sec and thus has been overestimated when applying a constant flow velocity. This applies also for major rivers with a high flow variance over the year, such as e.g. the Guadiana. Largest effects occur at discharge peaks, which generally increase by applying the variable flow velocity. Here the Nash-Sutcliffe-Coefficient improves at stations, where flood peaks have been underestimated before and vice versa. The effects on monthly discharge hydrographs are lower than expected. However, the improved representation of the residence time of the water in the river section is crucial for the simulation of water quality parameters. The degradation of non-conservative substances is dependent on the residence time of water in the river. The same is true for the transport and accumulation rate of conservative substances.

Three climate change projections for the 2050s have been used to drive WaterGAP3 to assess climate change impacts on flow velocity. The residence time of the water in the river system has been derived from the average flow velocity per grid cell and the distance to the river mouth. The three projections differ over large areas. However, they agree in projecting a decreased residence time in northern Europe and generally show an increasing residence time in parts of the Mediterranean, caused by declining water availability. An exception is the Spanish/Portuguese Guadiana catchment. Here flow velocity is projected to increase by all three GCM driven WaterGAP calculations. The results of our study confirm results of other studies, which conclude that the terrestrial water system of the Mediterranean region is susceptible to the projected climate change impacts. A number of studies project a decreased water availability in the Mediterranean caused by climate change impacts (IPCC, 2007a; Rothman et al., 2007), which is likely to be intensified through increased anthropogenic water consumption (Flörke and Alcamo, 2004).

Evidently, global models are not able to reach the accuracy of local scale models since they are not designed to simulate hydrological conditions of single watersheds. Global or continental scale models are rather suitable to detect large scale patterns which can be assessed in smaller scaled studies with more detail and accuracy. Regions in which a considerably change in flow velocity is likely, can be investigated in further detail within regional studies. Herein the effects of a flow velocity and river water residence time can be discussed region specific and if applicable, mitigation and adaptation strategies can be developed. Further, only climate change impacts have been investigated within the scope of this study. However, river discharge and thus the related flow velocity are affected by anthropogenic water use. This is especially true for the Mediterranean region, where a significant amount of water is extracted from the river system for irrigation. These impacts should be considered in follow up studies as well.

Chapter 7

Future Flood Risks in Europe: Assessing the Impact of Different Flood Indicators, Climate Change Projections and Time Series

7.1 Introduction

Floods are among the most frequent and most costly natural catastrophes. Major floods caused economic losses exceeding US\$ 200 Billion in the 1990s alone and the summer flood in Europe in 2002 generated costs exceeding 20 Billion Euro (MunichRe). It is commonly agreed that climate change induces an enhanced climate variability, which is expected to increase the risks of flooding in many areas (IPCC, 2007a; Kundzewicz et al., 2007). Extreme precipitation is projected to increase until the end of the 21st century in those regions that are relatively wet under present climate conditions, such as middle and northern Europe. Analogously, the number of consecutive dry days as indicator for dry extremes is projected to increase particularly in those regions that are already relatively dry under present climate conditions, for example the Mediterranean Region (Sillmann and Roeckner, 2008). Comparable results for total precipitation were found by a multi model simulation with global and regional climate models, which predict a precipitation increase in northern Europe and a decrease in southern Europe during all seasons, while in central Europe precipitation is projected to rise in winter and decline in summer (Christensen and Christensen, 2007). However, changes in extreme precipitation are not the only reason for changes in flood magnitudes. Floods are oftentimes arisen by snow melt in snow affected catchments. Due to temperature increase, the snow pack decreases and leads to lower snow melt induced flood peaks. Further, snow melt starts earlier within the year and leads to a temporal shift of the snow melt peak.

Most flood related climate change impact studies are performed on catchment scale (e.g. Graham et al., 2007; Menzel et al., 2006; Pinter et al., 2006; Booij, 2005; Dale, 2005; Menzel and Burger, 2002a) or investigate a number large catchments located throughout the world (Kleinen and Petschel-Held, 2007; Milly et al., 20002). Different types of flood maps exist for most European countries covering the entire or significant parts of their

territory (de Moel et al., 2009). The European countries are required to map flood hazards and risks in their territory to comply with the EU-directive (2007/60/EC). This directive has been adopted to transform the traditional (sub-)national flood defense strategies into a flood risk management approach at the basin scale in Europe. However, the application of different hydrological models in the various studies that are forced by results of a number of Global or Regional Circulation Models (GCMs, RCMs), the different scenarios applied as well as the related interpretations and presentation of the model results do not allow a consistent view over large areas such as Europe. To date we know about two studies investigating changes in flood frequencies in Europe with a consistent model, performed by Lehner et al. (2006) and more recently Dankers and Feyen (2008). Both studies investigated the future magnitude of a current 100-year-flood. In the Lehner et al. study, the global scale hydrological model WaterGAP has been driven by climate input of two GCMs for the 2020s and 2070s based on the IPCC-IS92a emission scenario. Dankers and Feyen used the European scale hydrological model LISFLOOD for their analysis, which was forced by SRES A2 and B2 scenarios for the 2050s in two different spatial resolutions. Both studies found opposed results for changes in flood frequency and intensity over north-eastern Europe as well as for parts of Western and Eastern Europe and agreed in their projections for the Iberian Peninsula. The main reasons for the contradictory results are the application of two hydrological models within the two studies, which were forced with diverse scenarios, calculated by different GCMs or GCM versions. Graham et al. (2007) found that the choice of the GCM impacts the projected hydrological change more than the selection of the emission scenario. Further, the Lehner et al. and Dankers and Feyers studies used different approaches to derive the future climate data that was used as model input. Dankers and Feyen (2008) applied the direct GCM output to force their models, whereas Lehner et al. (2006) scaled the future 30-year periods of average monthly climate with a dataset based on measured climate of the reference period by applying a delta-change-approach. Temporal changes in future climate variability are not considered when deriving future climate time series with the delta-change approach and consequently predictions of extreme flows might differ considerably (Lenderink et al., 2007). The comparison of the two continental scale studies shows that the results are sensitive on the selection and processing of the forcing climate input, which even leads to opposed results over large areas. To enhance the robustness and informative value of expected climate change impacts on flood hazards in Europe, this study aims at providing an assessment of the effect of

- different climate change projections,
- the difference between direct and delta-change derived GCM data to force the hydrological model, and
- different flood indicators.

Three climate change projections for the 2050s (2040-2069) have been selected, as calculated by three different GCMs: two representing the SRES A2 and one the SRES B1 scenario. The future time series of monthly precipitation and temperature were derived by (i) using the direct GCM output and (ii) scaling the average monthly values of the scenarios with climate of the reference period (delta-change-approach), respectively (Section 7.2.1). In addition to the 100-year-flood indicator for large flood events, we selected

two additional flood indicators for more frequent floods: the "discharge that is exceeded statistically in 1 of 100 days" and "the annual number of days, exceeding bankfull flow" (Section 7.2.2).

For flood simulations on European scale, we applied the global scale hydrological model WaterGAP3, which has a spatial resolution of 5 arc minutes. An earlier WaterGAP version has been used by Lehner et al. (2006). Since their analyses, WaterGAP has been further developed to improve the models ability to simulate floods (see Chapters 3-6). In addition, recent GCM results of future climate scenarios have been used to force WaterGAP. This makes the WaterGAP calculations presented in this study more comparable to the findings of Dankers and Feyen (2008) than the Lehner et al. (2006) results.

In the following section a short introduction to WaterGAP and the forcing data, i.e. the underlying GCMs and scenarios, is given. Then the selected flood indicators are explained in more detail and WaterGAP results as used for the analysis of the three indicators are evaluated by comparison to measured data. Subsequently, the results for the different projections and flood indicators are presented and (dis-)agreements are discussed. Finally "critical regions" in Europe are defined, in which significant changes of flood frequencies and intensities are likely to occur until the middle of this century.

7.2 Methodology

7.2.1 Forcing data

Historic WaterGAP Simulations

A combination of the datasets CRU TS 2.1 (Mitchell and Jones, 2005) and CRU TS 1.2 (Mitchell et al., 2004) has been used to drive the WaterGAP3 simulations for historic simulations, that have been used to validate the modeled flood discharges described in Section 7.2.3. The CRU TS 1.2 dataset has a spatial resolution of 10 arc minutes and covers the predominant part of Europe. The CRU TS 2.1 dataset with a spatial resolution of 0.5° has been applied to force WaterGAP at the grid cells that were not covered by the high resolved CRU TS 1.2 dataset. Both climate datasets have simply been disaggregated to a spatial resolution of 5 arc minutes. More details about the application of the CRU datasets within WaterGAP are described in Section 2.5.

Scenarios

Three climate change projections for the 2050s (2040-2069) from the ensemble of GCMs and scenarios analyzed within the Fourth IPCC Assessment Report (IPCC, 2007a) have been chosen to drive the WaterGAP3 scenario simulations. The climate projections chosen differ in magnitude and in some areas even in the direction of possible futures of the European climate. The wide range of scenario assumptions has been chosen to test the robustness of the predicted model results. Below the selected GCMs, underlying scenarios and characteristics of average annual temperature and precipitation are listed:

1. **IPCM-A2:** The IPSL-CM4 model from the Institute Pierre Simon Laplace, France, A2¹scenario:

The scenario indicates high temperature increase and low precipitation change (increase or decrease) in Europe ("dry" scenario).

2. **MIMR-A2:** The MICRO3.2 model from the Center for Climate System Research, University of Tokyo, Japan, A2 scenario:
In accordance with IPCM-A2, projects MIMR-A2 a high temperature increase over Europe in combination with a high precipitation increase or low decrease ("wet" scenario).
3. **MPEH-B1:** The ECHAM5/MPI-OM model from the Max-Planck Institute for Meteorology, Germany, B1¹ scenario:
This scenario predicts in contrast to the other two GCMs a small temperature increase and an average precipitation change ("intermediate" scenario).

The original GCM datasets have a spatial resolution of 1.875° x 1.875° (T63) and have been downscaled to a 5 arc minute grid by applying a simple bilinear interpolation approach. We used monthly temperature (T) and precipitation (P) results from the GCMs described above. The number of rain days per month and the cloudiness are taken from the reference period (1961-1990). Then the climate values are downscaled to daily climate as described in Section 2.5. Accordingly, a possible increase of climate variability at the daily scale is not taken into account. The simple approximation of pseudo-daily future climate input has been initially implemented in WaterGAP for studies of climate change impacts on long-term average discharge and may affect the simulated magnitude of high flows. Future monthly climate time series are derived by two different methods for each of the three scenarios:

1. The time series approach: the direct model output, i.e. monthly time series for P and T for 2040-2069, of the three GCMs are used to force WaterGAP3 and the spatial resolution is downscaled to a 5 arc-minutes raster by bilinear interpolation.
2. The delta-change-approach: monthly P and T time series of the CRU dataset (1961-1990) are scaled with the difference between 30-year average for both the reference period (1961-1990) and the 2050s (2040-2069) calculated by the GCMs (see Section 2.5).

The two approaches to derive time series of future climate differ in their extent of spatial and temporal information. The advantage of the delta-change-approach is that the spatial information density of the coarse resolution GCM output is improved by scaling the values with the CRU-dataset, which has a considerably higher spatial resolution. The temporal variability of future monthly time series is prejudicially not taken into account. It is implicit that changes in future monthly T and P variability are considered when using the direct GCM output. On the other hand, this method leads to less spatial variability compared to the delta change approach, especially when applying simple downscaling methods like the bilinear interpolation.

¹The SRES-A2 scenario "describes a very heterogeneous world with high population growth, slow economic development and slow technological change". The SRES-B1 world is a convergent world with a global population that peaks in mid-century and rapid changes in economic structures toward a service and information economy (IPCC, 2007a, p.44).

7.2.2 Flood Indicators

We have chosen three different flood indicators to investigate future flood magnitudes or frequencies in Europe. The indicators vary in their consideration of the flood magnitude, from rare extreme flood events to frequently recurring floods, but also in the complexity of their computation. The indicators are (i) the discharge of a 100-year flood, (ii) the discharge that is exceeded statistically in 1 of 100 days and (iii) the number of days over bankfull flow. The indicators have been derived from the 30-year time series of gridded daily river discharge results calculated by WaterGAP3 for the reference period (1961-1990) and the three scenarios (2040-2069).

100-year floods

One of the most frequently used indicators for large floods is the discharge of a 100-year flood, defined as a flood that statistically returns once in 100 years. 100-year floods are extreme flood events, causing especially high economical damage. Therefore the public interest is high in information about future changes of the magnitude or frequency of what is currently a 100-year flood. Further, this indicator is frequently used for the dimensioning of flood protection works.

To derive the discharge of a certain return period (e.g. 100-year flood), a series of extreme values, which is usually an annual maximum series (AMS) or a partial duration series (PDS), is ranked and fitted to a statistical distribution, or probability density function (pdf), which allows the extrapolation of the frequency distribution. There are several distribution functions available that serve this purpose. The choice of the distribution function alters the results, especially for events with a return period longer than 20-50 years (Dankers and Feyen, 2008). However, there is no single statistical distribution that fits all data. We have chosen the Pearson III distribution, which is oftentimes applied for flood frequency analysis (e.g. Lehner et al., 2006; Milly et al., 20002; Muzik, 2002; Roy et al., 2001) and suggested by national organizations as standard method for statistical flood analysis (US-ACWD, 1982; USGS, 1981; DVWK, 1979, 1999). The Pearson III distribution is described in detail e.g. in Haan (2002) or Rao and Hamed (2000).

At the beginning of our analysis, the annual maximum discharges of the 30-year time series of daily discharge have been derived for each grid cell. To fit the selected extreme values to the Log-Pearson-III distribution, the mean, the variance (V) and the skewness (S) have been calculated for the arithmetic and logarithmic values of each AMS. If S of the logarithmic AMS (S_{log}) is $S_{log} > 0$, a Log-Pearson III-distribution is applied. If $S_{log} < 0$ and $S_{arithm} > 0$, with S_{arithm} = skewness of arithmetic AMS, a Pearson III distribution is used, based on the arithmetic AMS. A particular case applies if $S_{log} < 0$ and $S_{arithm} < 0$. In this case an arithmetic Pearson-III distribution is applied with a corrected skewness ($S_{arithm} = 2V_{arithm}$) to avoid negative values of the distribution (DVWK, 1979; Maniak, 2005).

Due to the large variety of extreme value series derived in the grid cells covering Europe, the Pearson III distribution might not be suitable to serve as distribution for the AMS derived in a number of grid cells. Thus we have tested in each grid cell the goodness-of-fit of our AMS to the Pearson III distribution with a Chi^2 -test (significance level 1%). The statistical hypothesis test has been passed in 87% of the European grid cells, i.e. in these grid cells the Pearson III distribution is suitable to serve as statistical distribution

to derive the 100-year flood discharge from the AMS of the reference period (1961-1990). The Chi^2 -results for the scenarios showed only minor differences to those of the reference period. The grid cells that did not pass the Chi^2 -test have been blanked out in the related result maps (Figure 7.9)

Discharge exceeded by 1% of all discharges (daily Q1)

The second flood indicator applied is the discharge that is exceeded by 1% of all discharge values considered (daily Q1), which indicates more regular floods than the 100-year-flood (Figure 7.1). Consequently, the economical damages are lower and nature is usually well adapted to discharges of this magnitude or even dependent on the regular inundations. Anyhow, the investigation of altered magnitudes of more regular flood events is crucial, since nature and humans might have to adapt to significantly changed daily Q1 levels.

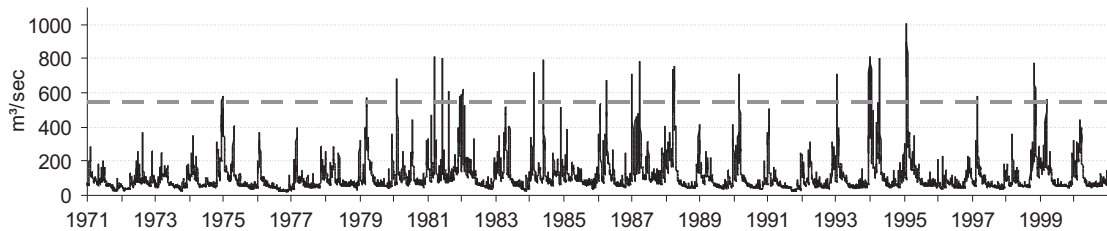


Figure 7.1— Daily discharge at the Weser River in Hann. Münden (Germany). The dashed line indicates the Q1 discharge level.

The daily Q1 discharge values do not allow drawing conclusions about its frequencies. No information is given by the indicator whether the Q1 discharge results from regular annual floods, as for example annual snow melt peaks in spring, or from a few irregular large floods, caused by extreme precipitation. Thus, the informative value, especially for planning purposes, might be lower than the more often applied discharge of certain return periods, such as 100-year flood discharge. This might be a reason why this indicator is applied seldomly. On the other hand this indicator is comparably easy to calculate, because it is derived by calculating the 99th percentile from the series of daily discharges of the 30 year time series of each grid cell covering Europe.

Number of days per year exceeding bankfull flow

The bankfull flow is defined as the point at which the river channel is full of its capacity and the flow just begins to enter the active floodplain (Leopold, 1994). If the river discharge exceeds the bankfull stage, adjacent areas such as floodplains, agricultural or urban areas are inundated, where no artificial flood protection is available. In order to estimate bankfull flow on global scale, an approach had to be found, which does not depend on in situ measurements. A number of studies worldwide have proven a relation between a certain flood return period and the bankfull stage. Therefore, we used flood frequency analysis to estimate bankfull flow. It is assumed that on the long-term average, bankfull flow

occurs at a certain time interval whereas best approximation is obtained by considering a flood recurrence period of 1.5 years (e.g. Dury et al., 1963; Leopold et al., 1964; Dunne and Leopold, 1978). Usually urban areas are well adapted to 1.5-year floods, so that no significant economical damages can be expected. This indicator is especially important for natural sites that rely on recurrent inundations, such as wetlands or the fauna and flora of water meadows. Changes in the annual inundation duration might alter the ecology of these ecosystems. Changes in the number of days exceeding bankfull flow between a reference period and future scenarios allow valuable interpretations about alterations in the flood duration. For example a decrease in the number of days with overbank flow and concurrent increase in flood magnitude allow the conclusion that the future flood durations will be shorter but with a higher flood magnitude, hence more intense.

However, our continental scale approach to derive this indicator is connected with a number of uncertainties. In most cases, the return period for the annual series is 1.5 years on average and ranged between 1 and 2 (Tricart, 1977; Harman et al., 1999) or 1 and 3 years (e.g. Tricart, 1977; Andrews, 1980; Castro and Jackson, 2001). On a few localities bankfull flow may diverge greatly from the suggested value of 1.5 years as shown by Williams (1978) and Mosley (1981). Another uncertainty derives from the fact that there is no clear agreement on the definition of bankfull flow. About 11 different definitions and ways to estimate bankfull stage in situ at a naturally shaped river cross section are applicable (Williams, 1978). This ambiguity of bankfull stage can lead to a maximum of 11 different bankfull levels at the same stream cross section.

The annual series has often been used to estimate bankfull flow but also has widely been criticized for being mathematically incapable of providing sub-annual recurrences intervals. To optimize the estimation of the comparably small return period of bankfull flow, we applied the partial-duration-series (PDS) approach to derive the extreme values from the 30-year time series of daily discharge values. The PDS approach takes all peak flows above a certain threshold into account, which is set in our analysis individually in each grid cell by different criteria. First, the threshold is set in a way so that the total number of extreme values is 2.5 times the length of the time series, which is here 30 years. Second, the threshold must be higher than the lowest annual maximum flood on record and third, only maxima of clusters of exceedance are considered as an extreme event. The extreme values are then fitted to a Pearson III distribution or Log-Pearson III distribution respectively as described in Section 7.2.2. A recurrence period of 0.92 is considered for bankfull flow in the partial-duration-series as suggested by Dunne and Leopold (1978), which corresponds to a recurrence period of 1.5 years as suggested for AMS.

One can conclude that bankfull flow can only be approximated with this continental approach, which should be considered when interpreting the results in the following section. Individual local conditions, anthropogenic changes to river depth, width or canalization are not considered. The approach is currently validated for different local sites in Europe by Schneider (2009).

7.2.3 Validation of WaterGAP for Flood Calculations

Lehner et al. (2006) performed a detailed analysis about WaterGAPs capability to model flood events. They found that WaterGAP is suitable to reasonably estimate large scale high flow regimes, general flood statistics and relative, basin-characteristic flood frequency

distributions. However, they pointed out that WaterGAP showed significant errors in the calculations of single flood events. As already mentioned above, WaterGAP has been further developed to enhance its ability to simulate flood events compared to the model version used by Lehner et al. (2006). They found that WaterGAP tends to overestimate snow induced flood peaks, presumably caused by the simple representation of snow melt. The snow algorithm has been improved since then (see chapter 3). Snow accumulation and melt is calculated on sub-grid scale in the WaterGAP version applied. This leads to an improved representation of the snow melt peak in spring. Further the spatial resolution of the model has been increased from 0.5° to 5 arc minutes globally (see Chapter 3). Thus the river network and the input data are represented with a higher level of detail. In addition, the lateral routing has been enhanced. A dynamic flow velocity has been implemented and the river length has been improved by an individual meandering factor per grid cell (see Chapters 5 and 6). However, WaterGAP still has some general limitations concerning the simulation of flood discharges. One should keep in mind that WaterGAP is a large scale water balance model, with a spatial resolution of 5 arc minutes. Thus, it is not explicitly designed to simulate single flood peaks. This requires a number of catchment specific information, which cannot be considered in a global scale model. Beside the general model structure is the spatial scale of the GCM data another source of uncertainty as well as the application of the number of wet days per month that is used to equally distribute the monthly precipitation to the single days of the month. For flood formations, the storage and retention of water in natural lakes and wetlands is of high importance. In WaterGAP simple storage functions are implemented (Döll et al., 2003; Kaspar, 2004). In addition, the retention in managed reservoirs is of major importance for the formation of flood peaks. However, reservoir management is not considered in the WaterGAP version applied for this study, which might also cause flood peak overestimations.

Validation of 100-year floods

Discharge of 100-year floods derived from measured and simulated discharge with the method described above has been used to verify the model results. Time series of 119 European gauging stations for the period 1950-2002 have been applied if existent, otherwise the available years with full data records of measured data. Figure 7.2 shows the 100-year flood discharge calculated from WaterGAP results and from measured discharge on a logarithmic scale. The results have an r^2 of 0.68 and it can be seen that WaterGAP is able to reproduce the 100-year flood discharge reasonably. The model equally under and overestimates the measured values. However, there is a conspicuous group of overestimated large flood values. Two stations in this group are located in the Dnjepr watershed. The discharge of the Dnjepr is highly regulated, which cannot be reproduced by WaterGAP. All other stations in this group are located in the lower Danube River. A reason for the overestimation might be that WaterGAP does not consider floodplains, which are usually flooded during large flood events. The model instead assumes a trapezoidal river cross section with a side slope of 0.5 (Section 6.2.2). Thus there is no temporal retention of flood discharge in the flood plains, which leads to an overestimation of flood peaks. In addition, the Danube is regulated, which is not considered by WaterGAP as already described above. However, if WaterGAP3 would be applied for detailed studies in specific case study catchments, the river cross section could be modified manually and floodplains

could be added if required.

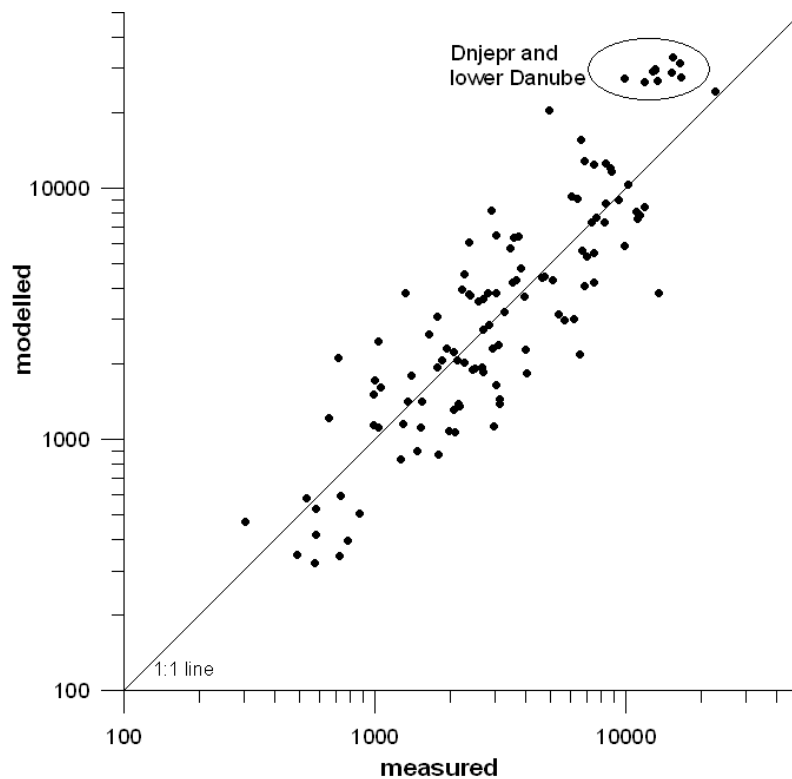


Figure 7.2— Comparison of 100-year flood discharge [m^3/sec] at 119 European gauging stations derived from measured and simulated time series.

The calculation of 100-year floods is based on the discharge of the largest annual flood peaks, which requires the simulation of single flood events. Figure 7.3 shows exemplarily the modeled and measured maximum annual time series of two rivers. In the Hungarian part of the Danube catchment at Dunaalmas, WaterGAP nearly equally under- or overestimates the measured annual maximum flow discharge during the time series shown (1961-1995). However, six discharge peaks (two in the early 1960s and four in the 1980s) are highly overestimated. At the river Rhine in Cologne, WaterGAP clearly underestimates the annual maximum flow discharge of most years between 1961 and 2002.

It can be seen that WaterGAP shows errors in simulating the discharge of single flood events at local sites. According to this, we minimize the uncertainty of the results shown, by investigating large scale patterns of change on the European scale. Further, we do not show absolute flood discharges in the results section and rather focus on changes of flood return between the reference and scenario period as shown in Figure 7.4.

Validation of discharge exceeded by 1% of all discharges (daily Q1)

The same 119 gauging stations as for the validation of the 100-year floods have been used to test WaterGAP's ability to simulate the daily Q1. The indicator has been calculated for the time period 1961 - 1990, which serves as reference period in the present study. In accordance with the results shown in the previous section, WaterGAP equally over-

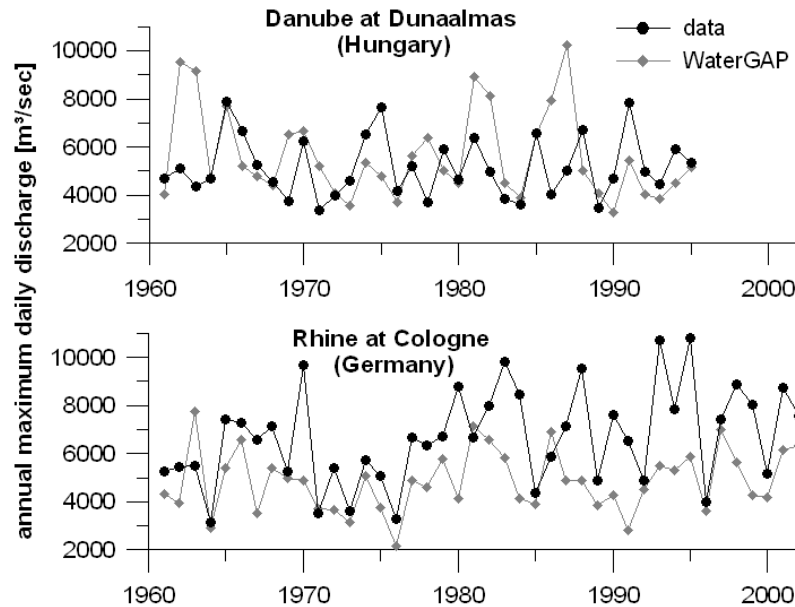


Figure 7.3— AMS of two gauging stations showing examples of average overestimation (top) and underestimation (bottom) of annual maximum daily flood peaks.

and underestimates the measured values (Figure 7.5). However, the comparison between measured and modeled values has an r^2 of 0.87, hence can better be reproduced by WaterGAP than the 100-year flood. A reason for this is that no peak values have to be modeled to derive the daily Q1 as for the 100-year flood. It has already been shown in previous studies that WaterGAP produces good results for the monthly Q10, which serves as high flow indicator (Hunger and Döll, 2008; Lehner et al., 2006).

Validation of number of days with overbank flow

The number of days, at which bankfull flow is exceeded and therefore leads to inundated floodplains cannot be validated on large scale. This indicator is most suitable for ecological tasks and should thus be validated on smaller scales and on areas that are especially vulnerable to alterations in inundation duration such as wetland areas. The development and validation of this indicator is neither part of this thesis nor performed by the author. The verification is currently carried out and not finalized yet. Nevertheless, first results of this indicator are presented, since valuable information for areas that rely on periodically inundation are presented. A detailed verification of this indicator and the application at selected case study regions will be presented by Schneider (2009).

Concluding comparison of the three flood indicators

A summary of the advantages and disadvantages of the three indicators presented are summarized in table 7.1.

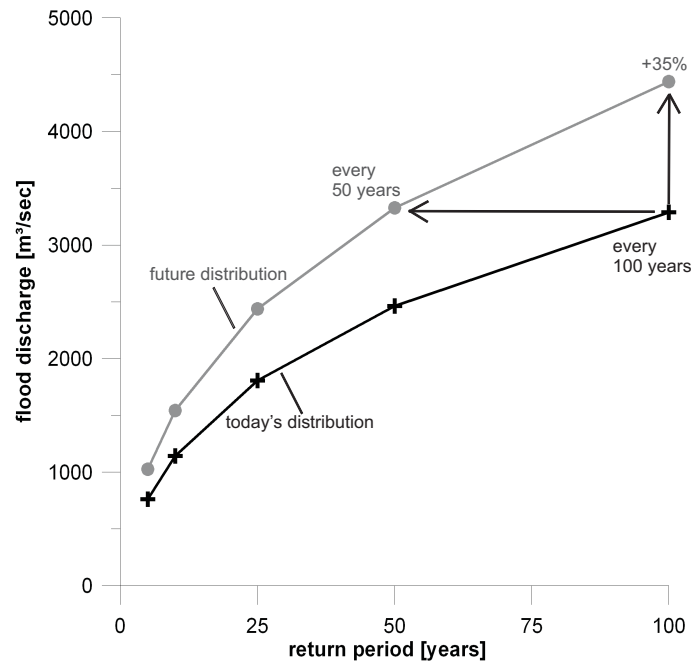


Figure 7.4— Characteristical relationship between a change in flood intensity and the corresponding change in the flood return period (after Lehner et al. (2006), modified)

7.3 Results

The changes in 100-year flood discharge, the daily Q1 as well as the number of days exceeding bankfull flow have been calculated using the results of the three GCMs (IPCM, MIMR and MPEH) according to the A2 and B1 emission scenarios, and the related control periods (1961-1990). WaterGAP has been driven by 30-year monthly time series of precipitation and temperature as calculated by the GCMs, without any bias correction (see Section 7.2). This results section is divided into two parts: first, the changes between the control periods (1961-1990) and the 2050s (2040-2069) for the three indicators and three scenarios are compared. Then, the impact of the method to derive forcing climate on the three indicators is analyzed for the MPEH climate (direct GCM time series vs. time series derived by the delta change method).

7.3.1 Changes in future precipitation

The magnitude of changes in precipitation differs between the three projections (compare Section 7.2.1). The IPCM-A2 climate is the "dry" projection with low precipitation change, MIMR-A2 is the "wet" projection with the largest precipitation increase and MPEH-B1 is an "intermediate" projection with average precipitation change (Figure 7.6). The different projections agree in predicting an increase in average annual precipitation over northern Europe and a decrease in southern Europe, more precisely the Iberian Peninsula and southeastern Europe. This agrees with the results found by multi model analyses of RCMs and GCMs within the scope of the PRUDENCE project (Christensen and Christensen, 2007) and the Fourth Assessment Report of the IPCC (IPCC, 2007a).

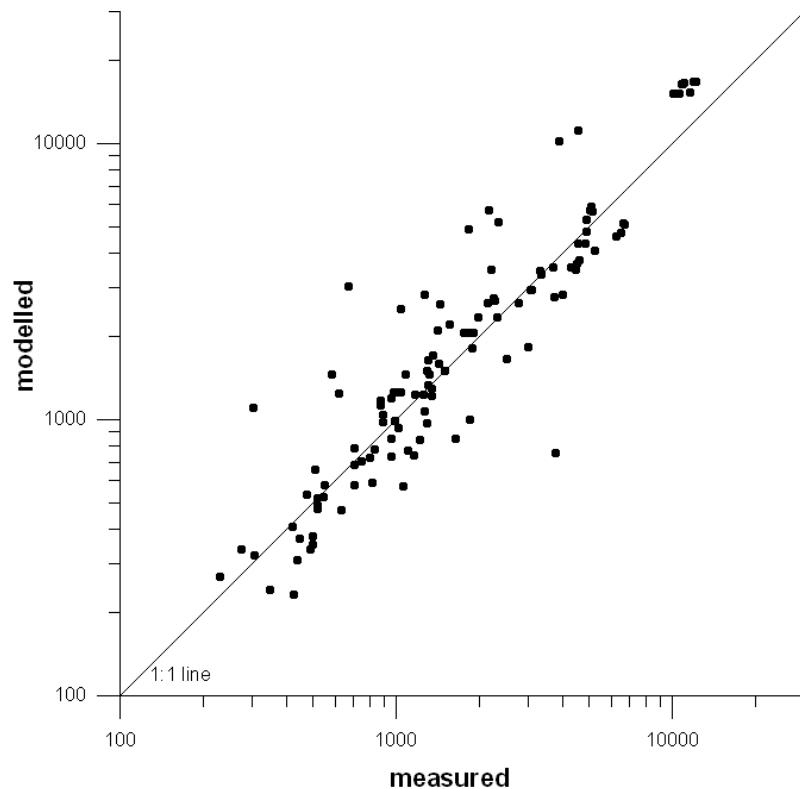


Figure 7.5— Discharge [m^3/sec] that is exceeded statistically in 1 of 100 days. Comparison between measured and WaterGAP3 modeled data for the period 1971-2000.

Regional differences are found in western and central Europe, as well as in the central Mediterranean region. In these regions IPCM-A2 projects a precipitation decrease and MIMR-A2 an increase. MPEH-B1 shows little changes ($\pm 5\%$) over wide areas of west and central Europe, increasing from west to east. MPEH-B1 further projects a precipitation increase in the northern Mediterranean region and a decrease more southerly.

However, the changes in precipitation vary significantly over the year. Figure 7.7 shows the changes in seasonal precipitation for IPCM4-A2². It can be seen that the GCM predicts a strong decline in summer precipitation exceeding 20% over southern Europe and less pronounced in central Europe. In contrast, winter precipitation is projected to increase significantly the Mediterranean, eastern Europe and most distinct in northern Europe, with a precipitation rise larger than 20% in northern Scandinavia. The consequence is a considerable increase of snow cover in northern Europe projected by IPCM-A2, since the temperatures remain below 0°C despite climate warming.

Table 7.1— Pros and Cons of the flood indicators as calculated by WaterGAP3

	Advantages	Disadvantages
100-year Flood	Indicator for extreme floods, causing high economic losses and damages to ecology and society Frequently applied	WaterGAP shows errors in reproducing the magnitude of single flood events. Complex to calculate compared to the other indicators.
Daily Q1	WaterGAP results show good agreement with measured data. Easy to calculate	Indicator for more regular floods e.g. caused by fast snow melt or extreme precipitation events. Thus relevance depends on scope of research.
Days exceeding bankfull flow	Indicator most relevant for ecological tasks regarding inundation of floodplains and other areas adjacent to the river. Provides information about changes in flood duration	Bankfull flow can be approximated on continental scale only and has a high uncertainty level. Individual local conditions and flood protection works cannot be considered area-wide. Validation of WaterGAP results over large areas is not possible and validation at local sites is not finished yet, fix return period (1.5 years (AMS), 0.92 (PSD)).

7.3.2 Changes in future flood magnitudes

7.3.3 Future changes in 100-year flood discharge

Figure 7.8 shows the changes in the magnitude of 100-year flood discharge, which goes along with a shorter flood return interval during the scenario period of what is 100-year flood discharge in the control run (Figure 7.9). All scenarios show both, increasing and decreasing 100-year flood levels over Europe with varying extent and magnitude. The results for the three scenarios agree in roughly 13% of Europe only. An increase of the 100-year flood discharge in 6.6% and a decrease of 6.5% of the European area is predicted. No change ($\pm 5\%$ change in 100-year flood discharge) is found in less than 1.2% of Europe. These numbers refer to grid cells with agreeing results and the areas of agreement are scattered. However, the scenarios agree in a number of large scale regions even though the exact location of agreement might not be identically. An increase of flood hazards has been found in parts of the Mediterranean area concordantly, although the average precipitation is predicted to decrease in this region. Parts of the Iberian Peninsula, Italy and the eastern Mediterranean region are affected, even though with different spatial extent and location. This is caused by an increase in heavy precipitation especially in fall and winter,

²the seasonal precipitation changes for MIMR-A2 and MPEH-B1 are shown in Figure B.1 and B.2 on page 131 ff.

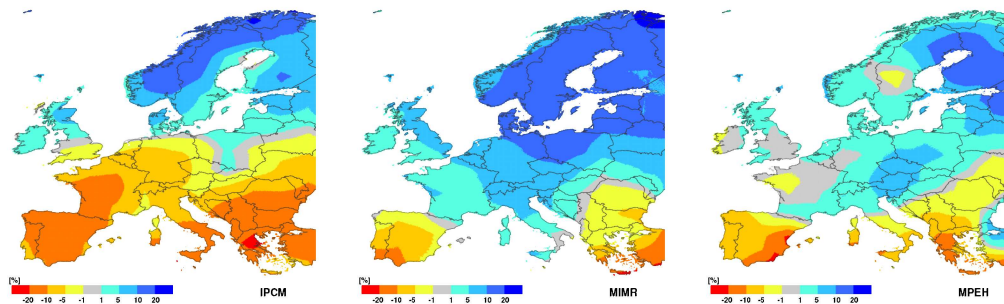


Figure 7.6— Changes in average annual precipitation between the baseline (1961-1990) and corresponding scenario period (2050s) derived from time series of the three GCMs.

which are the seasons with most rainfall in the Mediterranean. Increased 100-year flood levels are also shown by all scenarios in southern and northern Scandinavia, caused by a considerable increase in winter precipitation, especially for IPCM-A2 and MIMR-A2 (Figure 7.7 and B.1). Parts of central Europe are projected to suffer from increased flood magnitudes by all scenarios, with varying spatial extent and location. Shorter flood return periods (increasing flood magnitude) in west and parts of Mid-Europe are expected for IPCM-A2, MIMR-A2 predicts a flood magnitude rise in western Europe and MPEH-B1 primarily in eastern Europe. A decrease in 100-year flood levels is found in parts of eastern and central Europe by all scenarios to a varying degree, most pronounced by MIMR-A2. The scenarios concordantly show a decrease in the flood magnitudes in the Aegean, most distinct by IPCM-A2 and MPEH-B1, and in parts of the Iberian Peninsula.

IPCM-A2 projects 100-year flood levels to rise noticeably until the 2050s over wide parts of Europe (Figure 7.8), even though the scenario has been classified as "dry", based on annual precipitation. This contradiction is caused by the significant differences in precipitation change between the different seasons (Figure 7.7), showing a large increase of winter precipitation. This causes increasing flood hazards in regions with either maximum precipitation in winter, such as wide parts of the Mediterranean (Figure B.3, p.133), or in regions in which winter precipitation is stored as snow and the snow cover increase due to enhanced precipitation is larger than the reduction caused by climate warming. This applies for example for northern Europe. The decrease in 100-year flood level in south-east Europe and in the Pyrenees region is caused by a precipitation decrease all over the year, connected with less severe extreme precipitation events (Figure 7.7).

The "wet" MIMR-A2 simulations show that floods with the intensity of a 100-year flood of the control period are expected to occur more frequent over large parts of the Mediterranean region, western France and parts of eastern Europe as well as in most of Sweden and Finland (Figure 7.9) during the 2050s. The increase of flood hazards in Scandinavia is induced by a significant increase in winter precipitation (Figure B.1, p.131) as has already been described for IPCM-A2 above. This scenario shows a conspicuous decrease of 100-year flood levels over most of central Europe, which is related to less heavy rainfall events.

MPEH-B1 shows an increase of 100-year flood discharge in wide parts of the Mediterranean region and eastern Europe. A decrease of the flood level is found over wide areas of west and Mid-Europe as well as in Scandinavia. In contrast to the other two scenarios,

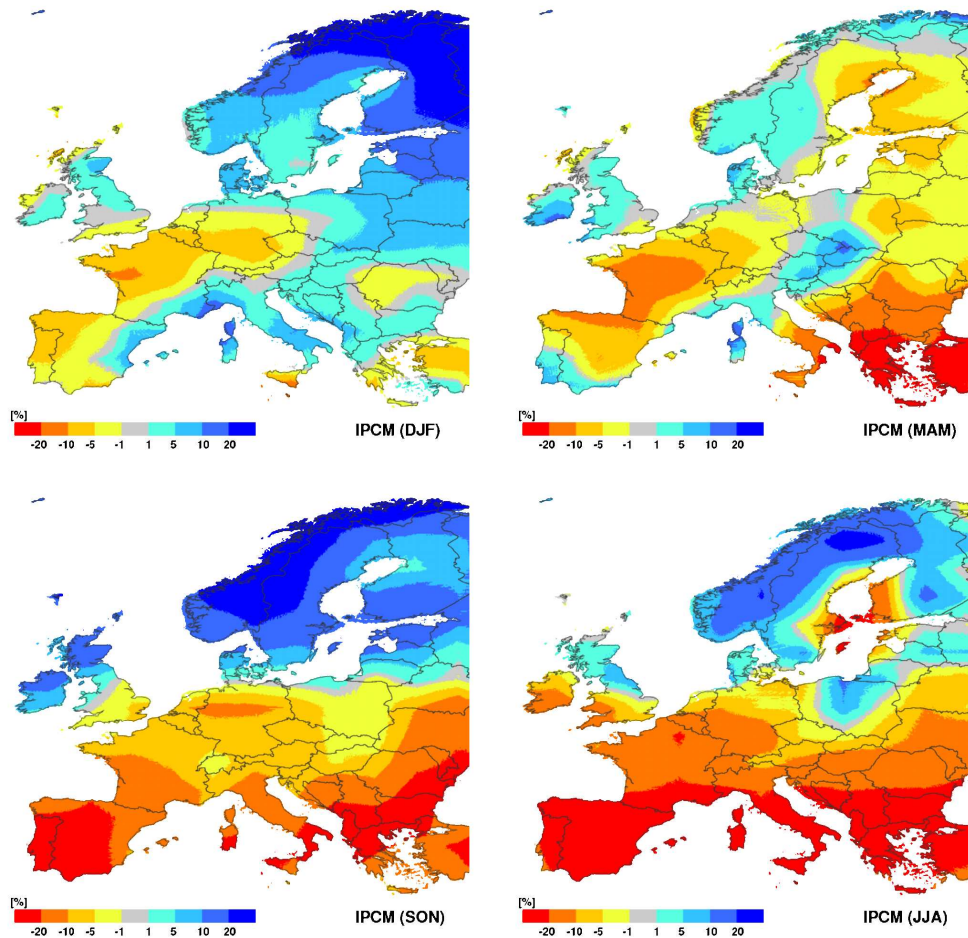


Figure 7.7— Seasonal changes in precipitation of IPCM-A2 (2050s) compared to the corresponding control run (1961-1990).

the MPEH-B1 shows a decreasing snow cover over most of Scandinavia (compare Figure 4.6, p. 56 and Figure A.1, p. 128). This leads to a decreased snow melt peak in spring and a lower 100-year flood level.

Future changes in daily Q1

The range of possible changes in future daily Q1 have been calculated for IPCM-A2, MIMR-A2 and MPEH-B1 (Figure 7.10). The agreement is considerably larger compared to the 100-year flood discharge. A decrease in daily Q1 over large parts of western Europe and southern Scandinavia as well as the Aegean is shown concordantly, covering 29% of the European area. The months with high discharges in most of western Europe and the Aegean are correlated to the months with maximum rainfall (Figure B.3, 133). The decreasing daily Q1 in Scandinavia can be attributed to a decreasing snow melt peak. The area agreeing in increasing daily Q1 is much smaller (3.4% of the European area) and is mainly located in parts of Great Britain and the northern Mediterranean region.

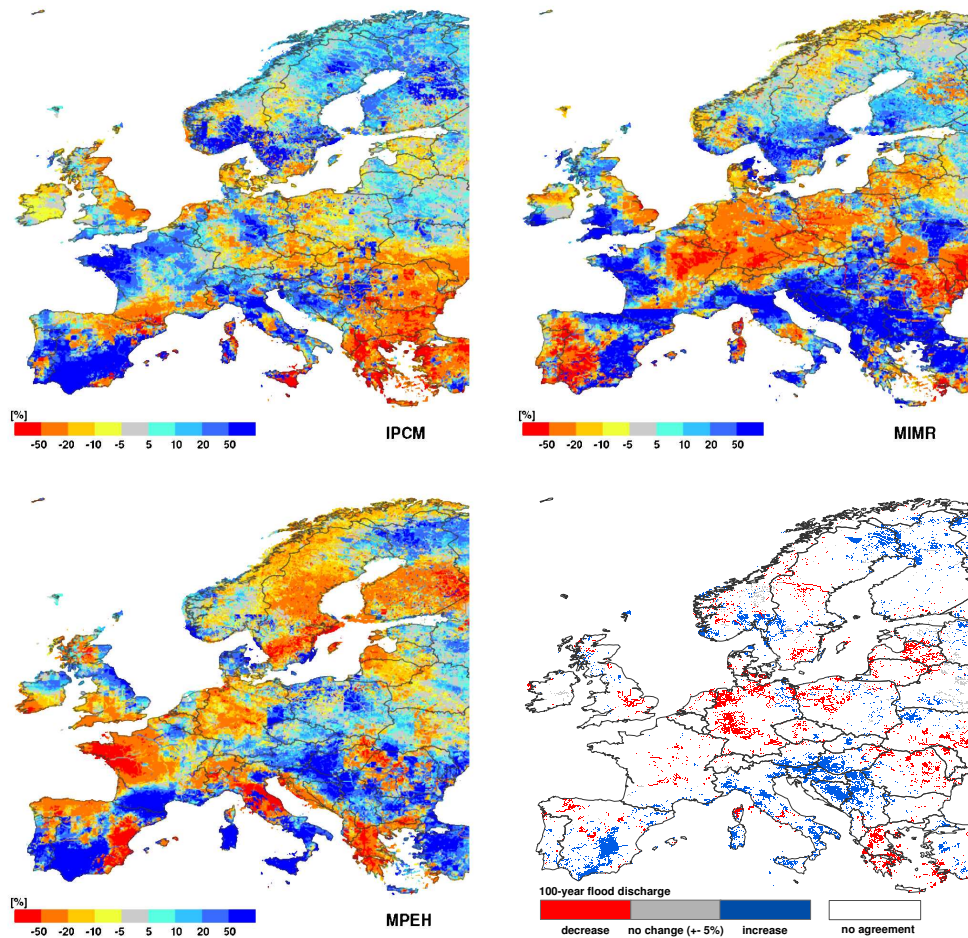


Figure 7.8— Change in 100-year flood discharge magnitude between the 2050s and the baseline (1961-1990) of the corresponding GCM.

The maps shown in Figure 7.10 represent the characteristics of climate projections IPCM-A2 (dry), MIMR-A2 (wet) and MPEH-B1 (intermediate) much better than the 100-year flood level maps (compare with figures 7.8 and 7.9). This can primarily be ascribed to the more regular floods that are covered by this indicator. These floods are rather induced by "normal" climate conditions, such as the regular annual snow melt peak or months with maximum precipitation, than by extreme precipitation events.

A decrease in daily Q1 by more than 10% is shown by IPCM-A2 of large areas of Mid- and eastern Europe as well as the southern Scandinavia. An increase in daily Q1 is projected for northern Scandinavia, Ireland and western Great Britain, due to increased precipitation over most of the year, as well as for parts of the Mediterranean, most pronounced in eastern Spain. Here the daily Q1 is expected to rise due to increased winter precipitation, which is the rainiest season in this area.

MIMR-A2 shows a strong west-east decline in daily Q1 with the exception of Scandinavia. An increase in daily Q1 is expected in west and Mid-Europe and most distinct in the Mediterranean region, with a daily Q1 rise exceeding 20%. In this region the scenario

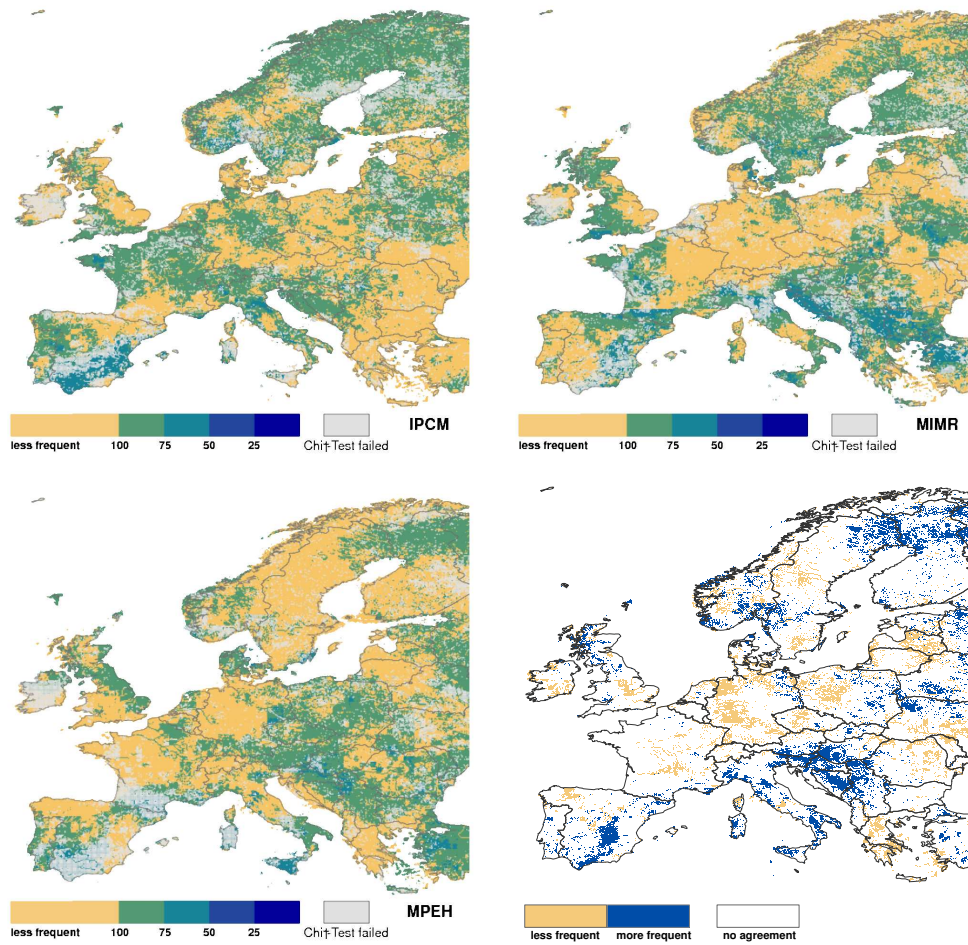


Figure 7.9— Future return periods of floods with the intensity of a 100-year flood of the control period (1961-1990).

shows a considerable increase in winter precipitation (Figure B.1, p. 131), which also applies for the rest of Europe except the Aegean.

Daily Q1 calculated from MPEH-B1 climate is projected to decrease over most of Scandinavia, eastern and Mid-Europe as well as in large parts of the Iberian Peninsula. The decrease in the latter region is induced by decreased precipitation during all seasons in the western Mediterranean (Figure B.2, p. 132). The changes in either direction as predicted by MPEH-B1 are less pronounced compared to IPCM and MIMR. This can be attributed to the less distinctive changes in precipitation (see Figures 7.7 and B.1, p. 131).

Future changes in days over bankfull flow

The third flood indicator investigated in this study is the number of days with overbank flow during the scenario period compared to the related control run (Figure 7.11). The agreement of large scale patterns between the three scenarios is large compared to the changes in 100-year flood discharge and daily Q1. It can be seen that IPCM-A2, MIMR-

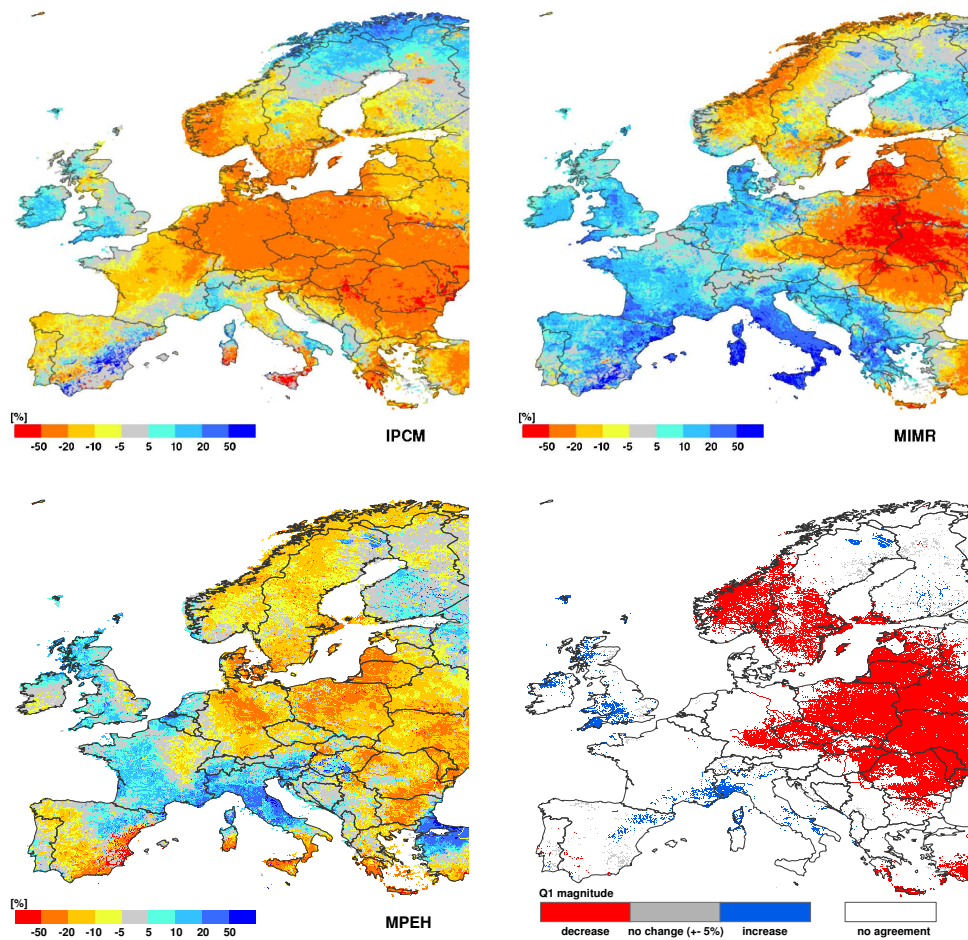


Figure 7.10— Projected changes in the discharge level that is exceeded by 1% of all discharges (daily Q1)

A2 and MPEH-B1 agree in predicting "no change", defined as change of ± 1 day, over most of west and south Europe, covering 35% of the European area. This does not allow drawing conclusions about the direction of change in flood frequency or magnitude, as can be seen from the results presented above. The indicator rather shows that the duration of the floods does not change, independent from the direction of predicted changes in flood magnitudes, as discussed above. The scenarios further agree in showing a decrease of days exceeding bankfull flow over most of eastern Europe, but with varying location and extent. The reduction of days is projected most spacious by the IPCM-A2 due to the generally reduced precipitation and discharge in this region. This is in accordance with the results found for the daily Q1 indicator. IPCM-A2 and MIMR-A2 project an enhanced number of days exceeding bankfull flow for parts of Scandinavia and the Baltic Region. MPEH-B1 shows least changes for this indicator, which is likely to be related to the moderate changes in precipitation.

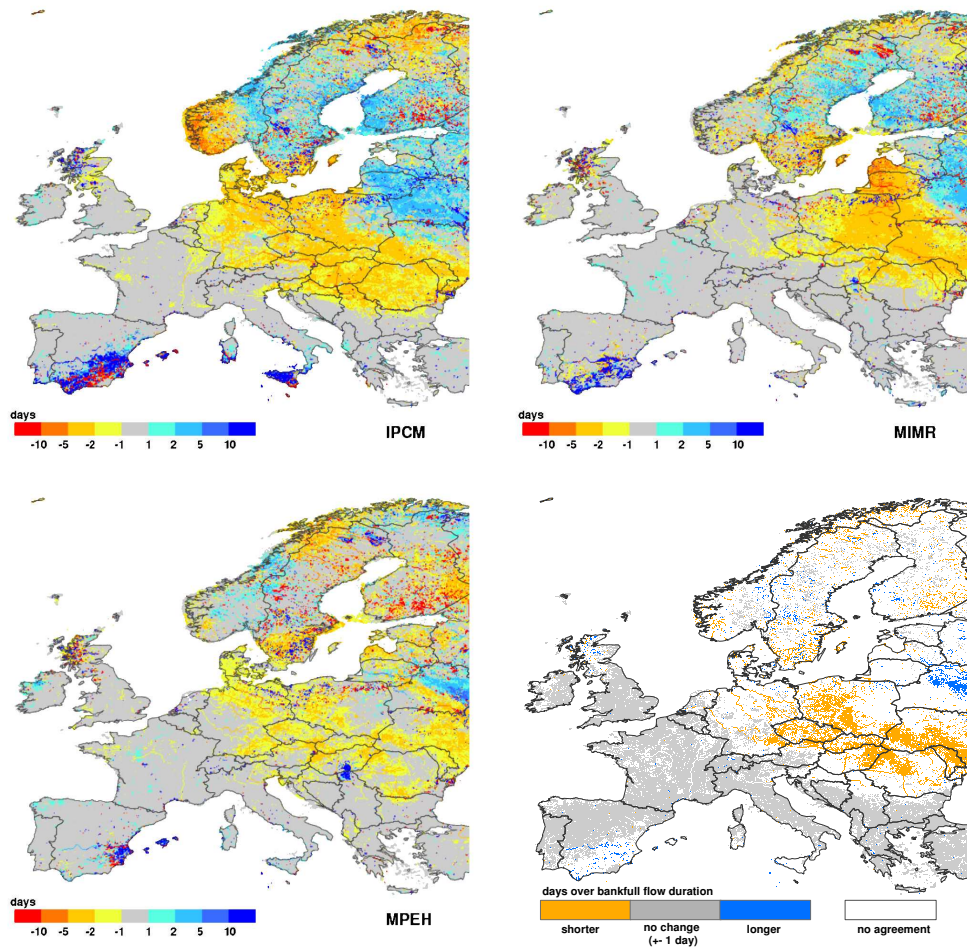


Figure 7.11— Absolute change in days over bankfull flow between reference period and scenario.

7.3.4 Comparison between scenario methods (delta change vs. future time series)

The time series applied to force WaterGAP can be derived by different methods. We have applied the direct monthly time series as calculated by the GCMs (TS) for the scenarios and the related control periods for the comparison between the single scenarios and flood indicators, described in Section 7.3.2. However, a common method to derive future time series of monthly climate for global scale hydrological studies is the application of the delta-change-method (DC): the time series of measured climate of the reference period (1961-1990) is scaled with the average monthly difference between the GCM control run and the scenario (see Section 7.2.1). For brevity, the impact of the two scenario methods on the three flood indicators is analyzed for MPEH-B1 only.

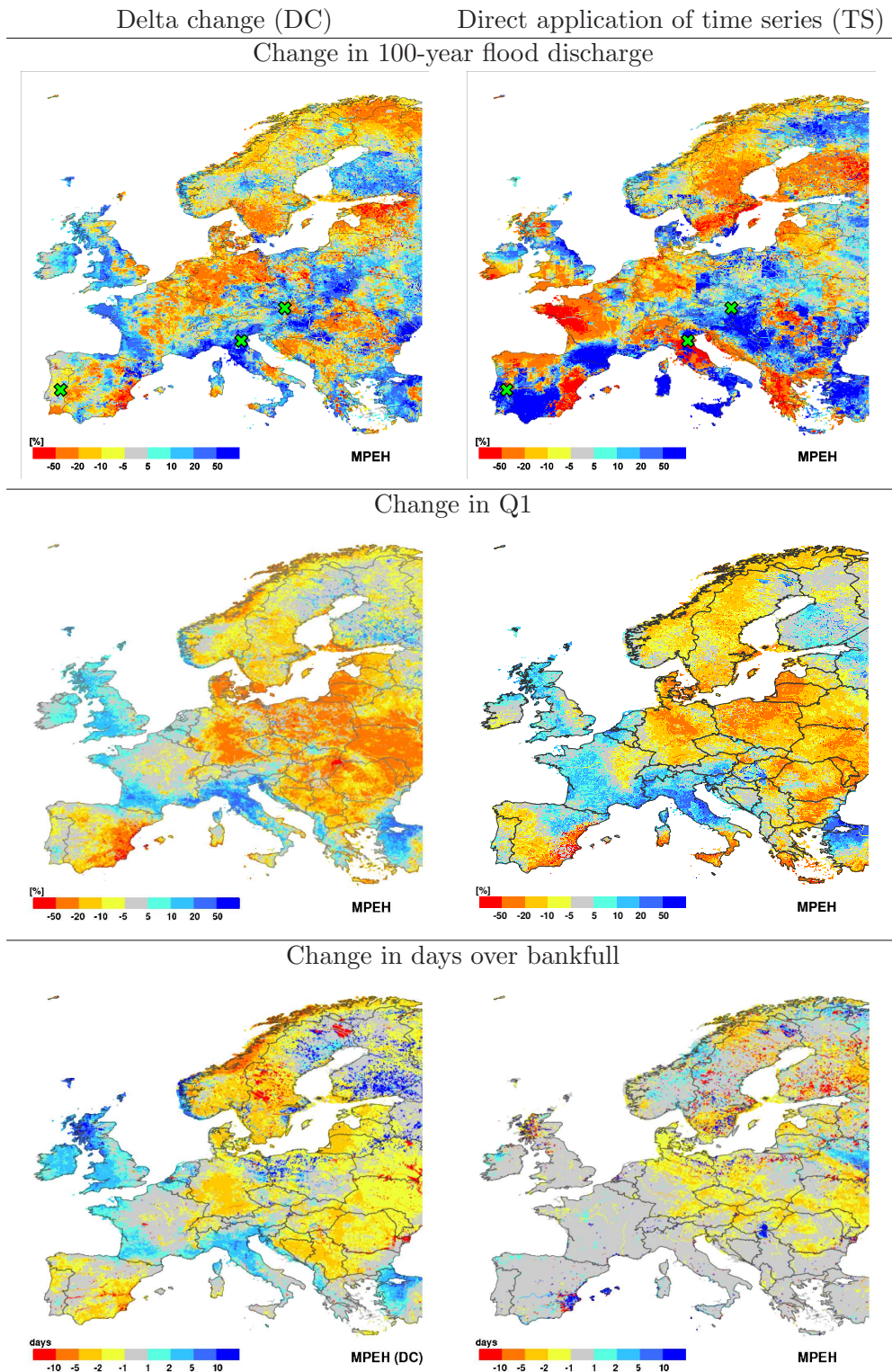


Figure 7.12— Comparison between the flood indicators calculated from MPEH5 climate. The forcing climate time series have been derived by the delta change method (left) or by the application of the direct GCM output (right). The crosses at the top figures indicate the location of gauging stations, which have been selected for further investigation

Results for Europe

The maps for Europe picturing the changes in the three flood indicators are compared in Figure 7.12, each calculated based on DC and TS climate (the TS-maps are identical with the maps shown in Section 7.3.2). The top maps in Figure 7.12 show the changes in 100-year flood discharge. It can be seen that the magnitudes of changes in either direction are more pronounced based on TS climate. Both maps show concordantly a decrease in 100-year flood discharge in most of Norway and Sweden, in parts of the Baltic Region, Mid-Europe and the Mediterranean region. An increase in 100-year flood level is found in parts of south-east and eastern Europe and the Mediterranean. But it is conspicuous that the calculated changes in 100-year floods based on DC and TS-climate leads to opposed results in different European areas. To investigate this effect in detail, we have selected the associated raster cells of three gauging stations in regions with contradictory changes in flood magnitude(see crosses on top maps on Figure 7.12), which are further analyzed in Section 7.3.4.

The differences between the maps showing the changes in daily Q1 (Figure 7.12, middle) are less contradictory between TS and DC compared to the 100-year flood discharge maps. The large scale patterns are basically the same over most of Europe with somewhat small differences in location, extent and magnitude. The magnitude of changes is more distinct for the TS climate, which has already been found for the changes in 100-year flood discharges. This shows that the daily Q1 is more robust against the scaling method than the changes in 100-year flood discharge.

The changes in the number of days exceeding bankfull changes are more pronounced when applying the DC climate (Figure 7.12, bottom). TS and DC agree in predicting a decrease in overbank flows over Mid- and Eastern Europe as well as in parts of the Baltic regions. Both methods show concordantly no change (± 1 day) in large areas especially all over Mid- and West-Europe, which is considerably larger for the TS climate. However the indicator derived by DC and TS disagrees in a number of European regions. The analysis of this finding is not part of this thesis, but is currently investigated within the scope of another study, which has not been finished yet.

Results for selected gauging stations

The direction of change for the 100-year flood discharge is contradictory in different European areas, as shown in Figures 7.8 and 7.9. However, the reasons behind the inconsistencies are complex and differ between single regions. Three gauging stations located in areas with opposed directions of change in 100-year flood discharge have been selected (see Figure 7.12, top and Table 7.2).

Figure 7.13 shows the AMS for the three gauging stations, each for the DC and TS climate and for 1961-1990 and the 2050s. The related daily discharge hydrographs for the third decade of the time series (1981-1990 and 2060-2069) are shown in Figure 7.14.

The Danube at Wien-Nussdorf shows a 13.5% decrease in the 100-year flood level for DC, whereas the TS projects an increase of 21% (Table 7.2). The AMS series of the MPEH-B1 control run is on a significantly higher level for the reference period (1961-1990) already compared to the CRU baseline (DC), which applies for the scenario period as well. Peak flows usually occur in spring (Figure 7.14) and are mainly snow melt induced, caused by tributaries originating in the Alps. The overestimation of the discharge peak in the TS

Table 7.2— Gauging stations selected for further investigations with changes in 100-year flood discharge for DC and TS.

River/ station	Routing area	Change in 100-year flood discharge between 1961-1990 and the scenario	
		DC-climate	TS-climate
Danube/ Wien Nussdorf (Austria)	101,700 km^2	-13.5%	+20.9%
Po/ Pontelagoscuro (Italy)	70,091 km^2	+37.75%	-20.55%
Tejo/ Vila Velha de Rodao (Portugal)	59,167 km^2	+3.28%	-12.6%

climate is likely attributed to an overestimation of the snow cover in the Alps due to errors in the representation of real climate in this heterogeneous terrain. The decrease in the discharge peak derived from DC climate can be ascribed to the reduced snow cover in the Alps due to climate warming (see Figure 4.6), leading to reduced snow melt induced flood peaks and a decreasing flood discharge during the whole range of return periods (Figure 7.13, top). The TS climate of the scenario period leads to a few large flood peaks, which are significantly above the level of flood peaks of the related control run. This results in increasing flood discharge of floods with return periods of 25 years or higher. The flood peaks of the TS scenario period at the Danube station do not generally exceed the peak flows of the related control run, quite the contrary: discharge of floods with return periods below 10 years are even projected to decrease.

The flood formation in the Po catchment can be attributed to both, snow melt in the Alps and heavy precipitation, especially in fall. Thus, flood peaks occurs either in fall or in spring, as shown by both methods, DC and TS (Figure 7.14). The AMS for DC and TS are on the same discharge level. However, the 100-year flood discharge of the DC method is projected to increase by 38%, whereas the comparable discharge based on TS climate is expected to decrease by approximately 20% (Table 7.2). The increase of the discharge level for the DC method is attributed to increased flood peaks in fall. The AMS of the control run and scenario period of the TS climate is on the same level for a large number of peaks. A few flood events of the control run caused high annual maximum flood peaks, leading to an increase of discharge for floods with return period larger than 10 years. The changes in more frequent return periods are marginal only.

For the Tejo river at Vila Velha de Rodao a slight increase (3%) of 100-year flood discharge is expected for the DC- and a decrease of 13% for the TS-method (Table 7.2). Floods in the Tejo catchment are usually caused by heavy winter precipitation with maximum discharges in January or February (Figure B.3, p. 133). Figures 7.13 and 7.14 show that both methods represent the discharge peaks within the same season but the magnitude differs significantly. The level of 100-year flood discharge peaks calculated with TS climate is considerably higher than those calculated from DC climate, which applies for the reference period as well as for the scenario period. The changes in 100-year floods in these regions are directly related to the changes in (extreme) winter precipitation, suggesting an overestimation of winter precipitation by MPEH-B1. There is only little difference in the discharge for flood return periods of 50 years or lower (TS-climate). The largest decrease is found for the 100-year flood. The discharge calculated from DC climate is expected to

vary marginally over the whole range of return periods (Figure 7.14).

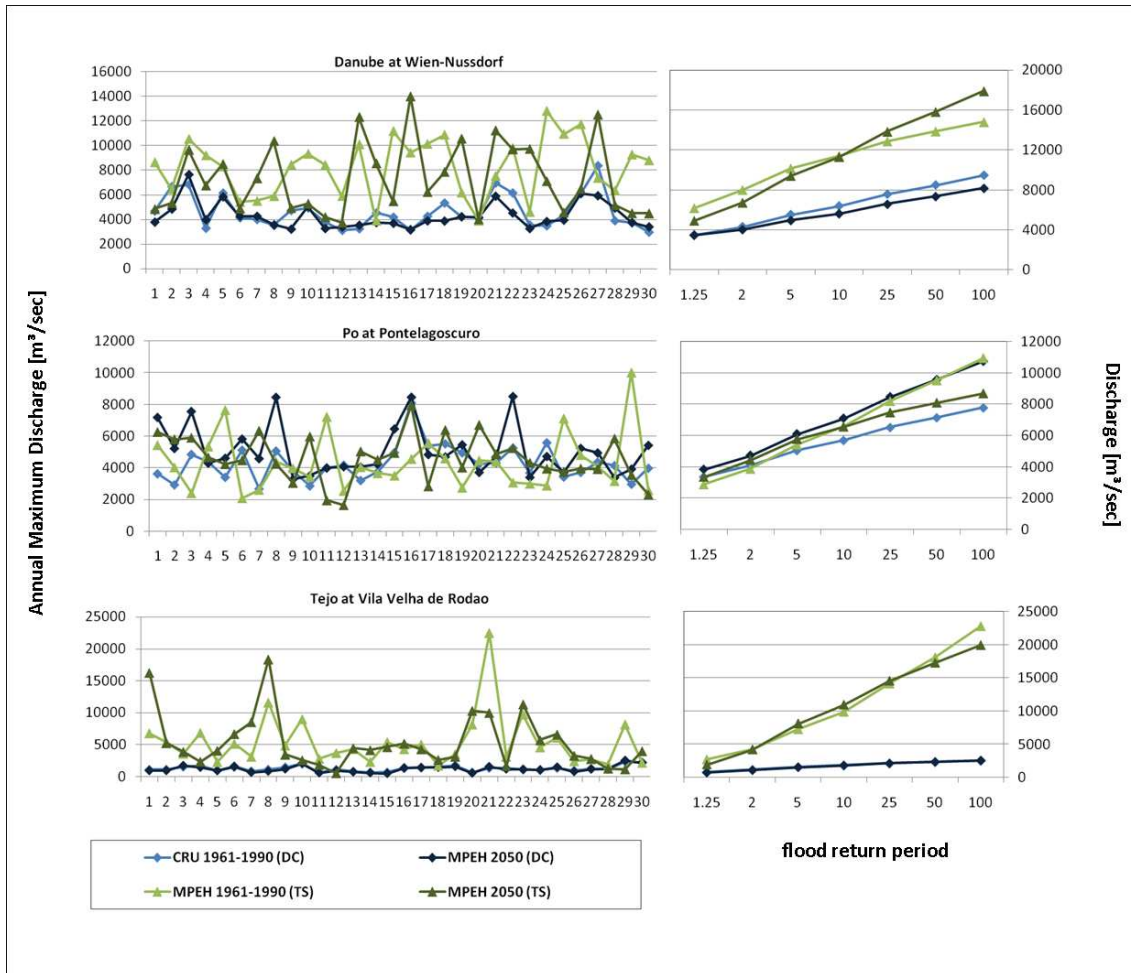


Figure 7.13— Changes in Annual Maximum Discharge (AMS) and the corresponding flood frequency distribution of the 30 year time series for the reference period (1961-1990) and the scenario period (2040-2069) for rivers showing opposed results in change in 100-year flood discharge for the DC and TS methods.

7.4 Discussion

The simulation of floods, in particular 100-year flood levels with WaterGAP is exposed to a number of uncertainties originating from the forcing climate and from WaterGAP itself. GCMs have difficulties in simulating precipitation consistent with observations (for a detailed analysis see Meehl et al., 2007), whereas the bias in simulated precipitation varies substantially with season and location between different climate models (Christensen et al., 2007). Sillmann and Roeckner (2008) investigated extreme events simulated by ECHAM5/MPI-OM, which is the GCM behind MPEH-B1, and found that the large scale patterns of precipitation extremes can be represented by the GCM, however with regional exceptions, such as areas with complex orography. This is attributed to the coarse resolution of the forcing climate (1.875° x 1.875°). The simple bilinear interpola-

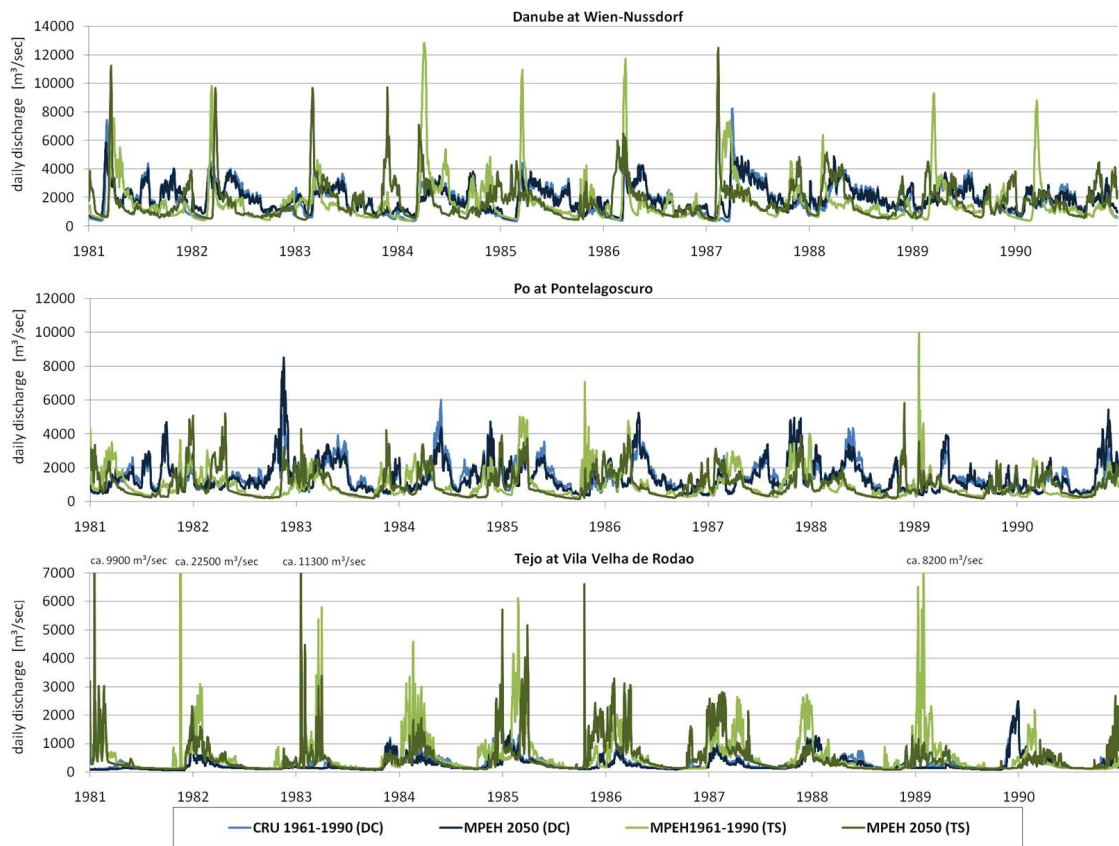


Figure 7.14— Hydrographs of the same stations as in Figure 7.13 but for 1981-1990 only (which is 2060-2069 in the scenario period)

tion that has been applied to downscale the GCM output to the 5 arc minutes resolution of WaterGAP, does not consider altitudinal effects on precipitation and temperature. Therefore, the climate and consequently the snow cover in the mountainous European regions such as the Alps, Pyrenees or the Carpathians neither represented well in the scenario runs nor in the related control runs. This has affected the results of the present study, where for example peak flows of snow affected Danube differed considerably between ECHAM5/MPI-OM (MPEH-B1) and CRU driven simulations. Another source for uncertainty is the applied pseudo-daily precipitation, derived from monthly GCM climate, which is distributed equally over the month on a fixed formation of wet days (see Section 2.5.3). Changes in the temporal precipitation variability are not considered accordingly, though it is important for flood related studies. The annual maximum 5-day accumulated rainfall, which is an indicator for extreme precipitation, is expected to change during the 21st century (e.g. Dankers and Feyen, 2008; Sillmann and Roeckner, 2008; Beniston et al., 2007). It would be reasonable to apply RCM output to force WaterGAP on European scale. State-of-the-art RCMs have a spatial extent between 12 km and 50km over Europe (Christensen and Christensen, 2007). Thus, they are well suitable to be used as input for WaterGAP3, which has a grid cell size of approximately 6x9 km in central Europe. Further, RCMs are able to simulate extreme precipitation more realistically than GCMs

(Fowler et al., 2007).

The simulation of 100-year flood discharge levels can be simulated with WaterGAP3 reasonably well, but it is connected to a number of uncertainties as has already been described in Section 7.2.3. The retention of extreme flood discharge, such as 100 year floods in reservoirs and flood plains is not represented within WaterGAP. Also the choice of the extreme value distribution to estimate the 100-year flood discharge influences the results (Dankers and Feyen, 2008). For a number of raster cells may distributions different from the Log-Pearson III type distribution be more suitable. We minimized the uncertainty by testing the suitability of the chosen Pearson III distribution with a Chi^2 -Test. Raster cells in which the selected distribution has not been suitable have been blanked out in the result maps. It has further been shown that the 100-year flood discharge is sensitive to the method of deriving future time series of forcing climate as well as to different scenarios. The projected changes in discharge that is exceeded statistically in 1 of 100 days (daily Q1) are less sensitive than the 100-year flood discharges. This applies for the comparison between different scenarios, where larger areas of agreement have been found, as well as to the method to derive time series of future climate. No single peak discharges are required to calculate the daily Q1, as is for deriving the 100-year flood discharge. This makes the calculation of the daily Q1 more robust and WaterGAP calculates more reliable results for the Q1 indicator compared to the 100-year flood discharge (Section 7.2.3). The daily Q1 copes frequent flood events, to which nature and humans are generally well adapted. It might be possible that public interest in the daily Q1 is lower than in the expected changes in the extreme 100-year flood discharge, even though these results are far more uncertain.

First results for the third flood indicator, the number of days per year exceeding bankfull flow, have been shown as well. The results should be treated as preliminary, since the validation in selected European watersheds has not been finished yet. In contrast to the other two indicators (100-year flood and daily Q1) is the agreement of large scale pattern with change in either direction and areas with "no change" comparably large. It has also been found that an increasing number of days with overbank flow should not be equated with increasing flood magnitudes and vice versa. The investigation of this effect is work in progress as well.

The study presented in this chapter has shown that the choice of the method to derive the time series of future climate affects simulated changes in flood discharge. Changes in flood levels driven by climate derived with a delta-change-method have been compared to results forced by direct GCM output. It has been found that largest effects of the "scaling method" occur for the changes in 100-year flood discharge. This is in agreement with results found by Graham et al. (2007) and Lenderink et al. (2007). Lenderink et al. found a stronger change of 100-year flood discharge of the Rhine from the delta change approach compared to the direct application of the time series. This agrees with the results found for IPCM-A2 of the present study but cannot be conveyed as general rule. Changes in 100-year flood discharge with opposed results in both directions have been found in the present study in different European areas with varying extent and location. The reasons behind the contradictory results vary between the regions and the factors behind the flood formation, most prominent snow melt and extreme precipitation. Thus it is important that both, the snow cover as well as the extreme discharge is represented well. The snow cover especially in the comparably small European mountains is represented significantly better

by WaterGAP results forced by CRU climate compared to the control runs of the GCMs (for 1961-1990). This is due to the much higher spatial resolution of the CRU dataset (10 arc-minutes over Europe) compared to the GCM climate. Yet, the CRU dataset has been scaled by a simple delta change approach to derive future time series of temperature and precipitation. This leads to reasonable changes in future snow cover, but changes in the variability of future precipitation cannot be considered, which is crucial for the simulation of changes in flood magnitudes. Changes in precipitation variability are considered when applying direct time series of GCMs. This applies for daily climate data naturally more than for the monthly climate time series as have been applied in the present study.

Recently, Dankers and Feyen (2008) investigated changes in 100-year flood discharges over Europe by driving the hydrological model LISFLOOD with RCM climate. They found a decrease of the flood level over northeastern Europe due to decreasing snow cover. This agrees with results found for MPEH-B1 in this study. In the same region show IPCM-A2 and MIMR-A2 increasing flood discharge caused by a significant increase in the snow cover and related snow melt peak flows. Dankers and Feyen further found a 100-year flood level decrease to a varying degree in central Europe as well as in parts of the Iberian Peninsula. This agrees with the results found in the present study, whereas Dankers and Feyen (2008) found a decrease in the southern part of the Iberian Peninsula, which agrees with MIMR-A2 only. IPCM-A2 and MPEH-B1 project decreases in the northern and eastern part (MPEH-B1 only) of this region. Strong increases in 100-year flood discharge have been found by Dankers and Feyen (2008) across much of western and central Europe, including parts of the Balkan, northern Italy as well as parts of Sweden and southern Norway. This agrees with the large patterns found in this study, but with varying extent between the scenarios.

Dankers and Feyen (2008) referred to Lehner et al. (2006), who performed the first analysis of changes in extreme floods over Europe, as has already been mentioned in Section 7.1. Lehner et al. (2006) applied an older model version of WaterGAP than the one used within the present study. Dankers and Feyen suggest that the inconsistencies between their and the WaterGAP results calculated by Lehner et al. might be "related to the much higher resolution of both the climate and the hydrological models used in the present study, or to an increase in daily rainfall variability, which was not taken into account in the Lehner et al. study". The WaterGAP results presented in this study are much closer to the results found by Dankers and Feyen. The spatial resolution of WaterGAP has been enhanced compared to the model version as applied by Lehner et al., but the effect cannot be validated based on the results of the present study. Another reason for the convergence of the model results might be the general improvement of WaterGAP (Chapters 2-6) for simulating floods but also the choice of the forcing climate. Lehner et al. (2006) applied climate based on the IPCC-IS92a scenario from the early years of this decade, which is comparably old and GCMs and RCMs have significantly been improved since then. It can be agreed with Dankers and Feyen that driving WaterGAP with daily climate produced by RCMs with a high spatial resolution could further improve the reliability of the flood projections with WaterGAP.

7.5 Summary and Conclusions

The global hydrological model WaterGAP has been applied to simulate floods on European scale. The results of the flood discharge validation have been encouraging. WaterGAP is able to reproduce the discharge level of 100-year floods reasonably well, which also applies for simulated daily Q1 (discharge that is exceeded statistically at one of 100 days). The daily Q1 can be represented more realistically by WaterGAP, because the indicator is more robust to errors of the simulated magnitude of peak flows compared to the 100-year flood discharge. It is likely that the results can further be improved by considering flood retention in managed reservoirs.

WaterGAP has been applied to assess the climate change impact on floods risks in Europe. Three climate change projections (results of three GCMs according to two emission scenarios (A2 and B1)) have been compared by calculating three different flood indicators (100-year flood, daily Q1, annual number of days with overbank flow). The agreement between the projections decreases with increasing flood magnitude covered by the respective indicator, i.e. the agreement between the projections for daily Q1 has been larger than for 100-year floods. This shows that the calculation of 100-year floods is less robust to differences between scenarios and GCMs as well as to errors in the representation of flood peak level by WaterGAP than the daily Q1, which covers regular floods. However, the interest of policy, public and science in expected changes of extreme floods is high, even though the results are uncertain. It would be reasonable to perform further research on the development of new flood indicators to enhance the informative value of flood studies to the public.

All scenarios applied in this study agreed in the projected changes of flood magnitudes in a number of large regions, however with varying spatial extent and location. Increasing flood risk is projected for parts of the Mediterranean area concordantly; more precisely parts of the Iberian Peninsula, Italy and the eastern Mediterranean region, although the average precipitation is predicted to decrease in this region. This is caused by a significant increase in precipitation especially in fall and winter. Increased 100-year flood levels have also been shown in agreement in south and north Scandinavia, caused by a considerable increase in winter precipitation, especially for the IPCM-A2 and MIMR-A2 scenarios. Further are parts of west, mid- and eastern Europe projected to suffer from increased flood magnitudes. A decrease in 100-year flood levels as well as in daily Q1 is expected in parts of eastern and central Europe by all scenarios to a varying degree. The scenarios further predict concordantly a decrease in the flood magnitudes in the Aegean and in parts of the Iberian Peninsula.

The preliminary results presented for the annual number of days exceeding bankfull flow show marginal changes over most of western and southern Europe. The scenarios further agree in showing a decrease of days exceeding bankfull flow over most of eastern Europe, but with varying location and extent. Further analysis of this indicator should be carried out and it would be reasonable to select selected case study regions, where changes in regular inundations are crucial.

The results of future changes in flood hazard are exposed to a number of uncertainties originating in WaterGAP itself and the forcing climate applied. Especially the calculation of future changes in 100-year floods is sensitive to the forcing climate. This has been shown by the comparison of results based on future climate time series scaled with a delta

change method compared to the direct application of GCM time series. The simulation of flood scenarios can presumably be improved by the application of RCM climate calculated, which have a higher spatial resolution than the GCM climate applied in this study. The representation of changes in daily climate variability could be enhanced by the usage of daily climate to force WaterGAP. Alternatively, more sophisticated methods to derive future time series of forcing climate and downscaling methods may improve the reliability of modelled changes in future flood hazards.

Chapter 8

Summary and Outlook

8.1 General Summary

The central theme of this dissertation is the (further) development of the global scale hydrological model WaterGAP to assess climate change effects on flood hazards worldwide. WaterGAP should be suitable to define regions on large scale, in which considerable changes in floods might be expected based on different climate change scenarios. The representation of the snow dynamics and the river flow velocity within WaterGAP have been assessed in detail, because these are important determining factors of the formation and simulation of floods. This included the validation of the model results as well as the investigation of climate change impacts on snow cover and river flow velocity. Further the spatial resolution of WaterGAP has been increased from 0.5° globally (WaterGAP 2.1) to 5 arc-minutes globally (WaterGAP3), which leads to a more realistic representation of the river network and naturally to a higher information density of static input maps (Chapter 2). Several research questions have been raised in the Introduction of this dissertation (Chapter 1), which were answered throughout this thesis and will be summarized in the following.

How can the simulation of snow dynamics and the representation of snow melt induced peak flows be improved? How does climate change affect the snow cover of snow dominated regions of the world?

Snow melt induced flood peaks in spring were overestimated in a large number of mountainous catchments, before the simulation of the snow dynamics has been improved within the scope of this thesis. The overestimation has been caused by the uniform simulation of the snow cover on a 0.5° grid cell, of which the snow of the entire grid cell started melting once the temperature exceeded 0°C . The simulation of the peak flow has been far more successful when implementing sub-scale information within each grid cell (Chapter 3): the altitudes of 100 sub-grid cells have been assigned to each 0.5° grid cell of WaterGAP and snow accumulation and melt is calculated individually on each sub-grid. The modeled extent of the Northern Hemisphere snow cover has been validated with satellite derived data. The results were encouraging and showed that WaterGAP is able to represent the snow cover well, which is especially true for North America, parts of Europe and in spacious plain areas such as northern Russia. The largest discrepancies

between observed and modeled snow cover extent occur in orographically heterogeneous regions like Central Europe and in regions with comparably imprecise climate data, e.g. the Hindu Kush-Himalaya region or eastern Asia. The snow module has been improved within the model version WaterGAP2 and has been implemented afterwards into WaterGAP3 as well.

A decrease in Northern Hemisphere snow cover has been observed during the last decades, which is very likely to further contract within the 21st century (e.g. IPCC, 2007a), showing that the snow cover is particularly susceptible to climate warming. WaterGAP2 has been applied to investigate the climate change impact on (i) seven large mountain regions worldwide and (ii) the Northern Hemisphere snow cover based on two climate change scenarios for the 2080s, each calculated by two different GCMs. As could be expected, all investigated mountains will be affected by climate change, with drastic impacts on their future snow cover, which is projected to decrease significantly in most mountains and which goes along with a significant rise of the snow line (Chapter 4). Mountains of the lower latitudes will suffer from a stronger decrease in snow cover than those located in the northern regions of the globe. Most affected are the Alps, the Andes and the Hindu Kush-Himalaya region. In contrary to other selected mountains, the snow cover magnitude of the Altai is expected to rise due to increasing precipitation and the extremely cold temperatures, which are despite climate warming far below the 0°C threshold.

The snow dominated areas of the Northern Hemisphere are expected to shrink, most pronounced in mountains, north-eastern Europe, northern USA and the Canadian west coast. This is shown in agreement by both GCMs and scenarios (Chapter 4). The decrease of the snow cover does also affect the discharge of large rivers located in the snow dominated areas of the Northern Hemisphere, draining into the Arctic Ocean. The total freshwater inflow into the Arctic Ocean provided by the nine largest Arctic rivers is projected to increase considerably. This is likely to alter the freshwater balance of the Arctic Ocean with possible impacts on sea ice formation and the thermohaline circulation.

How can the lateral transport of the water through the river network be improved? Does climate change affect the flow velocity of European rivers?

Originally, the river discharge was routed with a constant river flow velocity of 1m/sec through the river network of WaterGAP2. Thus, the spatial and temporal variability of the flow velocity was not considered, which is related to the actual river discharge, the river bed slope and the river bed roughness. The river flow velocity is simulated more realistically after model improvement by (i) increasing the spatial resolution of WaterGAP (Chapter 2), and (ii) implementing a variable river flow velocity (Chapter 6). The increased spatial resolution of WaterGAP3 leads to a more realistic representation of the river length, which has additionally been improved by considering an individual meandering factor for each grid cell, derived from a high resolution drainage direction map (Chapter 6). A temporally and spatially variable river flow velocity has been incorporated into WaterGAP3 within the scope of this thesis (Chapters 5 and 6). A way had to be found to model flow velocity simple enough to derive the required parameters from data globally available and sophisticated enough to deliver realistic flow velocity values for a large variety of environmental conditions. The river flow velocity is modeled based on

the Manning-Strickler formula, which consists of three factors that have been derived as follows: The river bed roughness (Manning's n) is approximated spatially explicit based on topography, the location of urban population and the river sinuosity. The hydraulic radius is estimated from actual river discharge and the river bed slope is derived by combining a high resolution DEM, a 5 arc-minute drainage direction map and the river sinuosity. It has been found that WaterGAP matches the level of measured velocities satisfyingly, by comparing modeled to measured river flow velocities of 22 US rivers. However, the model overestimates the average velocity at most investigated gauging stations. Despite the uncertainties of the modeled river flow velocity, the representation of the lateral transport has clearly been improved compared to the constant flow velocity applied in older WaterGAP versions. Largest effects of the variable flow velocity on river discharge occur at peak flows, which generally increase by applying the variable flow velocity. Hence, the representation of afore underestimated flood peaks improves and vice versa. The effects on monthly discharge hydrographs is marginal only.

Three climate change projections (results of three GCMs according to two emission scenarios (A2 and B1)) for the 2050s have been chosen to drive WaterGAP3 for assessing climate change impacts on flow velocity and related to this the residence time of the water in the river system. The results of the three projections differ for central and eastern Europe. They agree in predicting a decreased residence time in northern Europe and show an increasing residence time in parts of the Mediterranean, caused by declining water availability and, connected to this, slower river flow velocity. It can be concluded that climate change does affect the river flow velocity, which is related to average discharge, but the changes are comparably small. Larger effects can be expected by considering the effects of anthropogenic water consumption on river discharge and river flow velocity.

How can floods be simulated on global scale and which climate change impacts on flood hazards can be expected in Europe? Which impact has the method of deriving future climate time series on the flood calculations?

WaterGAP3 has been applied to simulate discharge levels of 100-year floods on European scale as well as the daily Q1, defined as discharge that is exceeded statistically at one of 100 days and which covers more regular floods (Chapter 7). The results of the flood discharge validation have been encouraging. WaterGAP is able to reproduce the measured flood levels satisfyingly. The daily Q1 is represented more realistically by WaterGAP, and it has been found that this indicator is more robust to errors in simulated magnitudes of peak flows than the 100-year flood discharge. WaterGAP has problems to match the exact level of large flood peaks. For this reason, only the changes in flood discharges have been analyzed in the climate change impact study.

The climate change impacts on floods hazards in Europe have been assessed based on the same three climate change projections for the 2050s that have already been applied for the flow velocity investigations. The changes between the control period (1961-1990) and the scenario period have been compared for three different flood indicators: (i) the 100-year flood discharge, (ii) the daily Q1, and (iii) the number of days with overbank flow (Chapter 7). The agreement between the projections decreases with increasing flood magnitude covered by the respective indicator, i.e. the agreement between the projections for daily Q1 has been larger than for 100-year floods. An increased flood risk is predicted

for large parts of Europe by all projections, but with varying spatial extent and location, which will be discussed with more detail in the following. All projections show rising flood discharge in parts of the Mediterranean area concordantly, although the average annual precipitation is predicted to decrease in this region. This is caused by a significant precipitation increase especially in fall and winter. Enhanced 100-year flood discharge levels have also been shown in agreement in southern and northern Scandinavia, caused by increasing winter precipitation. Further, parts of west, mid- and eastern Europe are projected to suffer from rising flood magnitudes. A decrease in 100-year flood levels as well as in daily Q1 is predicted for parts of eastern and central Europe by all projections to a varying degree. The projections further predict concordantly a decrease in flood magnitudes in the Aegean and in parts of the Iberian Peninsula. The number of days with overbank flow is going to change marginally only over most of western and southern Europe. This finding suggests that the duration of the floods does not change necessarily, when the flood magnitude changes in either direction. The three projections agree in showing a decrease of days with overbank flow over most of eastern Europe, but with varying location and extent. Two of the three projections predict an enhanced number of days with overbank flow for parts of Scandinavia and the Baltic region.

It can be concluded that the number and magnitude of extreme flood hazard are expected to increase until the 2050s in many European areas. However, the spatial extent and location varies considerably between the three scenarios, which particularly applies for changes in 100-year flood discharge. Further analyzes and scenario studies are required to reduce the uncertainty of the projected changes of large floods and to enhance the informative value for the public.

Time series of forcing climate can be derived by different methods. Two methods have been compared within the scope of this study and changes in flood levels have been calculated based on (i) the direct application of GCM time series for the control period (1961-1990) and the scenario period (2040-2069), and (ii) average climate of the scenario period scaled with a delta change method on measured climate (CRU dataset). The choice of the method used to derive the time series of future climate affects simulated changes in flood discharge considerably (Chapter 7). Largest effects have been found in for the changes in 100-year flood discharge, which even shows opposed results in both directions in different European areas and with varying extent and location. The impact on the daily Q1 results have been comparably small, which shows that the daily Q1 is less sensitive to the method of deriving the climate time series. The reasons behind the contradictory results for the 100-year flood discharge vary between the regions and the regional representation of snow melt and extreme precipitation. The snow cover especially in the comparably small European mountains is represented significantly better by WaterGAP results forced by CRU climate compared to the control runs of the GCMs. This has been caused by the much higher spatial resolution of the CRU dataset. The application of the delta change method leads to reasonable changes in future snow cover, but changes in the variability of future precipitation cannot be considered, which is crucial for the simulation of changes in flood magnitudes. However, by using the direct GCM time series is the snow cover represented less satisfyingly but changes in precipitation variability are considered. This applies for daily climate data naturally more than for the monthly climate time series as applied in the study presented in Chapter 7.

8.2 Concluding Remarks and Outlook

It can generally be concluded that the objective of this dissertation, the further development of WaterGAP for assessing climate change effects on flood hazards worldwide, has been realized successfully. But the last open question is, whether large flood events can be modeled more realistically with the improved model version WaterGAP3, compared to the original WaterGAP version that has been used as basis for the improvements performed within the scope of this dissertation (WaterGAP2.1e). 100-year flood discharge derived from measured discharge of European gauging stations is compared to the respective flood levels of WaterGAP 2.1e and WaterGAP 3.1, respectively (Figure 8.1). The r^2 of the WaterGAP3 simulated flood discharge is larger than for WaterGAP 2.1e, showing that on average large flood discharges are represented better by WaterGAP3 compared to WaterGAP 2.1e.

However, the flood analyzes described and discussed in Chapter 7 of this thesis shows

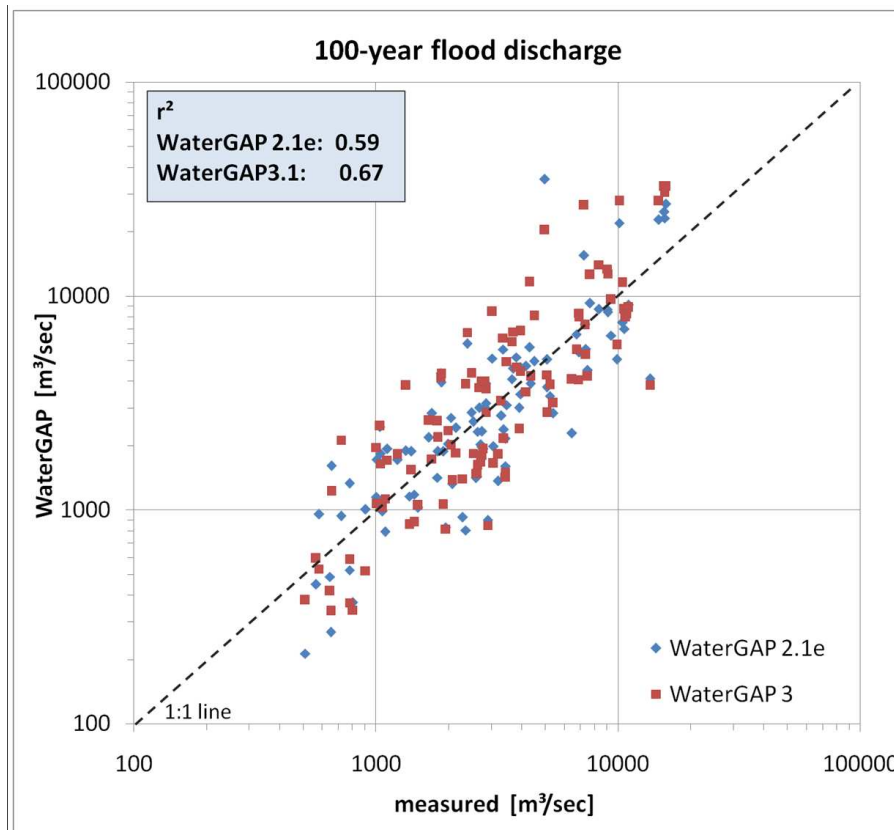


Figure 8.1— Validation of 100-year flood discharge modeled by two WaterGAP versions: before (WaterGAP 2.1e) and after (WaterGAP3.1) implementing the improvements performed within the scope of this dissertation.

first WaterGAP3 results only and it has been discussed that there is still potential for improvement. WaterGAP3 is prepared to simulate floods worldwide, but the model has been validated for Europe only and further validation should be performed for other regions of the world. The forcing climate influences the modeled flood discharges considerably and it

is likely that the results can further be improved by the application of climate from RCMs. The high spatial resolution of RCMs compared to GCMs would presumably lead to a better representation of climate conditions in mountains and thereby improve the simulation of snow cover as well as snow melt induced peak flows. Furthermore, the representation of precipitation extremes is more reliable in RCMs compared to GCMs (Fowler et al., 2007). The climate used to drive WaterGAP could generally be improved by using sophisticated spatial downscaling methods, which consider the impact of topography on the climatic conditions. Additionally, more elaborated methods to derive bias corrected scenarios to drive WaterGAP may represent the variability of precipitation more realistically, which would consequently lead to a better representation of discharge extremes (Leander and Buishand, 2007). It would be worthwhile to find a way to derive future climate time series, which reasonably represents the variability and magnitude of precipitation as well as the snow cover. Flood related analyzes based on WaterGAP3 calculations could additionally be improved by the use of daily climate time series for both, the reference period and the scenario.

This study has shown average annual changes in flood magnitudes only. However, the predicted precipitation changes vary considerably between the single seasons. Thus, an analysis of seasonal changes of extreme floods is advisable. The interest of policy, public and science in expected changes of extreme floods is high, even though the results are uncertain. Further research should therefore be carried out on the choice or even development of new flood indicators, which are less uncertain than the 100-year flood and would consequently enhance the informative value of flood studies for the public.

Appendix A

Appendix to Chapter 4

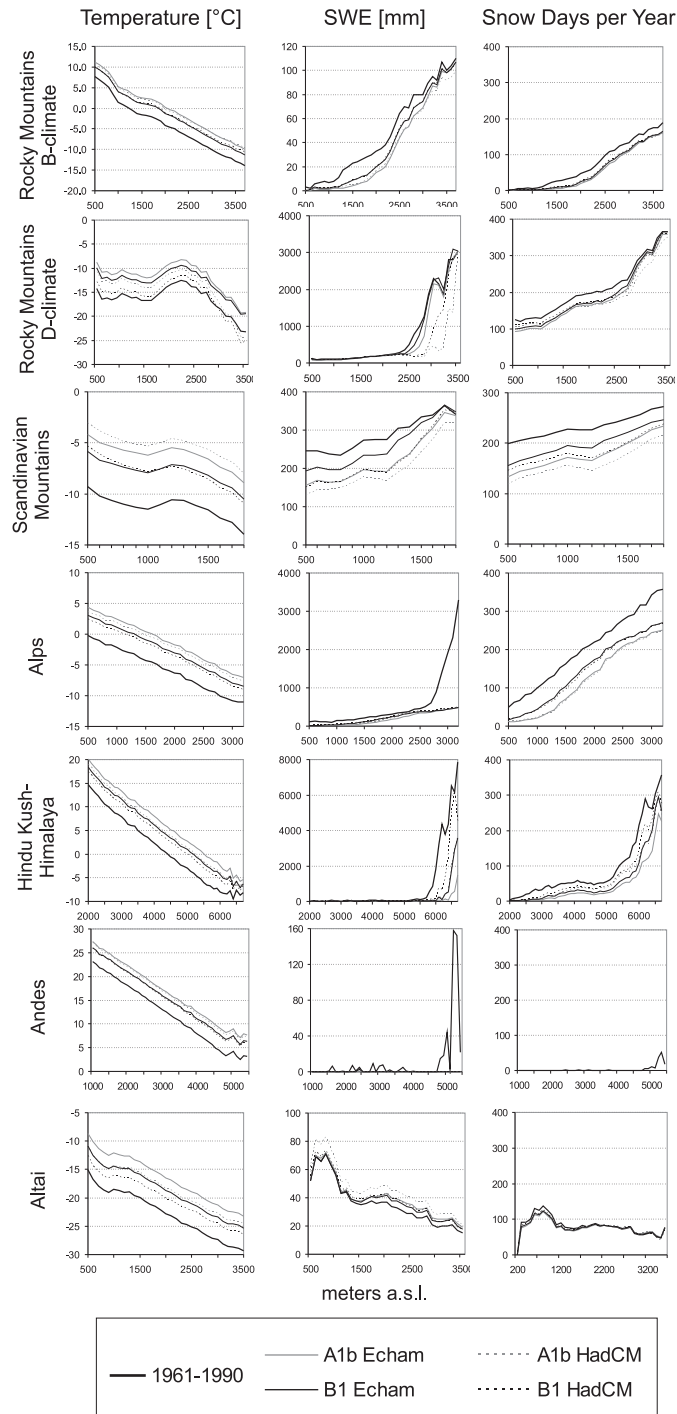


Figure A.1— Average January or April temperature and SWE (depending on annual SWE maximum) and annual number of snow days over the altitude [m a.s.l.] of seven selected mountain ranges during the reference period 1961-1990 and the four scenarios of the 2080s. We show results for altitudinal belts that include more than 5 sub grids.

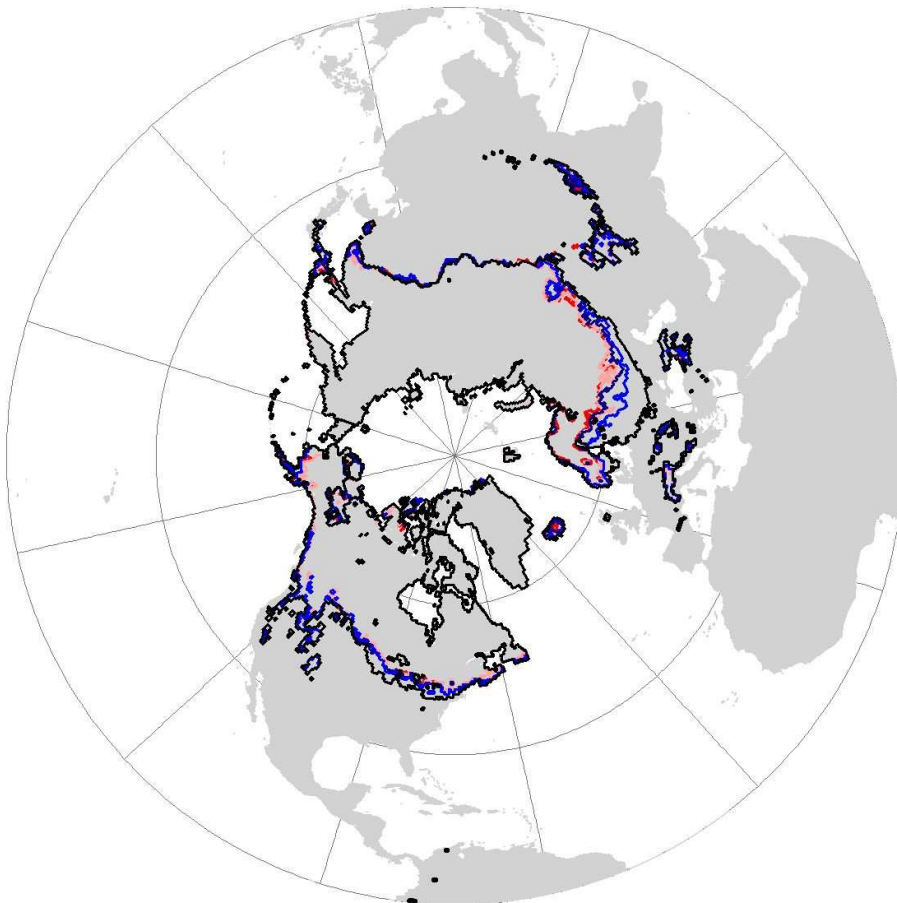


Figure A.2— Snow dominated area of the reference period (1961-1990, black line) and for the four scenarios of the 2080s: Echam5 - A1b: pink, Echam5 - B1: light blue, HadCM - A1b: red, HadCM - B1: dark blue.

Appendix B

Appendix to Chapter 7

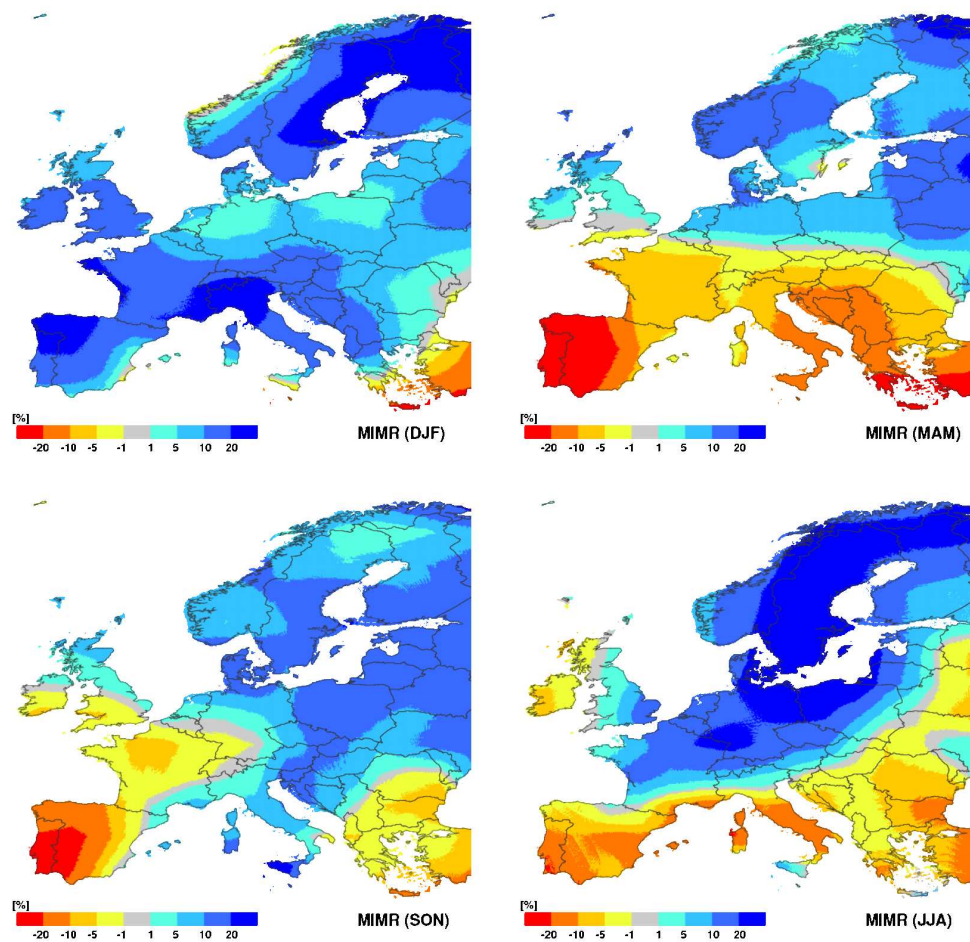


Figure B.1— Seasonal changes in precipitation of the MIMR scenario (2050s) compared to the corresponding control run (1961-1990).

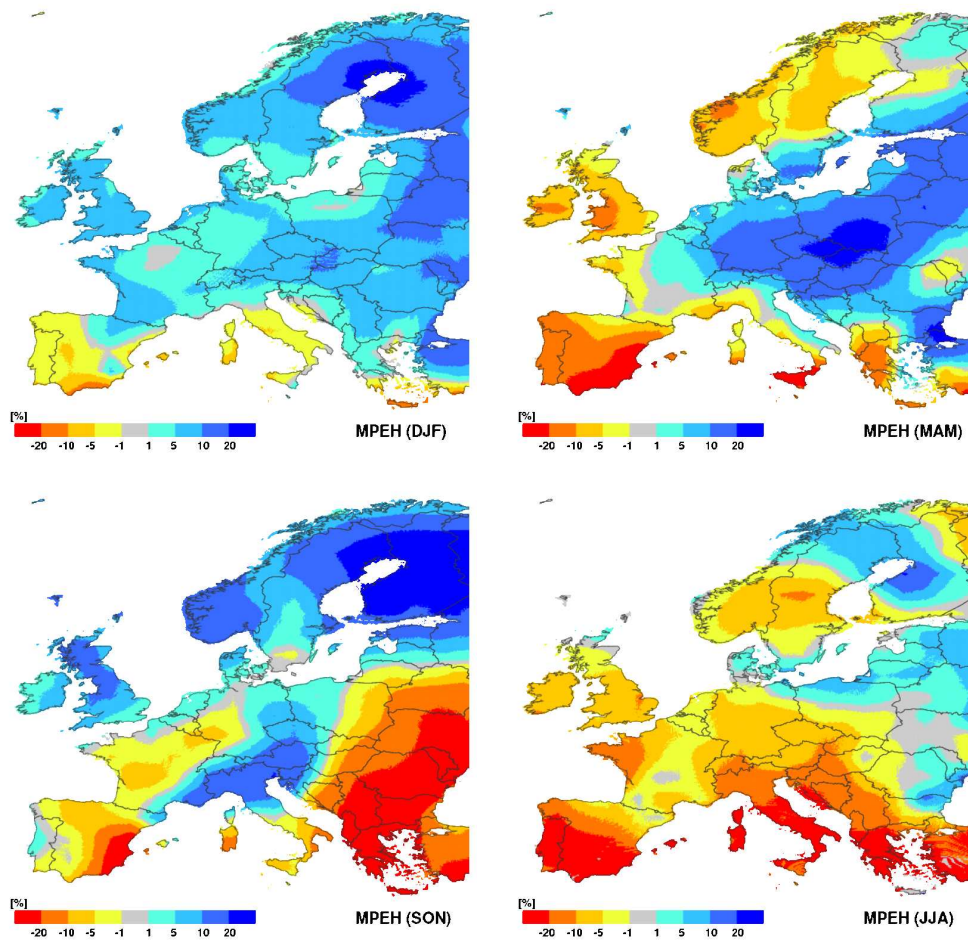
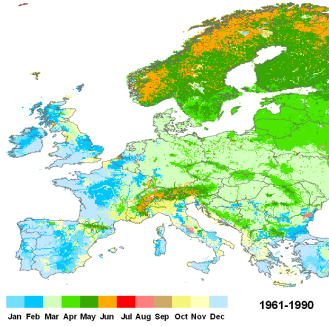


Figure B.2— Seasonal changes in precipitation of the MPEH scenario (2050s) compared to the corresponding control run (1961-1990).

1961-1990 CRU climate



1961-1990 GCM time series

2050s GCM time series

2050s scaled with delta change method

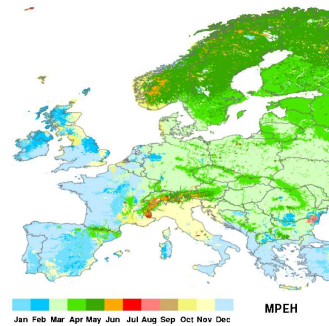
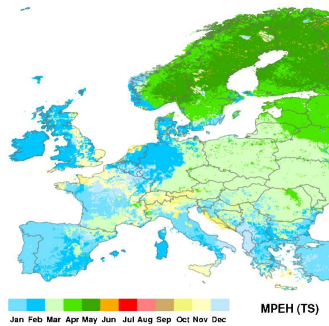
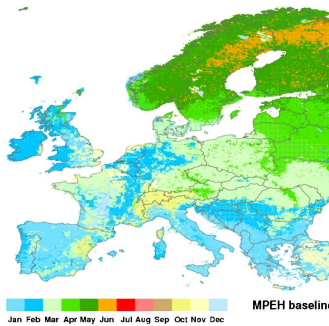
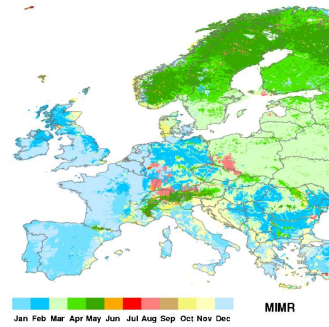
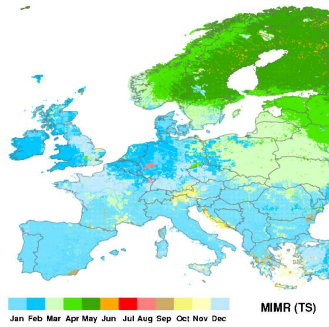
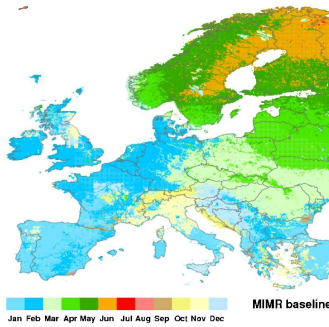
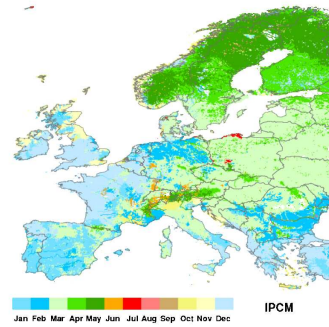
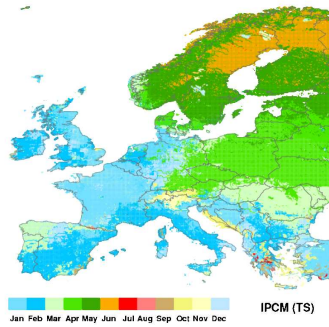
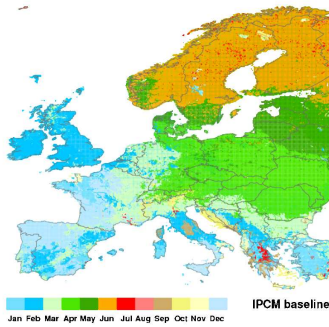


Figure B.3— Month with maximum discharge for reference period (CRU-climate), control period (GCM) and the scenarios derived by DC and TS, respectively

Bibliography

- ACIA: Arctic Climate Impact Assessment., Cambridge University Press, <http://www.acia.uaf.edu>, 2005.
- Alcamo, J., Kreileman, E., Krol, M., Leemans, R., Bollen, J., Minnen, J. v., Schaeffer, M., Toet, S., and Vries, B. d.: Global Change Scenarios of the 21st Century. Results of the IMAGE 2.1 Model, chap. Global modelling of environmental change: an overview of IMAGE 2.1, pp. 3–94, Pergamon, Oxford, 1998.
- Alcamo, J., Döll, P., Henrichs, T., Kaspar, F., Lehner, B., Rösch, T., and Siebert, S.: Development and Testing of the WaterGAP 2 Global Model of Water Use and Availability, *Hydrological Science*, 48 (3), 317–337, 2003a.
- Alcamo, J., Döll, P., Henrichs, T., Kaspar, F., Lehner, B., Rösch, T., and Siebert, S.: Global estimation of water withdrawals and availability under current and "business as usual" conditions, *Hydrological Science*, 48 (3), 339–348, 2003b.
- Alcamo, J., Van Vuuren, D., Cramer, W., Alder, J., Bennett, E., Carpenter, S., Christensen, V., Foley, J., Märker, M., Masui, T., Morita, T., O'Neill, B., Peterson, G., Ringler, C., Rosegrant, M., and Schulze, K.: Ecosystems and human well-being, Scenarios, findings of the Scenarios Working Group, Millennium Ecosystem Assessment., chap. Changes in ecosystem services and their drivers across the scenarios. Chapter 9, pp. 297–373., Island Press, Washington, 2005.
- Alcamo, J., Flörke, M., and Märker, M.: Future long-term changes in global water resources driven by socio-economic and climatic changes, *Hydrological Sciences Journal*, 52(2), 247–275, 2007.
- Allen, P. M., Arnold, J. G., and Byars, B. W.: Downstream channel geometry for use in planning-level models, *Water Resources Bulletin*, 30(4), 663–671, 1994.
- Andrews, E.: Effective and bankfull discharges in the Yampa River basin, Colorado and Wyoming., *Journal of Hydrology*, 46, 311–330, 1980.
- Armstrong, R., Brodzik, M., and Knowles, K.: Northern Hemisphere Snow Cover, Version 2, Digital media, 2003.
- Armstrong, R., Brodzik, M., Knowles, K., and Savoie, M.: Global monthly EASE-Grid snow water equivalent climatology, Digital media, 2005.
- Arnell, N.: Implications of climate change for freshwater inflows to the Arctic Ocean, *Journal of Geophysical Research*, 110, D07105, 2005.

- Arnell, N. and Reynard, N.: The effects of climate change due to global warming on river flows in Great Britain, *Journal of Hydrology*, 183, 397–424, 1996.
- Arnell, N. W.: A simple water balance model for the simulation of streamflow over a large geographic domain, *Journal of Hydrology*, 217, 314–335, 1999.
- Arora, K. and Boer, G.: A variable velocity flow routing algorithm for GCMs, *Journal of Geophysical Research*, 104, 30,965–30,979, 1999.
- Barnes, H.: Roughness characteristics of natural channels., Tech. rep., United States Geological Survey Water Supply Paper, 1849, 1967.
- Barry, R.: Mountain weather and climate. 2nd edition, Routledge: London, New York, 1992.
- Batjes, N.: Development of a world data set of soil water retention properties using pedotransfer rules, *Geoderma*, 71, 31–52, 1996.
- Beniston, M., Stephenson, D. B., Christensen, O. B., Ferro, C. A. T., Frei, C., Goyette, S., Halsnaes, K., Holt, T., Jylhä, K., Koffi, B., Palutikof, J., Schöll, R., Semmler, T., and Woth, K.: Future extreme events in European climate: an exploration of regional climate model projections, *Climatic Change*, 81, 71–95, DOI 10.1007/s10584-006-9226-z, 2007.
- Bergström, S.: The HBV Modell – its structure and applications., Tech. rep., SMHI Reports Hydrology, No. 4, April 1992, 1992.
- Booij, M.: Impact of climate change on river flooding assessed with different spatial model resolutions, *Journal of Hydrology*, 303, 176–198, 2005.
- Bouwman, A. F., Drecht, G. V., Knoop, J. M., Beusen, A. H. W., and Meinardi, C. R.: Exploring changes in river nitrogen export to the world's oceans, *Global Biogeochem. Cycles*, 19, GB1002, doi:10.1029/2004GB002314, 2005.
- Brown, J., Jr., O. F., Heginbottom, J., and Melnikov, E.: Circum-Arctic Map of Permafrost and Ground-Ice Conditions. In International Permafrost Association Standing Committee on Data Information and Communication (comp.). 2003. Circumpolar Active-Layer Permafrost System, Version 2.0. Edited by M. Parsons and T. Zhang, CD-ROM, 1998.
- Brown, J., Hinkel, K., and Nelson, F.: The Circumpolar Active Layer Monitoring (CALM) program: research design and initial results, *Polar Geography*, 24(3), 166–258, 2000.
- Castro, J. and Jackson, P.: Bankfull Discharge Recurrence Intervals And Regional Hydraulic Geometry Relationships: Patterns In The Pacific Northwest, USA., *Journal Of The American Water Resource Association*, 37(5), 1249 – 1262, 2001.
- Chang, J. and Hanna, S.: Air quality model performance evaluation, *Meteorology and Atmospheric Physics*, 87(1-3), 167–196, 2001.
- Chow, V.: Open-channel hydraulics., New York, McGraw- Hill Book Co., 1959.

- Christensen, J., Hewitson, B., Busuioc, A., Chen, A., Gao, X., Held, I., Jones, R., Kolli, R., Kwon, W.-T., Laprise, R., Rueda, V. M., Mearns, L., Menéndez, C., Räisänen, J., Rinke, A., Sarr, A., and Whetton, P.: Climate Change 2007: The Physical Science Basis. Contribution of Working Group I to the Fourth Assessment Report of the Intergovernmental Panel on Climate Change, chap. Regional Climate Projections, pp. 847–940, Cambridge University Press, Cambridge, United Kingdom and New York, NY, USA., 2007.
- Christensen, J. H. and Christensen, O. B.: A summary of the PRUDENCE model projections of changes in European climate by the end of this century, *Climatic Change*, 81, 7–30, 2007.
- Cowan, W.: Estimating hydraulic roughness coefficients,, *Agricultural Engineering*, 37(7), 573–475, 1956.
- Dale, M.: Impact of climate change on UK flooding and future predictions, in: *Proceedings of the Institution of Civil Engineers-Water Management*, vol. 158 (4), pp. 135–140, 2005.
- Dankers, R. and Feyen, L.: Climate change impact on flood hazard in Europe: An assessment based on high-resolution climate simulations, *Journal of Geophysical Research*, 113, D19 105, doi:10.1029/2007JD009 719., 2008.
- de Moel, H., van Alphen, J., and Aerts, J. C. J. H.: Flood maps in Europe – methods, availability and use, *Natural Hazards and Earth System Science*, 9, 289–301, 2009.
- Döll, P. and Flörke, M.: Global-Scale Estimation of Diffuse Groundwater Recharge. Frankfurt Hydrology Paper 03, Tech. rep., Institute of Physical Geography, Frankfurt University, Frankfurt am Main, Germany, 2005.
- Döll, P. and Lehner, B.: Validation of a new global 30-min drainage direction map, *Journal of Hydrology*, 258(1-4), 214–231, 2002.
- Döll, P. and Siebert, S.: Global Modeling of Irrigation Water Requirements, *Water Resources Research*, 38 (4), 8.1–8.10, 2002.
- Döll, P., Kaspar, F., and Lehner, B.: A Global Hydrological Model for Deriving Water Availability Indicators: Model Tuning and Validation, *Journal of Hydrology*, 270(1-2), 105–134, 2003.
- Déry, S. and Wood, E.: Decreasing river discharge in northern Canada, *Geophysical Research Letters*, 32, L10 401, doi:10.1029/2005GL022 845, 2005.
- Déry, S. J. and Brown, R. D.: Recent Northern Hemisphere snow cover extent trends and implications for the snow-albedo feedback, *Geophysical Research Letters*, 34, L22 504, doi:10.1029/2007GL031 474, 2007.
- Dunn, S. and Colohan, R.: Developing the snow component of a distributed hydrological model: a step-wise approach based on multi-objective analysis, *Journal of Hydrology*, 223(1), 1–16, 1999.

- Dunne, T. and Leopold, L.: Water in environmental planning, Freeman, San Francisco, 1978.
- Dury, G., Hails, J. R., and Robbie, H. B.: Bankfull Discharge and the Magnitude Frequency series, *Australian Journal of Science*, 26, 123–124, 1963.
- DVWK: Empfehlungen zur Berechnung der Hochwasserwahrscheinlichkeit, Tech. rep., DVWK-Regeln zur Wasserwirtschaft, H. 101, Verlag Paul Parey, Hamburg, 1979.
- DVWK: Statistische Analyse von Hochwasserabflüssen., Tech. rep., DVWK-Merkblatt 251/1999, Wirtschafts- und Verl.-Ges. Gas und Wasser, 1999.
- Dyck, S. and Peschke, G.: Grundlagen der Hydrologie, Verlag für Bauwesen, Berlin., 1995.
- EB: Encyclopedia Britannica, <http://www.britannica.com/> (15.01.2009), 2009.
- EEA: Corine Land Cover 2000 - Mapping a decade of change Document Actions, Tech. Rep. Brochure No 4/2004, EEA (European Environment Agency), 2004.
- FAO: Digital Soil Map of the World and Derived Soil Properties. Rev. 1. (CD Rom), <http://www.fao.org/ag/AGL/agll/dsmw.htm> (21-Oct-2008), 2003.
- Farr, T. G., Rosen, P. A., Caro, E., Crippen, R., Duren, R., Hensley, S., Kobrick, M., Paller, M., Rodriguez, E., Roth, L., Seal, D., Shaffer, S., Shimada, J., Umland, J., Werner, M., Oskin, M., Burbank, D., and Alsdorf, D.: The Shuttle Radar Topography Mission, *Reviews of Geophysics*, 45, RG2004, doi:10.1029/2005RG000183, 2007.
- Flörke, M. and Alcamo, J.: European Outlook on Water Use, Final Report EEA/RNC/03/007, Center for Environmental Systems Research — University of Kassel, 2004.
- Fowler, H. J., Ekström, M., Blenkinsop, S., and Smith, A. P.: Estimating change in extreme European precipitation using a multimodel ensemble., *Journal of Geophysical Research*, 112, D18 104, doi:10.1029/2007JD008619, 2007.
- Gerrard, A. J.: Mountain environments: An examination of the physical geography of mountains, Belhaven, London, 1990.
- Gordon, C., Cooper, C., Senior, C., Banks, H., Gregory, J., Johns, T., Mitchell, J., and Wood, R.: The simulation of SST, sea ice extents and ocean heat transports in a version of the Hadley Centre coupled model without flux adjustments, *Climate Dynamics*, 16, 147–168, 2000.
- Graham, L., Andreasson, J., and Carlsson, B.: Assessing climate change impacts on hydrology from an ensemble of regional climate models, model scales and linking methods - a case study on the Lule River basin, *Climatic Change*, 81, 293–307, 2007.
- GRDC: GRDC Station Catalog, <http://www.bafg.de/html/internat/grdc/download.html> (10.01.2003), 1999.

- GRUMP: Global Rural-Urban Mapping Project (GRUMP), Alpha Version: Urban Extents., Available at <http://sedac.ciesin.columbia.edu/gpw>. (29.05.2008), 2004.
- Haan, C.: Statistical methods in hydrology, 2nd edition, Iowa State Press, Ames, Iowa., 2002.
- Hagemann, S. and Dümenil, L.: A parameterization of lateral water flow for the global scale, *Climate Dynamics*, 14, 17–41, 1998.
- Harman, W., Jennings, G., Patterson, J., Clinton, D., Slate, L., Jessup, A., Everhart, J., and Smith, R.: Bankfull Hydraulic Geometry Relationships for North Carolina Streams, in: *AWRA Wildland Hydrology Proceedings*, edited by Olsen, D. and Potyondy, J. P., pp. 401–408, AWRA Summer Symposium. Bozeman, Montana, 1999.
- Henrichs, T. and Kaspar, F.: EuroWasser: Model-based assessment of European water resources and hydrology in the face of global change., chap. Baseline-A: a reference scenario of global change, pp. 4-1 – 4-8, *Kassel World Water Series 5*. Centre for Environmental Systems Research, University of Kassel, Kassel, Germany, 2001.
- Hirabayashi, S., Kanae, S., Emori, T., Oki, T., and Kimoto, M.: Global projections of changing risks of floods and droughts in a changing climate, *Hydrological Sciences Journal*, 53(4), 754–773, 2008.
- Hosaka, M., Nohara, D., and Kitoh, A.: Changes in snow coverage and snow water equivalent due to global warming simulated by a 20km-mesh global atmospheric model, *Scientific Online Letters on the Atmosphere*, 1, 93–96, 2005.
- Hunger, M. and Döll, P.: Value of river discharge data for global-scale hydrological modeling, *Hydrology and Earth System Sciences*, 12, 841–861, 2008.
- IPCC: *Climate Change 2001: The Scientific Basis*. Contribution of Working Group I to the Third Assessment Report of the Intergovernmental Panel on Climate Change, Cambridge University Press, Cambridge, United Kingdom and New York, NY, USA, 2001.
- IPCC: *Climate Change 2007: Synthesis Report*. Contribution of Working Groups I, II and III to the Fourth Assessment Report of the Intergovernmental Panel on Climate Change., IPCC, Geneva, Switzerland, 2007a.
- IPCC: *Climate Change 2007: The Physical Science Basis*. Contribution of Working Group I to the Fourth Assessment Report of the Intergovernmental Panel on Climate Change, chap. IPCC, 2007: Summary for Policymakers., pp. 1–18, Cambridge University Press, Cambridge, United Kingdom, 2007b.
- Jungclaus, J., Botzet, M., Haak, H., Keenlyside, N., Luo, J., Latif, M., Marotzke, J., Mikolajewicz, U., and Roeckner, E.: Ocean circulation and tropical variability in the coupled model ECHAM5/MPI-OM, *Journal of Climate*, 19, 3952–3972, 2006.
- Kaspar, F.: *Entwicklung und Unsicherheitsanalyse eines globalen hydrologischen Modells*, PhD thesis, Kassel University Press, ISBN 3-89958-071-0, 139 pages, 2004.

- Kleinen, T. and Petschel-Held, G.: Integrated assessment of changes in flooding probabilities due to climate change, *Climatic Change*, 81, 283–312 DOI 10.1007/s10584-006-9159-6, 2007.
- Klug, W., Graziani, G., Grippa, G., Pierce, D., and Tassone, C.: Evaluation of Long Range Atmospheric Transport Models Using Environmental Radioactivity Data from the Chernoby Accident: The ATMES Report., Elsevier Applied Science, London, 1992.
- Koenigk, T., Mikolajewicz, U., Haak, H., and Jungclaus, J.: Arctic freshwater export in the 20th and 21st centuries, *Journal of Geophysical Research*, 112, G04S41, doi:10.1029/2006JG000274, 2007.
- Kundzewicz, Z., Mata, L., Arnell, N., Döll, P., Kabat, P., Jiménez, B., Miller, K., Oki, T., Sen, Z., and Shiklomanov, I.: Freshwater resources and their management. *Climate Change 2007: Impacts, Adaptation and Vulnerability. Contribution of Working Group II to the Fourth Assessment Report of the Intergovernmental Panel on Climate Change*, Cambridge University Press, Cambridge, UK, 2007.
- Lammers, R., Shiklomanov, A., Vorosmarty, C., Fekete, B. M., and Peterson, B.: Assessment of Contemporary Arctic River Runoff Based on Observational Discharge Records, *Journal of Geophysical Research - Atmospheres*, 106(D4), 3321–3334, 2001.
- Leander, R. and Buishand, T. A.: Resampling of regional climate model output for the simulation of extreme river flows, *Journal of Hydrology*, 332, 487–496, 2007.
- Lehner, B. and Döll, P.: Development and validation of a global database of lakes, reservoirs and wetlands, *Journal of Hydrology*, 296(1-4), 1–22, 2004.
- Lehner, B., Döll, P., Alcamo, J., Henrichs, T., and Kaspar, F.: Estimating the impact of global change on flood and drought risks in Europe: a continental integrated analysis, *Climatic Change*, 75, 273–299, 2006.
- Lehner, B., Verdin, K., and Jarvis, A.: New global hydrography derived from spaceborne elevation data, *Eos, Transactions, AGU*, 89(10), 93–94, <http://hydrosheds.cr.usgs.gov> (21-Oct-2008), 2008.
- Lemke, P., Ren, J., Alley, R., Allison, I., Carrasco, J., Fujii, G. F. Y., Kaser, G., P.Mote, Thomas, R., and Zhang, T.: *Climate Change 2007: The Physical Science Basis. Contribution of Working Group I to the Fourth Assessment Report of the Intergovernmental Panel on Climate Change*, chap. Observations: Changes in Snow, Ice and Frozen Ground, pp. 337–384, Cambridge University Press, Cambridge, 2007.
- Lenderink, G., Buishand, A., and van Deursen, W.: Estimates of future discharges of the river Rhine using two scenario methodologies: direct versus delta approach, *Hydrology and Earth System Sciences*, 11(3), 1145–1159, 2007.
- Leopold, C., Süß, M., and Breitbart, J.: Programming for Malleability with Hybrid MPI-2 and OpenMP: Experiences with a Simulation Program for Global Water Prognosis., in: *European Conference on Modelling and Simulation*, Bonn, pp. 665 – 670, 2006.

- Leopold, L. and Maddock, T.: The hydraulic geometry of stream channels and some physiographic implications: Professional Paper 252, Tech. rep., United States Geological Survey, 1953.
- Leopold, L. B.: A view of the River, Harvard University Press, Cambridge, Massachusetts., 1994.
- Leopold, L. B., Wolman, M. G., and Miller., J. P.: Fluvial Processes in Geomorphology, W.H. Freeman and Co., San Francisco, California, 1964.
- Maniak, U.: Hydrologie und Wasserwirtschaft – eine Einführung für Ingenieure, Springer, Berlin., 2005.
- Marsh, P.: Snowcover formation and melt: recent advances and future prospects, Hydrological Processes, 13, 2117–2134, 1999.
- Meehl, G., Stocker, T., Collins, W., Friedlingstein, P., Gaye, A., Gregory, J., Kitoh, A., Knutti, R., Murphy, J., Noda, A., Raper, S., Watterson, I., Weaver, A., and Zhao, Z.-C.: Climate Change 2007: The Physical Science Basis. Contribution of Working Group I to the Fourth Assessment Report of the Intergovernmental Panel on Climate Change, chap. Global Climate Projections, Cambridge University Press, Cambridge, United Kingdom and New York, NY, USA, 2007.
- Menzel, L. and Burger, G.: Climate change scenarios and runoff response in the Mulde catchment (Southern Elbe, Germany), Journal of Hydrology, 267(1-2), 53–64, 2002a.
- Menzel, L. and Burger, G.: Climate change scenarios and runoff response in the Mulde catchment (Southern Elbe, Germany), Journal of Hydrology, 267 (1-2), 53–64, 2002b.
- Menzel, L. and Lang, H.: Global Change in Mountain Regions – An Overview of Current Knowledge., chap. Spatial heterogeneity of snow conditions and evapotranspiration in the Swiss Alps, pp. 275–282, Dordrecht (Springer), 2005.
- Menzel, L., Thielen, A., Schwandt, D., and Bürger, G.: Impact of climate change on the regional hydrology - Scenario based modelling studies in the German Rhine catchment, Natural Hazards, 38, 45–61, 2006.
- Meybeck, M.: Treatise on Geochemistry Volume 5, Surface and Ground Water, Weathering and Soils, chap. Global occurrence of major elements in rivers, Drever JI (ed.). Elsevier/Pergamon, 207224, 2003.
- Meybeck, M., Green, P., and Vörösmarty, C.: A new typology for mountains and other relief classes, Mountain Research and Development, 21, 34–45, 2001.
- Milly, P., Wetherald, R., and Dunne, K.A .and Delworth, T.: Increasing risk of great floods in a changing climate, Nature, 415, 514–517, 20002.
- Mitchell, T. D. and Jones, P. D.: An improved method of constructing a database of monthly climate observations and associated high-resolution grids, International Journal of Climatology, 26(6), 693 – 712, 2005.

- Mitchell, T. D., Carter, T. R., Jones, P. D., Hulme, M., and New, M.: A comprehensive set of high-resolution grids of monthly climate for Europe and the globe: the observed record (1901-2000) and 16 scenarios (2001-2100)., Tech. rep., Tyndall Centre for Climate Change Research, Working Paper 55, 2004.
- Mosley, M.: Semi-determinate hydraulic geometry of river channels, South Island, New Zealand, *Earth Surface Processes*, 6, 127–138, 1981.
- Mosley, M. P. and McKerchar, A. I.: Handbook of Hydrology, chap. Streamflow, p. 8.1–8.39, McGraw-Hill, New York, 1993.
- MunichRe: Land under water – flood loss trend, www.munichre.com (20.02.2009).
- Muzik, I.: A first-order analysis of the climate change effect on flood frequencies in a sub-alpine watershed by means of a hydrological rainfall–runoff model, *Journal of Hydrology*, 267, 65–73, 2002.
- Ngo-Duc, T., Oki, T., and Kanae, S.: A variable streamflow velocity method for global river routing model: model description and preliminary results, *Hydrol. Earth Syst. Sci. Discuss*, 4, 4389–4414, 2007.
- Nijssen, B., Lettenmaier, D., Liang, X., Wetzel, S., and Wood, E.: Streamflow simulation for continental-scale river basins, *Water Resources Research*, 33(4), 711–724, 1997.
- Nijssen, B., O’Donnell, G., Hamlet, A., and Lettenmaier, D.P. ., .: Hydrologic sensitivity of global rivers to climate change, *Climatic Change*, 183, 397–424, 2001.
- NSIDC: National Snow and Ice Data Center, World glacier inventory, <http://nsidc.org/data/g01130.html> 23.10.2008, digital media, 1999, updated 2007.
- Peterson, B., Holmes, R., McClelland, J., Vörösmarty, C., Lammers, R., Shiklomanov, A., Shiklomanov, I., and Rahmstorf, S.: Increasing River Discharge to the Arctic Ocean, *Science*, 298(5601), 2171–2173, 2002.
- Pinter, N., van der Ploeg, R., Schweigert, P., and G.Hoefer: Flood magnification on the River Rhine., *Hydrological Processes*, 20, 147–164, 2006.
- Rao, A. and Hamed, K.: Flood Frequency Analysis., CRC Press New York, 2000.
- Röckner, E., Bäuml, G., Bonaventura, L., Brokopf, R., Esch, M., Giorgetta, M., Hagemann, S., Kirchner, I., Kornbluh, L., Manzini, E., Rhodin, A., Schlese, U., Schulzweida, U., and Tompkins, A.: The atmospheric general circulation model ECHAM5. Part I: Model description, Tech. rep., Max Planck Institute for Meteorology, Hamburg, Germany, Rep 349, 127 pp, 2003.
- Rothman, D., Agard, J., Alcamo, J., Alder, J., Al-Zubari, W., Beek, T. a. d., Chenje, M., Eickhout, B., Flörke, M., Galt, M., Ghosh, N., Hemmings, A., Hernandez-Pedresa, G., Hijioka, Y., Hughes, B., Hunsberger, C., Kainuma, M., Kartha, S., Miles, L., Msangi, S., Odongo Ochola, W., Pichs Madruga, R., Pirc-Velkarvh, A., Ribeiro, T., Ringler, C., Rogan-Finnemore, M., Sall, A., Schaldach, R., Stanners, D., Sydnor, M., Ruijven, B. v.,

- Vuuren, D. v., Verburg, P., Verzano, K., and Zöckler, C.: United Nations Environment Programme, Global Environment Outlook GEO 4 Environment for Development (Section E - The Outlook - Towards 2015 and Beyond, Chapter 9), chap. The Future Today, pp. 397–454, UNEP, 2007.
- Rowland, R. and Thompson, J.: A method for comparing fallout patterns, Tech. rep., DNA 2929, DOD Nuclear Information and Analysis Centre, General Electric Co., TEMPO, Santa Barbara, 93102, 1972.
- Roy, L., Leconte, R., Brissette, F. P., and C., M.: The impact of climate change on seasonal floods of a southern Quebec River Basin, *Hydrological Processes*, 15, 3167–3179, 2001.
- Schneider, C.: Estimation of Bankfull Flow for Large Scale Modeling Analyses, (in preparation), 2009.
- Schulze, E.-D., Kelliher, F. M., Körner, C., Lloyd, J., and Leuning, R.: Relationships among maximum stomatal conductance, ecosystem surface conductance, carbon assimilation rate, and plant nitrogen nutrition: A global ecology scaling exercise, *Annual Review of Ecology and Systematics*, 25, 629–660, 1994.
- Schulze, K., Hunger, M., and Döll, P.: Simulating river flow velocity on global scale, *Advances in Geosciences*, 5, 133–136, 2005.
- Scurlock, J., Asner, G., and Gower, S.: Worldwide historical estimates of Leaf Area Index 1932-2002, Tech. rep., ORNL Oak Ridge National Laboratory (US), 2001.
- Semádeni-Davies, A.: Monthly snowmelt modelling for large-scale climate change studies using the degree day approach, *Ecological Modelling*, 101, 303–323, 1997.
- Siebert, S., Döll, P., Hoogeveen, J., Faures, J.-M., Frenken, K., and Feick, S.: Development and validation of the global map of irrigation areas, *Hydrology and Earth System Sciences*, 9, 535–547, 2005.
- Sillmann, J. and Roeckner, E.: Indices for extreme events in projections of anthropogenic climate change, *Climatic Change*, 86, 83–104, 2008.
- SMHI: IHMS – Integrated Hydrological Modelling System, Version 4.0, Manual., Tech. rep., Swedish Meteorological and Hydrological Institute Norrköpping, Sweden, 1996.
- Snir, M., Otto, S. W., Huss-Lederman, S., Walker, D. W., and Dongarra, J.: MPI : The Complete Reference, MIT Press, 1996.
- Straume, A.: A More Extensive Investigation of the Use of Ensemble Forecasts for Dispersion Model Evaluation, *Journal of Applied Meteorology*, 40, 425–445, 2001.
- Tricart, J.: *Precis de Geomorphologie Dynamique Generale (tome2)*, Sedes, Paris, 1977.
- Troll, C.: High mountain belts between the polar caps and the equator: their definition and lower limit, *Arctic and Alpine Research*, 5, A19–A27, 1973.

- US-ACWD: US Interagency Advisory Committee on Water Data - Guidelines for determining flood flow frequency. Bulletin 17B of the Hydrology Subcommittee., Tech. rep., US Geological Survey, Office of Water Data Coordination: Reston, Virginia., 1982.
- U.S. Geological Survey, E. D. C.: GTOPO30 Digital Elevation Model, <http://edcdaac.usgs.gov/gtopo30/gtopo30.html> (10.01.2003), 2003.
- USGS: <http://waterdata.usgs.gov/nwis/> (26.08.2004).
- USGS: Flood Flow Frequency, Bulletin 17B of the Hydrological Subcommittee, Tech. rep., U.S. Geological Survey, 1981.
- USGS: U.S. Geological Survey, EROS Data Centre (2006) GTOPO30 Digital Elevation Model., <http://edc.usgs.gov/products/elevation/gtopo30/gtopo30.html> (27.12.2006), 2006.
- USGS: Global Land Cover Characterization (GLCC), available at: <http://edc.usgs.gov/products/landcover/glcc.html> (12.12.2008), 2008.
- Verzano, K. and Menzel, L.: Hydrology in Mountain Regions: Observations, Processes and Dynamics, chap. Snow conditions in mountains and climate change - a global view, p. (in press), IAHS-Publication, 2008.
- Verzano, K. and Menzel, L.: Snow Hydrological Conditions in Mountains and Cold Regions: Current State and Future Projections, In preparation, 2009.
- Verzano, K., Voss, F., Bärlund, I., and Lehner, B.: Modeling variable river flow velocity on continental scale: current situation and climate change impacts, in preparation, 2009.
- Viviroli, D. and Weingartner, R.: The hydrological significance of mountains: from regional to global scale, *Hydrology and Earth System Sciences*, 8(6), 1016–1029, 2004.
- Vöröshmarty, C. J., Moore, B., Grace, A. L., and Gildea, M. P.: Continental scale models of water balance and fluvial transport: an application to South America, *Global Biogeochemical Cycles*, 3(3), 241–265, 1989.
- Vörösmarty, C. and Meybeck, M.: Vegetation, Water, Humans and the Climate: A New Perspective on an Interactive System., chap. Responses of continental aquatic systems at the global scale: new paradigms, new methods., IGBP Synthesis Series. Springer Verlag: Berlin; 375413, 2004.
- Waszkewitz, J., Lenzen, P., and Gillet, N.: The PINGO Package - Procedural Interface for Grib Formatted Objects. DKRZ Technical Report 11, Tech. rep., DKRZ, Hamburg, Germany. <http://www.dkrz.de/forschung/reports.html>, 1996.
- Weiß, M., Voß, F., and Menzel, L.: Regionalisation of the Priestly Taylor coefficient for use in global hydrological modelling, *Hydrological Processes*, p. submitted, 2009.
- Williams, G.: Bank-Full Discharge of Rivers, *Water Resources Research*, 14(6), 1141–1154, 1978.

-
- Wu, P., Wood, R., and Scott, P.: Human influence on increasing Arctic river discharges, *Geophysical Research Letters*, 32, L02 703, doi:10.1029/2004GL021 570, 2005.
- Yates, D. N.: Approaches to continental scale runoff for integrated assessment models, *Journal of Hydrology*, 201, 289–310, 1997.
- Zhang, X., Ikeda, M., and Walsh, J. E.: Arctic sea ice and freshwater changes driven by the atmospheric leading mode in a coupled sea iceocean model, *Journal of Climate*, 16, 2159– 2177, 2003.

Danksagung

Die vorliegende Arbeit entstand im Rahmen meiner Tätigkeit als wissenschaftliche Mitarbeiterin am Center for Environmental Systems Research (CESR) der Universität Kassel. Dem Direktor des Zentrums, Prof. Joseph Alcamo, danke ich für seine Unterstützung während meiner Zeit am CESR und die konstruktiven Diskussionen. Auch meinem Betreuer Prof. Lucas Menzel sowie Prof. Petra Döll möchte ich für die zahlreichen Ratschläge und Diskussionen danken. Ich habe die Möglichkeit bekommen, die vorliegende Dissertation im Rahmen der International Max Planck Research School on Earth System Modeling durchzuführen, was mir viele wertvolle Einblicke in die globale Klimamodellierung ermöglicht hat. Ich möchte insbesondere Antje Weitz für ihre Unterstützung und die ermutigenden und netten e-mails und Gespräche während meiner ausgedehnten IMPRS Zeit danken.

Meinen Kolleginnen und Kollegen am CESR möchte ich für die tolle Arbeitsatmosphäre danken. Ulla und Kirsten sei gedankt für die viele ungeschene administrative Arbeit und die netten Plaudereien im Sekretariat. Achim danke ich für seine Hilfe in allen technischen Belangen und die Einblicke in die Welt des Sportkletterns. Ein ganz besonderer Dank geht an meine Bürokollegen Martina, Frank und Christoph für das kritische Korrekturlesen und ihre großartige Mithilfe während der Abschlussphase, die zahlreichen Diskussionen und Gespräche und die spaßige Zeit, die wir miteinander hatten. Besonders gedankt sei an dieser Stelle auch Ellen, die bei der Umsetzung zahlreicher Programme geholfen hat und bei programmiertechnischen Fragen immer helfend zur Seite stand.

Ohne eine liebevolle und zuverlässige Kinderbetreuung wäre die Fertigstellung dieser Arbeit nicht möglich gewesen. Deshalb möchte ich mich an dieser Stelle ganz herzlich bei Frau Contreras-Schlüsselburg und ihrer Familie sowie bei Marga und Katja vom Kinderneest für die wunderbare Zeit bedanken. Bei meinen Eltern möchte ich mich herzlichst dafür bedanken, dass sie mir in allen Lebenslagen mit Rat und vor allem Tat zu Seite standen. Von ganzem Herzen danke ich Rudi für seine große Geduld und sein Verständnis während der Fertigstellung dieser Arbeit. Und meinen Kindern Simeon und Liam danke ich dafür, dass sie mir die Augen für die vielen wichtigen kleinen Dinge auf dieser Welt öffnen.

Die gesamten Veröffentlichungen in der Publikationsreihe des MPI-M
„Berichte zur Erdsystemforschung“,
„Reports on Earth System Science“,
ISSN 1614-1199

sind über die Internetseiten des Max-Planck-Instituts für Meteorologie erhältlich:

<http://www.mpimet.mpg.de/wissenschaft/publikationen.html>

